Louisiana State University

LSU Scholarly Repository

4-4-2018

The Effects of Metal Speciation, Content and Cluster Size in Fly Ash on PCDD/F Formation

Xia Guan
Louisiana State University and Agricultural and Mechanical College

Follow this and additional works at: https://repository.lsu.edu/gradschool_dissertations

Part of the Environmental Sciences Commons

Recommended Citation

THE EFFECTS OF METAL SPECIATION, CONTENT AND CLUSTER SIZE IN FLY ASH ON PCDD/F FORMATION

A Dissertation

Submitted to the Graduate Faculty of the
Louisiana State University and
Agricultural and Mechanical College
in partial fulfillment of the
requirements for the degree of
Doctor of Philosophy

in

The Department of Environmental Sciences

by
Xia Guan
B.S., Henan Normal University, 1998
Ph.D., Fudan University, 2011
May 2018

ACKNOWLEDGEMENTS

TABLE OF CONTENTS

LIST OF ABBREVIATIONS

PCDD/Fs - polychlorinated dibenzo-*p*-dioxins and polychlorinated dibenzofurans

EPFRs - environmentally persistent free radicals

2-MCP - 2-monochlorophenol

STDS - system for thermal diagnostic studies

GC/MS - gas chromatograph / mass spectrometer

XRD - x-ray diffraction

XPS - x-ray photoelectron spectroscopy

TEM - transmission electron microscope

EPR - electron paramagnetic resonance

DPPH - 2,2-diphenyl-1-picrylhydrazyl

DF - dibenzofuran

DD - dibenzo-*p*-dioxin

MCDF - 4-monochlorodibenzofuran

MCDD - 1-monochlorodibenzo-*p*-dioxin

DCDF - 4,6-dichlorodibenzofuran

DCDD - 2,7-dichlorodibenzo-*p*-dioxin

TriCDD - 1,2,3-trichlorodibenzo-*p*-dioxin

TeCDD - 2,3,7,8-tetrachlorodibenzo-*p*-dioxin

TCB - tetrachlorinated biphenyl

PeCB - pentachlorinated biphenyl

HxCB - hexachlorinated biphenyl

HpCB - heptachlorinated biphenyl

OCB - octachlorinated biphenyl

PCB - polychlorinated biphenyl

PeCDD - pentachlorinated dibenzo-*p*-dioxin

HxCDD - hexachlorinated dibenzo-*p*-dioxin

HpCDD - heptachlorinated dibenzo-*p*-dioxin

OCDD - octachlorinated dibenzo-*p*-dioxin

TCDF - tetrachlorinated dibenzofuran

PeCDF- pentachlorinated dibenzofuran

HxCDF - hexachlorinated dibenzofuran

HpCDF - heptachlorinated dibenzofuran

OCDF- octachlorinated dibenzofuran

ABSTRACT

Transition metal oxides present in waste incineration systems have the ability to catalyze the formation of polychlorinated dibenzo-*p*-dioxins and dibenzofurans (PCDD/Fs) through surface mediated condensation of organic dioxin precursors. Current studies have concentrated on the catalytic effects of individual transition metal oxides, while the complex composition of fly ash introduces the possibility of synergistic or antagonistic effects between multiple, catalytically active components. In addition, there is at present hardly a quantitative link between fly ash physical properties/chemical reactivity and PCDD/Fs yield.

We have tested fly ash surrogates containing different ratios of iron (III) oxide and copper (II) oxide to study the cooperative effects between two transition metals. The presence of both iron and copper oxides increased the oxidative power of the fly ash surrogates in oxygen rich conditions and led to extremely high PCDD/F yields under pyrolytic conditions (up to >5% yield) from 2-monochlorophenol precursor. PCDD/F congener profiles from the mixed oxide samples are similar to results obtained from only CuO, however the total PCDD/F yield increases with increasing Fe_2O_3 content. Careful analysis of the reaction products and changes to the oxidation states of active metals indicate the CuO surface sites are condensation reaction centers while the Fe_2O_3 is affecting the bond energy in CuO and increasing the ability of copper centers to form surface-bound radicals that are precursors to PCDD/Fs.

Three fly ash surrogates containing 1%, 2.5%, and 4% of Fe_2O_3 were prepared and their effects on the PCDD/F formation were investigated and compared to typical 5% iron oxide sample. The results showed that under pyrolysis conditions, the total dioxin

yields increased with the increasing content of iron in the fly ash surrogates. To understand the effects of the content and morphology of iron and the formation of PCDD/F, the surrogates were characterized using transmission electron microscopy (TEM) and X-ray diffraction (XRD). TEM and XRD analysis confirmed that 1% of Fe_2O_3 fly ash surrogate was amorphous, and crystallinity increased with the increasing iron content. Our results demonstrate the amount of iron in the fly ash influences the morphology and size of the Fe_2O_3 nanoclusters, determining the furan congeners' distribution and total PCDD/F yield.

CHAPTER 1 INTRODUCTION

1.1 Introduction to PCDD/F

Dioxins are generic names of polychlorinated dibenzo-p-dioxins (PCDD) and polychlorinated dibenzofurans (PCDF). PCDD/Fs are formed as byproducts in combustion processes,[1-2] especially the thermal treatment of municipal solid waste. [3-4] They are a group of tricyclic aromatic compounds with similar chemical properties. Each compound comprises two benzene rings interconnected by oxygen atoms. In PCDDs' structure, the benzene rings are joined by two oxygen bridges, and in PCDFs, the benzene rings are connected by a carbon bond and an oxygen bridge. There are 75 PCDD and 135 PCDF congeners, each differing in the number and position of the chlorine atoms. PCDD/Fs are highly toxic in biological systems due to their teratogenic, mutagenic and carcinogenic properties. [5-6] Their strong lipophilic nature leads to bioaccumulation in the food chain, mainly in the fatty tissue of animals. In PCDD/F family, 2,3,7,8-tetrachlorodibenzo-p-dioxin (TCDD) is the most toxic; other congeners' toxicities can be expressed as fractional equivalencies of TCDD. Of the 210 possible PCDD/F congeners, only the seventeen 2,3,7,8-chloro-substituted congeners are considered toxic and bioaccumulative. These 17 congeners have a range of toxic potency, and each has been assigned a toxic equivalency factor (TEF) based on the relative potency compared with the most toxic congener, 2,3,7,8-tetrachlorodibenzo-p-dioxin (TCDD). [7] A toxic equivalent (TEQ) is then defined as the summation of all toxic congener concentrations weighted by their TEF to provide a single unit to measure the toxic concentration of all the PCDD/Fs. In addition to PCDD/Fs, some polychlorinated biphenyls (PCBs) have similar chemical structures and physical-chemical properties, accordingly, they invoke common toxic

responses. Certain members of the PCDD/Fs and PCB family are termed as "dioxin-like"

products and are assigned TEF values in Table 1.1. [8] Figure 1.1 shows the generic

structures of PCDDs, PCDFs and PCBs, respectively. In this document, dioxins are

referred to PCDDs and PCDFs.

Table 1.1. Recommended Toxicity Equivalence Factors (TEFs) for Human Health Risk Assessment of Polychlorinated Dibenzo-*p*-dioxins, Dibenzofurans, and Dioxin-like Polychlorinated Biphenyls [8]	
Compound	TEF
PCDDs	
2,3,7,8-TCDD	1
1,2,3,7,8-PeCDD	1
1,2,3,4,7,8-HxCDD	0.1
1,2,3,6,7,8-HxCDD	0.1
1,2,3,7,8,9-HxCDD	0.1
1,2,3,4,6,7,8-HpCDD	0.01
OCDD	0.0003
PCDFs	
2,3,7,8-TCDF	0.1
1,2,3,7,8-PeCDF	0.03
2,3,4,7,8-PeCDF	0.3
1,2,3,4,7,8-HxCDF	0.1
1,2,3,6,7,8-HxCDF	0.1
1,2,3,7,8,9-HxCDF	0.1
2,3,4,6,7,8-HxCDF	0.1
1,2,3,4,6,7,8-HpCDF	0.01
1,2,3,4,7,8,9-HpCDF	0.01
OCDF	0.0003
PCBs	
3',4,4'-TCB	0.0001
3,4,4',5-TCB	0.0003
3,3',4,4',5-PeCB	0.1
3,3',4,4',5,5'-HxCB	0.03
2,3,3',4,4'-PeCB	0.00003
2,3,4,4',5-PeCB	0.00003
2,3',4,4',5-PeCB	0.00003
2,3,3',4,4', 5-HxCB	0.00003
2,3,3',4,4',5'-HxCB	0.00003
2,3',4,4',5,5'-HxCB	0.00003
2,3,3',4,4',5,5'-HpCB	0.00003

1.2 Emission Sources of PCDD/F

According to the dioxin source inventory issued by the U.S. Environmental Protection Agency (EPA),[9] the major identified sources of environmental releases of dioxin-like compounds are grouped into six broad categories: combustion sources, metals
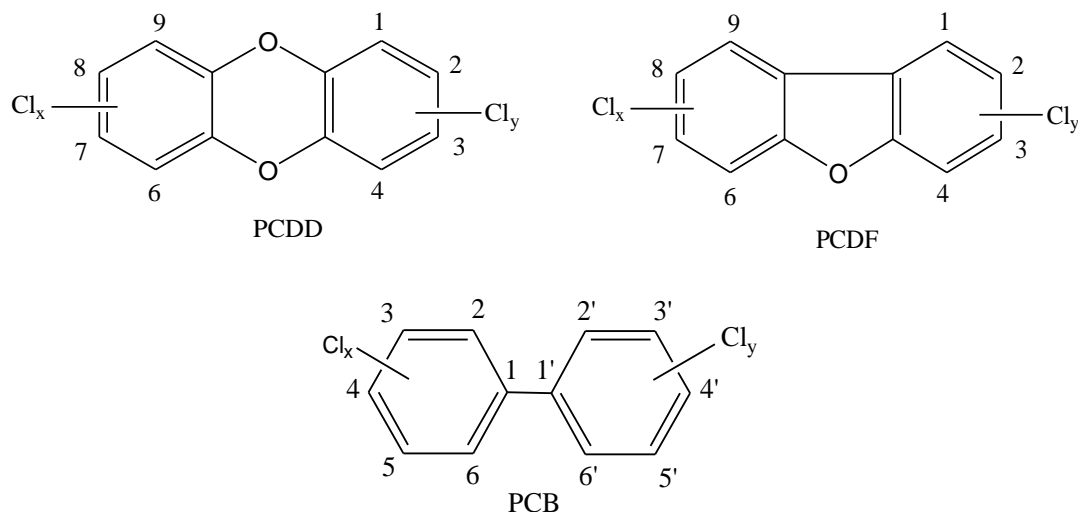
Figure 1.1. Chemical Structural Formulas for PCDD, PCDF and PCB

smelting, refining and process sources, chemical manufacturing sources, natural sources, and environmental reservoirs. Combustion is a dominant source of dioxin emission. [10] "Dioxins" are produced from biomass burning, [11-12] municipal solid waste incineration (MSWI), [13-16] medical waste incineration,[17] backyard barrel burning of refuse, etc. Metallurgical industries [18-19] such as iron ore sintering and secondary non-ferrous metal smelting have also been identified as primary source of PCDD/F emission. Other sources include co-fired utility boilers,[20] automobile exhaust,[21] pulp and paper mills,[22-23] forest fire, [24] volcanic activities, pesticide production, [25] etc. The EPA inventory report shows that environmental releases of dioxin-like compounds decreased by approximately 90% between 1987 and 2000; the leading source of dioxin-like compounds in 2000 was the backyard burning of refuse in barrels because it was unregulated on a national level.

In the Toxics Release Inventory reporting facilities from 2010 to 2016, since 2010, dioxin released increased by 114%. This increase is largely driven by increased on-site land disposal from a non-ferrous metal smelting and refining facility.

1.3 Environmental Laws and "Dioxins"

U.S. EPA has released laws and guidelines to minimize emissions of dioxins and protect human health. [26]

Comprehensive Environmental Response, Compensation and Liability Act (CERCLA) / Resource Conservation and Recovery Act (RCRA): In 2009, former Administrator Lisa Jackson directed EPA to accelerate work underway to reassess the human health risks from exposures to dioxin including completing the development of draft interim preliminary remediation goals (PRGs) for dioxin in soil. PRGs are goals for lowering the concentration of specific chemicals in specific media like soil, sediment, at Superfund sites, federal facilities and RCRA sites. They serve as a target to use during the initial development, analysis, and selection of cleanup options. These goals are designed to protect human health and the environment, and comply with all applicable, relevant and appropriate regulations (ARARs) for all exposure pathways being addressed.

Hazardous Air Pollutants for Hazardous Waste Combustors and Clean Air Act: EPA announced the final rule Final Standards for Hazardous Air Pollutants for Hazardous Waste Combustors in 2005. The rule established national emission standards for hazardous air pollutants (like dioxins) for sources that burn hazardous waste: commercial and onsite incinerators, cement kilns, lightweight aggregate kilns, boilers, and hydrochloric acid production furnaces. These standards were promulgated pursuant to

Section 112 (d) of the Clean Air Act, which requires EPA to issue technology-based standards reflecting the performance of the Maximum Achievable Control Technology (MACT).

Toxic Substances Control Act (TSCA): under TSCA section 8(e), any person who manufactures (including imports), processes, or distributes in commerce a chemical substance (including, generally, dioxin) or mixture and who obtains information which reasonably supports the conclusion that such substance or mixture presents a substantial risk of injury to health or the environment to immediately inform EPA, except where EPA has been adequately informed of such information. Under 40 CFR part 766, testing by manufacturers and processors of certain specified chemical substances to ascertain whether those substances may be contaminated with halogenated dibenzo-*p*-dioxins (HDDs)/dibenzofurans (HDFs) is required under TSCA section 4, and under TSCA section 8 manufacturers and processors of certain chemicals are required to report certain information to EPA.

Emergency Planning and Community Right-to-Know Act (EPCRA): Section 313 of the EPCRA of 1986 requires certain facilities manufacturing, processing or otherwise using listed chemicals to report their environmental releases of such chemicals annually. The list of reportable chemicals, known as the EPCRA section 313 list and also referred to as the Toxics Release Inventory, or TRI list, was originally identified in the statute and was comprised of more than 300 individual chemicals and 20 chemical categories.

Safe Drinking Water Act (SDWA): under the Safe Drinking Water Act (SDWA), EPA has established a maximum contaminant level for dioxin in drinking water.

China is one of the largest dioxin-emitting counties in the world, with estimated total annual dioxin emissions from the 17 main industrial sectors of 6 kg toxic equivalent (TEQ) in 2008.[27] In 2000, China issued the first dioxin emission standard for waste incineration. In October 2010, China issued Guidance on the Strengthening of Dioxin Pollution Prevention, which requires key dioxin-emitting industries to carry out comprehensive actions to reduce dioxin emissions. [28] This is a major historical milestone in China's fight against dioxin pollution.

European Union has presented three progress reports on dioxins and PCBs since 2004. [29] Between 1990 and 2007 industrial emissions of newly formed dioxins, furans and PCBs were reduced in the European Union by 80%. In order to address the health and environmental concerns due to these pollutants the Commission adopted in 2001 a Communication to the Council, the European Parliament and the Economic and Social Committee setting out a Community Strategy for dioxins, furans and PCBs. This dioxin strategy consists of two parts: one part containing actions for reducing the presence of dioxins, furans and PCBs in the environment and one part containing actions for reducing their presence in feed and food.

1.4 PCDD/F Formation Mechanisms

Fly ash from MSWI has been known as hazardous waste because of the high content of metals and PCDD/Fs. [30-31] PCDD/Fs are formed as byproducts in combustion processes, especially the thermal treatment of municipal waste. Studies have shown the highest load of PCDD/Fs released from waste incineration is mainly adsorbed on fly ash. [32] The metals include Al, Fe and Zn, Cr, Cu and Pb, etc. The content and form of the metals is related with the leaching behavior and potential environment risk of the fly ash.

[31, 33] Since the discovery of PCDD/Fs in MSWI fly ash and flue gas, the formation mechanisms of PCDD/Fs [34-36] and the role of metal oxides in promoting or suppressing the formation of PCDD/Fs has been thoroughly studied. Among transition metals, copper and iron have been identified to be the most active in the formation of PCDD/F.[37-39]

Chlorophenols have been demonstrated to be the predominant and direct precursors of PCDD/Fs in thermal systems. [40-43] Chlorophenols can be found ubiquitously in the environment due to their extensive and long-term use in industry and in daily life. In addition to chlorophenols, chlorobenzenes[44-46] have also been shown to be the precursors of PCDD/F formation via different mechanisms.

PCDD/Fs are formed by two general pathways: homogeneous and heterogeneous pathways. Homogeneous pathways involve the reaction of structurally related precursors in the gas phase, in the higher temperature region of 500-800 °C. Heterogeneous pathways involve two routes in 100-500 °C: "de novo" synthesis and transition metal catalyzed precursor mechanisms. De novo synthesis occurs from carbonaceous materials in soot, which releases PCDD/F congeners in the presence of oxygen and catalyst without the gas-phase precursor. Transition metal catalyzed condensation reaction of precursors.

1.4.1 Homogeneous Pathway

Gas phase formation of PCDD/F from structurally related precursors includes three principal steps: [34] self-condensation of the precursors; cyclization of the initial intermediates from the first step to produce PCDD/F; chlorination/dichlorination reactions. Specifically, the production of the phenoxy radical ($C_6H_5O\cdot$) from a phenol molecule is an important step. This reaction might be initiated through thermal decomposition. Then, the

phenoxy radicals experience self-condensation and keto-enol tautomization to form bis-enol intermediates. PCDFs are formed through a radial-radial coupling while PCDDs formation involves radical/radical, molecule/radical or molecule/molecule coupling.

1.4.2 Heterogeneous Pathways

In heterogeneous reactions, when gas molecules adsorb and desorb at a catalytically active surface and interact with each other, as well as with the surface itself, various reaction mechanisms have been proposed. Three main reaction mechanisms: (a) Langmuir-Hinshelwood mechanism, (b) Eley-Rideal mechanism, (c) Mars-Van Krevelen mechanism are shown in Figure 1.2. In Langmuir-Hinshelwood mechanism, both reactant A and B first adsorb onto the surface, then a reaction takes place and the reaction product desorbs from the surface. In Eley-Rideal mechanism, only reactant A adsorbs onto the surface, the other reactant B interact and react with the adsorbed A directly from the gas phase, followed by the desorption of the reaction product. In Mars-Van Krevelen mechanism, the surface itself is an active part in the reaction, which involves transfer of oxygen atoms from the surface to the adsorbate. When the reaction product desorbs, a vacancy is left behind the surface and it will be filled by a reactant atom from the bulk. The characteristic feature of this mechanism is that some products of the reaction leave the solid catalysts' surface with one or more constituents of the catalysts' lattice.

De novo **Formation**

The emission of PCDD/F from native carbon in MSWI fly ash and sources of oxygen, chlorine and hydrogen is referred to de novo pathway. The phenomenon of dioxin
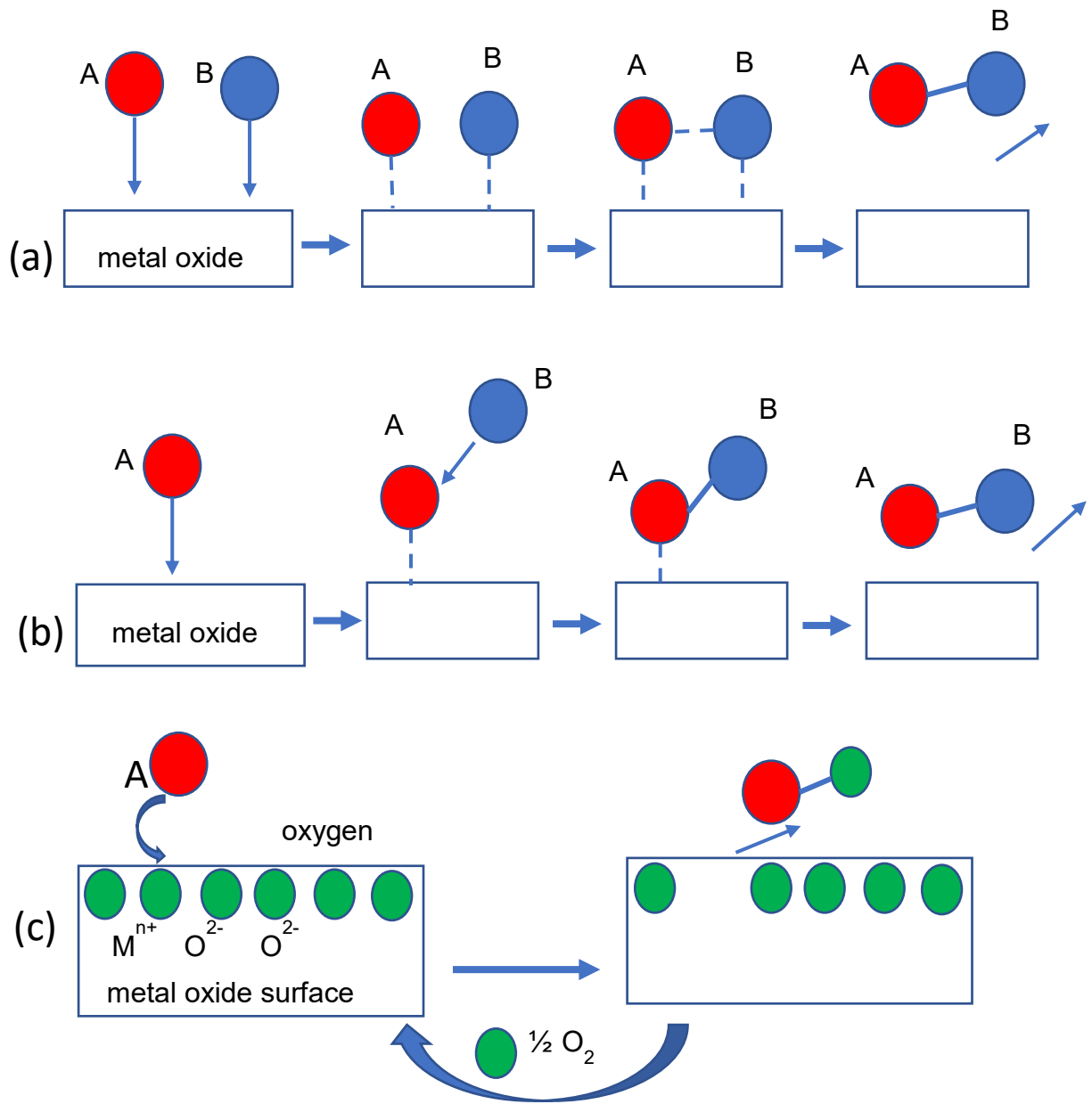
Figure 1.2. (a) Langmuir-Hinshelwood mechanism, (b) Eley-Rideal mechanism, (c) Mars-Van Krevelen mechanism

formation from residual carbon in fly ash was originally discovered by Vogg and Stieglitz in 1986. [47] They suggested that the formation of PCDD/F could be regarded as a de novo synthesis from carbon and inorganic chloride in fly ash. Since then, many laboratories have performed de novo studies under different experimental conditions. Milligan and Altwicker studied the relationship between de novo synthesis of PCDD/F and carbon gasification in fly ash. [48] A clear correlation was observed between carbon gasification rates and PCDD/F formation rates for all four fly ashes. Huang and Buekens [49] developed a kinetic model for the formation of PCDD/F based on the de novo pathway. Three reactions are considered:

Reaction 1: $C + aO_2 \rightarrow bCO + cCO_2 + dAr + e(PCDD/Fs)s$

Reaction 2: $(PCDD/Fs)s \rightarrow (PCDD/Fs)g$

Reaction 3: $(PCDD/Fs)g \rightarrow other\ products$
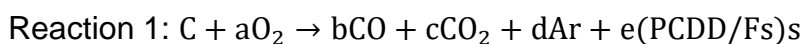
Reaction 1 describes carbon gasification and PCDD/F formation; reaction 2 is the desorption of solid phase PCDD/F to the gas phase; reaction 3 is the degradation of PCDD/F to other product. Kinetic parameters for the three reactions were all adopted from previous literature data. Based on their calculation, de novo synthesis of PCDD/F is dominant in industrial incinerators.

Cu is thought to be the key catalyst of the de novo synthesis in both modeled and real fly ash. Li [50] studied the effect of 0.1 wt% Cu, Cr, Ni, Zn and Cd chloride or oxide model fly ash on the de novo synthesis of PCDD/F. They found that combining the function of chlorinating agent and catalyst, chlorides are more active than oxides. $CuCl_2$ is the most active PCDD/F catalyst. By using the fly ash from an MSWI in Taiwan, Wang

[51] also concluded the formation of PCDD/Fs was significantly increased by $CuCl_2$ after comparing the results from 10 wt% $FeCl_2$, $ZnCl_2$ and $CuCl_2$ into the fly ash medium.

Fe^{3+}, also redox-active, is almost the highest concentration transition metals in fly ash. Depending on the MSWI facilities and sampling time, the content of iron oxide in fly ashes is from 0.85-5.02 %. [31] Early research has focused on the destruction rather than formation of PCDD/Fs. [52-53] Recently, the effect of iron (III) on the PCDD/F formation has been realized and extensively studied both in de novo pathway [54-57] and in precursor pathway. [38, 58]

Transition Metal Catalyzed Precursor Condensation Pathway

Transition metals are present in the fly ashes in the exhaust and air pollution control devices of most combustion systems. It is known that transition metal oxides and chlorides play an important role in dioxin formation.[59] Specifically, substituted aromatic species chemisorb to metal oxide or hydroxide surface sites to form a phenoxy-type, persistent free radicals (EPFRs). These surface-associated phenoxy radicals can then react with each other to form PCDD/Fs and other pollutant. Scheme 1.1 shows the EPFR formation mechanisms. [38] Two pathways of chemisorption have been identified for chlorophenols: (1) elimination of H_2O (2) elimination of both H_2O and HCl. The mechanism of chemisorption of phenols and other substitute aromatic species on transition metal surfaces suggests that the surface catalyzed precursor reaction involving transition metals is a significant source of PCDD/F emissions. It is believed that ~70% [60] of PCDD/F emissions are due to transition-metal mediated surface reactions in the post-flame, cool zone of combustors. Lomnicki and Dellinger suggested that the formation of PCDFs follows a Langmuir-Hinshelwood mechanism while the formation of PCDDs

follows a Eley-Rideal Mechanism.[61] The formation mechanisms are shown in scheme 1.2 and scheme 1.3, respectively. Nagnai further proposed an additional mechanism of PCDF formation (scheme 1.4). [38] The bidentate intermediate depicted in Scheme 1.1 could form a surface-associated phenoxyl radical through back-electron transfer, the phenoxyl radical then converts to keto mesomer, two keto mesomers then react to form DF.

As known from the previous results, PCDFs were the dominant products over iron oxide. DF's maximum output temperature was above 350 °C and 4,6-DCDF was < 350 °C; for copper oxide, PCDD and PCDF product yields are comparable, with no DF was observed. Different PDDD/F congener profiles formed on iron and copper indicated different chemisorption mechanism. For copper oxide, 2-chlorophenoxyl radial is the dominant intermediate and it proceeds to form 4,6-DCDF while for iron oxide, both 2-chlorophenoxy radial and bidentate species could form through chemisorption. Bidentate species further react to produce phenoxyl radicals that forms DF. [38]

1.5 Real Fly Ash vs. Fly Ash Surrogate

Fly ash is one of the combustion residues from MSWI. It has complex structures and variable properties. [31] After the combustion process, most metals remain in fly ash and could be transported by fly ash particles. The metals may be in the forms of oxides, chlorides, sulfates and carbonates. The amount of transported metals depends on the size, shape, density of particles and combustion conditions. The smaller particle size of fly ash having the larger mass fraction of metals. Particulates less than 10 μm in diameter can easily penetrate into the lungs, thus executing a significant toxicity to human health.[62-64] The morphology of fly ash is irregular, with both amorphous structures and polycrystalline aggregates. Generally, metals are mainly present in the forms of aerosol
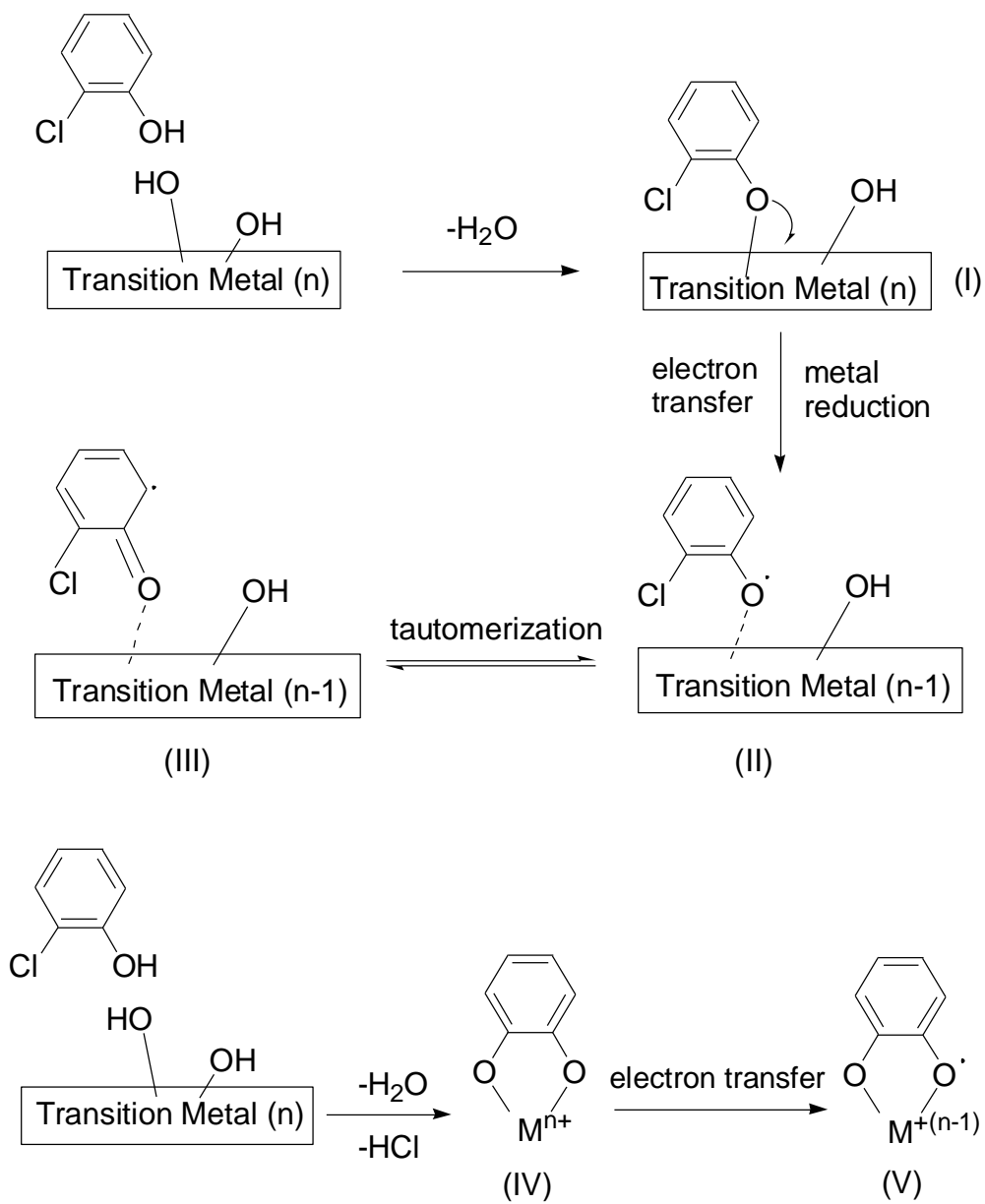
Scheme 1.1. EPFRs formation mechanism (adapted from [38])
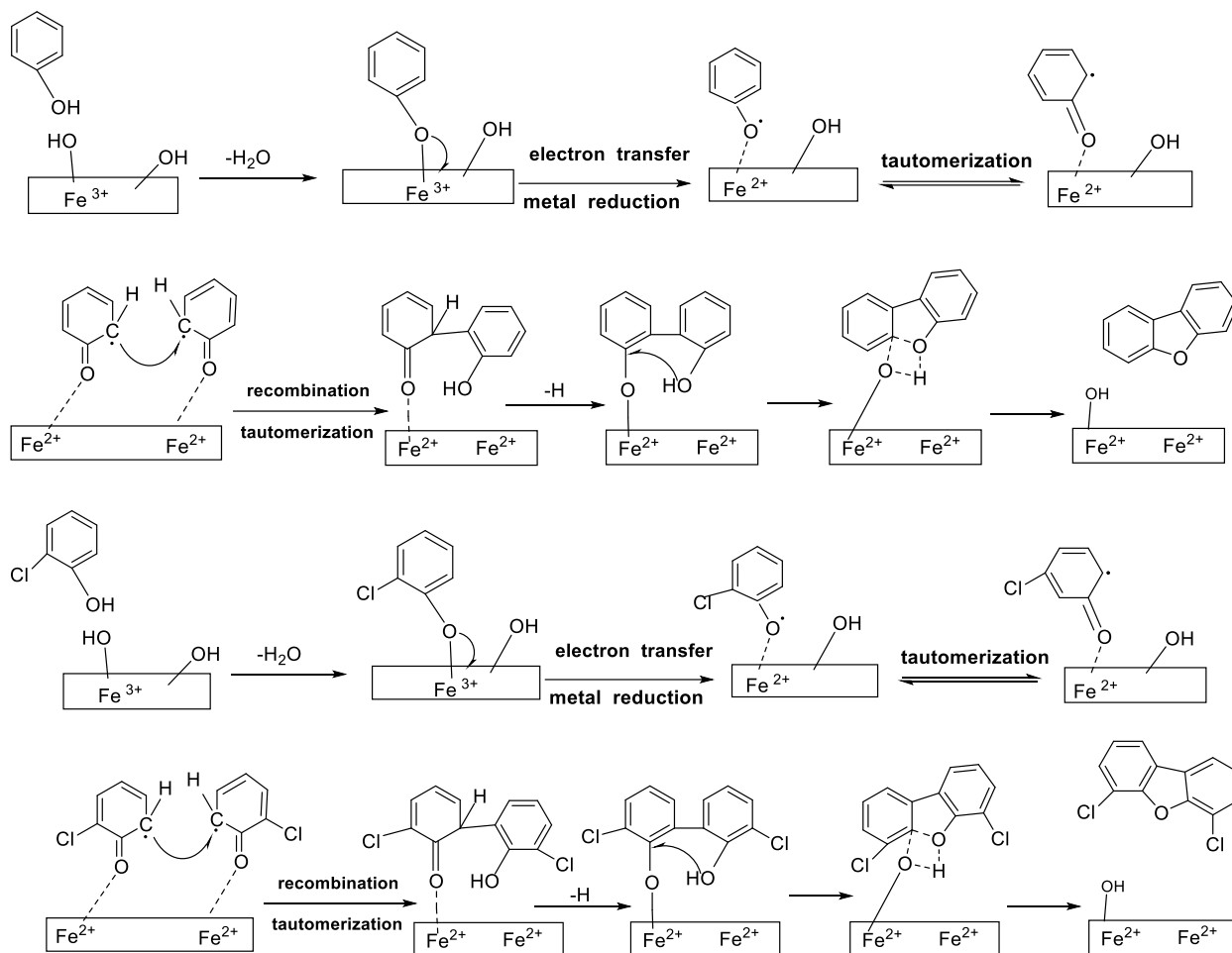
Scheme 1.2. Langmuir-Hinshelwood Mechanism for DF and DCDF Formation

14
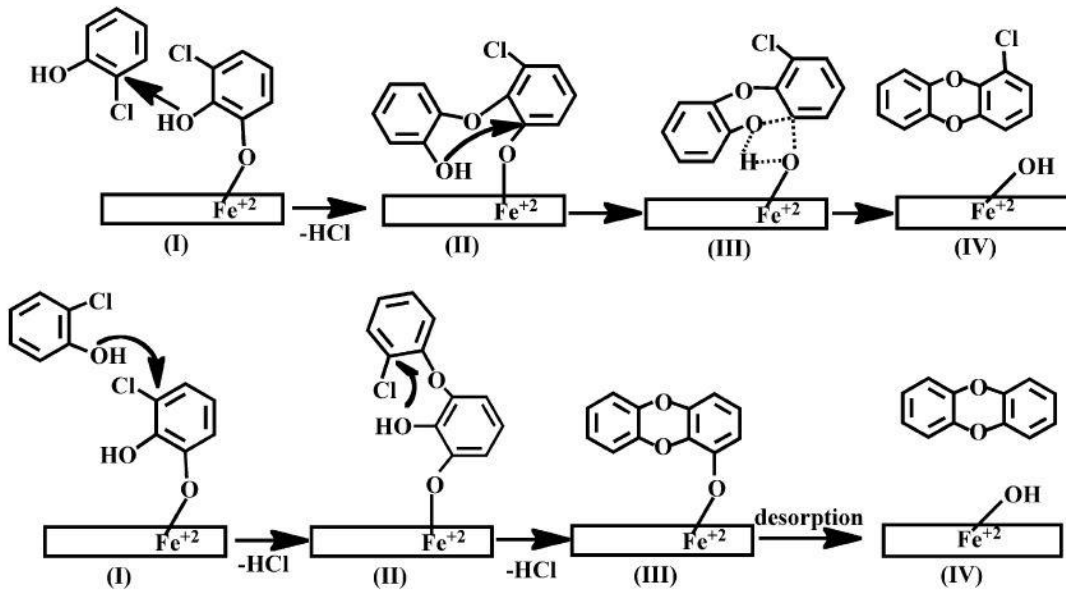
Scheme 1.3. Eley-Rideal Mechanism for DD and MCDD Formation (adapted from [58])
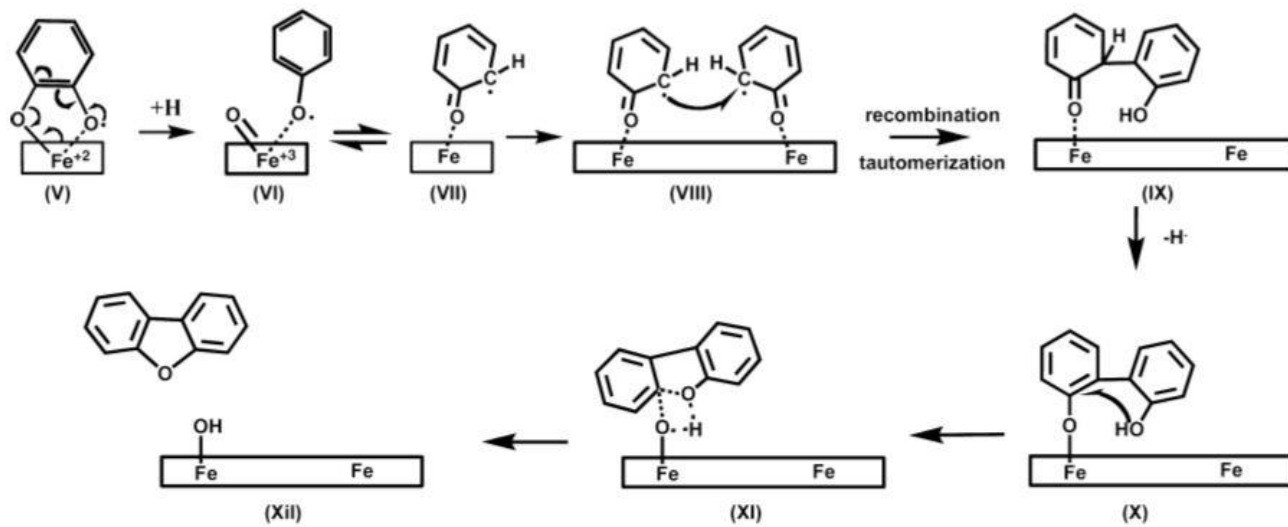
Scheme 1.4. Bidentate Intermediate Mechanism for DF Formation [38]

particulates or tiny particulates enriched on surfaces of fly ash particles. Jiang [31] collected

fly ash samples from the baghouses of six urban waste combustion facilities in China and

analyzed their basic properties. The primary metals include Zn, Pb, Cr, Cu, Fe, etc. The

content (w/w) of Fe_2O_3 is between 0.85~5.02% while that of CuO is between 0.09~0.51%.

Typical fly ashes generated from combustion contain complex components; it is

very difficult to detect the effect of a specific metal. Fly ash is collected at the end of the

combustion system after they have been exposed to multiple organics, and their activities

might be changed compared to that of fresh, in situ generated fly ash. These fly ashes

are only representative of the specific combustion facilities under the operating conditions

at the time of collection.[38]

As opposed to real fly ash, whose metal content varies significantly depending on

its source, the fly ash surrogates were appropriate tools to formulate a reaction

mechanism as synthetic model fly ash has similar characteristics to the fly ash produced

from MSWI and they are uniform in the composition and their chemical makeup is easily

reproducible, which allows an interpretation of eventual changes of fly ash state and

composition clearly and easily. Therefore, model fly ash has been a useful tool to simulate

PCDD/F formation.[65-67]

1.6 Human Exposure-Case Studies

Human exposure to dioxins and dioxin-like substances has been associated with

a range of toxic responses. Dietary intake of animal fat is the major route of exposure for

the general population. Local populations have been accidentally exposed to high dioxin

levels, e.g. in Seseo , Italy after an explosion at a chemical factory. [68]

A pilot study was conducted to evaluate the relationship between concentrations of PCDD/F in house dust and residential proximity to known sources.[69] Samples from vacuum bag dust from homes of 40 residents of Detroit, Los Angeles, Seattle, or Iowa were analyzed. Higher concentrations of certain PCDD/F in homes near cement kilns, freight routes, and major roads suggest that these outdoor sources are contributing to indoor environmental exposures.

In 2013, US Department of Agriculture published their study about the farm-raised catfish contamination by dioxin.[70] Under the Pesticide Data Program, catfish samples were collected and analyzed for 17 toxic PCDD/Fs. Comparison of the dioxin congener patterns in commercial catfish to known sources of PCDD/Fs showed strong similarities to the pattern of PCDD/Fs found in kaolin clays which have often been used as anti-caking agents in animal feeds. The study indicated mineral clays used in feeds as the potential source, which is a critical control point for PCDD/Fs entrance to the food supply.

Risk mitigation recommendations include: [71] Inventory and reduce emissions of dioxins and dioxin-like substances; Clean up and safely dispose of industrial waste containing PCDD/F; reduce contamination in food and feed and monitor PCDD/Fs in food items and human milk.

1. 7 References

1.   Tame, N. W.; Dlugogorski, B. Z.; Kennedy, E. M., PCDD/F formation in flaming combustion, smoldering, and oxidative pyrolysis of 'eco-friendly'treated wood. *Proceedings of the Combustion Institute* **2005,** *30* (1), 1237-1243.

2.   Tame, N. W.; Dlugogorski, B. Z.; Kennedy, E. M., Formation of dioxins and furans during combustion of treated wood. *Progress in Energy and Combustion Science* **2007,** *33* (4), 384-408.

3.   Shin, D.; Choi, S.; Oh, J.-E.; Chang, Y.-S., Evaluation of polychlorinated dibenzo-p-dioxin/dibenzofuran (PCDD/F) emission in municipal solid waste incinerators. *Environmental science & technology* **1999,** *33* (15), 2657-2666.

4.   Vehlow, J.; Bergfeldt, B.; Hunsinger, H., PCDD/F and related compounds in solid residues from municipal solid waste incineration-a literature review. *Waste management & research* **2006,** *24* (5), 404-420.

5.   Flesch-Janys, D.; Berger, J.; Gum, P.; Manz, A.; Nagel, S.; Waltsgott, H.; Dwyer, J. H., Exposure to polychlorinated dioxins and furans (PCDD/F) and mortality in a cohort of workers from a herbicide-producing plant in Hamburg, Federal Republic of Germany. *American journal of epidemiology* **1995,** *142* (11), 1165-1175.

6.   Birnbaum, L. S., The mechanism of dioxin toxicity: relationship to risk assessment. *Environmental health perspectives* **1994,** *102* (Suppl 9), 157.

7.   Van den Berg, M.; Birnbaum, L. S.; Denison, M.; De Vito, M.; Farland, W.; Feeley, M.; Fiedler, H.; Hakansson, H.; Hanberg, A.; Haws, L., The 2005 World Health Organization reevaluation of human and mammalian toxic equivalency factors for dioxins and dioxin-like compounds. *Toxicological sciences* **2006,** *93* (2), 223-241.

8.   U.S. EPA (Environmental Protection Agency). (2010) Recommended Toxicity Equivalence Factors (TEFs) for Human Health Risk Assessments of 2, 7,8-Tetrachlorodibenzo-p-dioxin and Dioxin-Like Compounds. **2010,** Risk Assessment Forum, Washington, DC. EPA/600/R-10/005. .

9.   Cleverly, D.; Schweer, G.; Lee, R.; McAloon, K.; Peck, C.; Randall, M.; Riley, K., An inventory of Sources and Environmental Releases of Dioxin-like Compounds in the United States for the Years 1987, 1995, and 2000. *US EPA, Washington DC* **2006**.

10.   Stanmore, B., The formation of dioxins in combustion systems. *Combustion and flame* **2004,** *136* (3), 398-427.

11.   Zhang, M.; Buekens, A.; Li, X., Dioxins from biomass combustion: an overview. *Waste and Biomass Valorization* **2017,** *8* (1), 1-20.

12.   Gullett, B. K.; Touati, A.; Huwe, J.; Hakk, H., PCDD and PCDF emissions from simulated sugarcane field burning. *Environmental science & technology* **2006,** *40* (20), 6228-6234.

13.   Thacker, N.; Sheikh, J.; Tamane, S.; Bhanarkar, A.; Majumdar, D.; Singh, K.; Chavhan, C.; Trivedi, J., Emissions of polychlorinated dibenzo-p-dioxins (PCDDs), dibenzofurans (PCDFs), and dioxin-like polychlorinated biphenyls (PCBs) to air from waste incinerators and high thermal processes in India. *Environmental monitoring and assessment* **2013,** *185* (1), 425-429.

14.   Cieplik, M. K.; De Jong, V.; Bozovič, J.; Liljelind, P.; Marklund, S.; Louw, R., Formation of dioxins from combustion micropollutants over MSWI fly ash. *Environmental science & technology* **2006,** *40* (4), 1263-1269.

15.   Ni, Y.; Zhang, H.; Fan, S.; Zhang, X.; Zhang, Q.; Chen, J., Emissions of PCDD/Fs from municipal solid waste incinerators in China. *Chemosphere* **2009,** *75* (9), 1153-1158.

16.   McKay, G., Dioxin characterisation, formation and minimisation during municipal solid waste (MSW) incineration. *Chemical Engineering Journal* **2002,** *86* (3), 343-368.

17.   Düwel, U.; Nottrodt, A.; Ballschmiter, K., Simultaneous sampling of PCDD/PCDF inside the combustion chamber and on four boiler levels of a waste incineration plant. *Chemosphere* **1990,** *20* (10-12), 1839-1846.

18.   Yang, L.; Liu, G.; Zheng, M.; Jin, R.; Zhu, Q.; Zhao, Y.; Zhang, X.; Xu, Y., Atmospheric occurrence and health risks of PCDD/Fs, polychlorinated biphenyls, and polychlorinated naphthalenes by air inhalation in metallurgical plants. *Science of the Total Environment* **2017,** *580,* 1146-1154.

19.   Lechtanska, P.; Wielgosinski, G.; Grochowalski, A.; Holtzer, M.; Cwiakalski, W., Dioxin emission from some metallurgical processes. *International Journal of Environment and Pollution* **2017,** *61* (3-4), 261-277.

20.   Sanchez-Hervas, J.; Armesto, L.; Ruiz-Martinez, E.; Otero-Ruiz, J.; Pandelova, M.; Schramm, K., PCDD/PCDF emissions from co-combustion of coal and PVC in a bubbling fluidised bed boiler. *Fuel* **2005,** *84* (17), 2149-2157.

21.   Marklund, S.; Andersson, R.; Tysklind, M.; Rappe, C.; Egebäck, K.-E.; Björkman, E.; Grigoriadis, V., Emissions of PCDDs and PCDFs in gasoline and diesel fueled cars. *Chemosphere* **1990,** *20* (5), 553-561.

22.   Clement, R.; Tashiro, C.; Suter, S.; Reiner, E.; Hollinger, D., Chlorinated dibenzo-p-dioxins (CDDs) and dibenzofurans (CDFs) in effluents and sludges from pulp and paper mills. *Chemosphere* **1989,** *18* (1-6), 1189-1197.

23.   Kuehl, D. W.; Butterworth, B. C.; Devita, W. M.; Sauer, C. P., Environmental contamination by polychlorinated dibenzo-p-dioxins and dibenzofurans associated with pulp and paper mill discharge. *Biological Mass Spectrometry* **1987,** *14* (8), 443-447.

24.   Prange, J. A.; Gaus, C.; Weber, R.; Päpke, O.; Müller, J. F., Assessing forest fire as a potential PCDD/F source in Queensland, Australia. *Environmental science & technology* **2003,** *37* (19), 4325-4329.

25.   Holt, E.; Weber, R.; Stevenson, G.; Gaus, C., Polychlorinated dibenzo-p-dioxins and dibenzofurans (PCDD/Fs) impurities in pesticides: a neglected source of contemporary relevance. *Environmental science & technology* **2010,** *44* (14), 5409-5415.

26.   US Environmental Protection Agency. Environmental Laws that Apply to Dioxin, https://www.epa.gov/dioxin/learn-about-dioxin#tab-2.

27.   Nie, Z.; Yue, B.; Wang, Q.; Huang, Q., Perspective on China's Dioxin Reduction Goal. *Water, Air, & Soil Pollution* **2014,** *225* (4), 1917.

28.   Zhao, B.; Zheng, M.; Jiang, G., Dioxin emissions and human exposure in China: a brief history of policy and research. *Environmental health perspectives* **2011,** *119* (3), A112.

29.   Communication from the commission to the concil, the European Parliament, the European Economic and Social Committee, On the implementation of the Community Strategy for dioxins, furans, and polychlorinated biphenyls (COM(2001)593) – Third progress report, **2010,** http://eur-lex.europa.eu/legal-content/EN/TXT/?uri=CELEX:52010DC0562.

30.   Yao, J.; Li, W.; Xia, F.; Zheng, Y.; Fang, C.; Shen, D., Heavy metals and PCDD/Fs in solid waste incinerator fly ash in Zhejiang province, China: chemical and bio-analytical characterization. *Environmental Monitoring and assessment* **2012,** *184* (6), 3711-3720.

31.   Jiang, J.-g.; Xin, X.; Jun, W.; Yang, S.-j.; Zhang, Y., Investigation of basic properties of fly ash from urban waste incinerators in China. *Journal of Environmental Sciences* **2007,** *19* (4), 458-463.

32.   Kakuta, Y.; Matsuto, T.; Tanaka, N.; Masuda, T., Influence of residual carbon on the decomposition process of PCDD/Fs in MSWI fly ash. *Chemosphere* **2005,** *58* (7), 969-975.

33.   Xiong, Y.; Zhu, F.; Zhao, L.; Jiang, H.; Zhang, Z., Heavy metal speciation in various types of fly ash from municipal solid waste incinerator. *Journal of Material Cycles and Waste Management* **2014,** *16* (4), 608-615.

34.   Altarawneh, M.; Dlugogorski, B. Z.; Kennedy, E. M.; Mackie, J. C., Mechanisms for formation, chlorination, dechlorination and destruction of polychlorinated dibenzo-p-dioxins and dibenzofurans (PCDD/Fs). *Progress in energy and combustion science* **2009,** *35* (3), 245-274.

35.   Lustenhouwer, J. W.; Olie, K.; Hutzinger, O., Chlorinated dibenzo-p-dioxins and related compounds in incinerator effluents: a review of measurements and mechanisms of formation. *Chemosphere* **1980,** *9* (7-8), 501-522.

36.   Addink, R.; Olie, K., Mechanisms of formation and destruction of polychlorinated dibenzo-p-dioxins and dibenzofurans in heterogeneous systems. *Environmental science & technology* **1995,** *29* (6), 1425-1435.

37.   Ismo, H.; Kari, T.; Juhani, R., Formation of aromatic chlorinated compounds catalyzed by copper and iron. *Chemosphere* **1997,** *34* (12), 2649-2662.

38.   Nganai, S.; Lomnicki, S.; Dellinger, B., Ferric oxide mediated formation of PCDD/Fs from 2-monochlorophenol. *Environmental science & technology* **2008,** *43* (2), 368-373.

39.   Lomnicki, S.; Dellinger, B., A detailed mechanism of the surface-mediated formation of PCDD/F from the oxidation of 2-chlorophenol on a CuO/silica surface. *The Journal of Physical Chemistry A* **2003,** *107* (22), 4387-4395.

40.   Zhang, Y.; Zhang, D.; Gao, J.; Zhan, J.; Liu, C., New understanding of the formation of PCDD/Fs from chlorophenol precursors: a mechanistic and kinetic study. *The Journal of Physical Chemistry A* **2014,** *118* (2), 449-456.

41.   Ryu, J.-Y.; Mulholland, J. A.; Kim, D. H.; Takeuchi, M., Homologue and isomer patterns of polychlorinated dibenzo-p-dioxins and dibenzofurans from phenol precursors: Comparison with municipal waste incinerator data. *Environmental science & technology* **2005,** *39* (12), 4398-4406.

42.   Briois, C.; Ryan, S.; Tabor, D.; Touati, A.; Gullett, B. K., Formation of polychlorinated dibenzo-p-dioxins and dibenzofurans from a mixture of chlorophenols over fly ash: influence of water vapor. *Environmental science & technology* **2007,** *41* (3), 850-856.

43.   Zhang, Q.; Li, S.; Qu, X.; Shi, X.; Wang, W., A quantum mechanical study on the formation of PCDD/Fs from 2-chlorophenol as precursor. *Environmental science & technology* **2008,** *42* (19), 7301-7308.

44.   De Jong, V.; Cieplik, M. K.; Louw, R., Formation of dioxins in the catalytic combustion of chlorobenzene and a micropollutant-like mixture on Pt/γ-Al$_2$O$_3$. *Environmental science & technology* **2004,** *38* (19), 5217-5223.

45.   Nestrick, T.; Lamparski, L.; Crummett, W., Thermolytic surface-reaction of benzene and iron (III) chloride to form chlorinated dibenzo-p-dioxins and dibenzofurans. *Chemosphere* **1987,** *16* (4), 777-790.

46.   Ballschmiter, K.; Braunmiller, I.; Niemczyk, R.; Swerev, M., Reaction pathways for the formation of polychloro-dibenzodioxins (PCDD) and -dibenzofurans (PCDF) in combustion processes: II. Chlorobenzenes and chlorophenols as precursors in the formation of polychloro-dibenzodioxins and -dibenzofurans in flame chemistry. *Chemosphere* **1988,** *17* (5), 995-1005.

47.   Vogg, H.; Stieglitz, L., Thermal behavior of PCDD/PCDF in fly ash from municipal incinerators. *Chemosphere* **1986,** *15* (9-12), 1373-1378.

48.   Milligan, M. S.; Altwicker, E., The relationship between de novo synthesis of polychlorinated dibenzo-p-dioxins and dibenzofurans and low-temperature carbon gasification in fly ash. *Environmental science & technology* **1993,** *27* (8), 1595-1601.

49.   Huang, H.; Buekens, A., Chemical kinetic modeling of de novo synthesis of PCDD/F in municipal waste incinerators. *Chemosphere* **2001,** *44* (6), 1505-1510.

50.   Zhang, M.; Yang, J.; Buekens, A.; Olie, K.; Li, X., PCDD/F catalysis by metal chlorides and oxides. *Chemosphere* **2016,** *159*, 536-544.

51.   Chin, Y.-T.; Lin, C.; Chang-Chien, G.-P.; Wang, Y.-M., PCDD/F formation catalyzed by the metal chlorides and chlorinated aromatic compounds in fly ash. *Aerosol Air Qual. Res* **2012,** *12* (2), 228-236.

52.   Lomnicki, S.; Dellinger, B., Development of supported iron oxide catalyst for destruction of PCDD/F. *Environmental science & technology* **2003,** *37* (18), 4254-4260.

53.   Wang, H. C.; Chang, S. H.; Hung, P. C.; Hwang, J. F.; Chang, M. B., Catalytic oxidation of gaseous PCDD/Fs with ozone over iron oxide catalysts. *Chemosphere* **2008,** *71* (2), 388-397.

54.   Zhang, M.; Buekens, A.; Ma, S.; Li, X., Iron chloride catalysed PCDD/F-formation: Experiments and PCDD/F-signatures. *Chemosphere* **2018,** *191*, 72-80.

55.   Heeb, N. V.; Zennegg, M.; Haag, R.; Wichser, A.; Schmid, P.; Seiler, C.; Ulrich, A.; Honegger, P.; Zeyer, K.; Emmenegger, L., PCDD/F formation in an iron/potassium-catalyzed diesel particle filter. *Environmental science & technology* **2013,** *47* (12), 6510-6517.

56.   Ryan, S. P.; Altwicker, E. R., Understanding the role of iron chlorides in the de novo synthesis of polychlorinated dibenzo-p-dioxins/dibenzofurans. *Environmental science & technology* **2004,** *38* (6), 1708-1717.

57.   Ryan, S. P.; Altwicker, E. R., The formation of polychlorinated dibenzo-p-dioxins/dibenzofurans from carbon model mixtures containing ferrous chloride. *Chemosphere* **2000,** *40* (9-11), 1009-1014.

58.   Nganai, S.; Lomnicki, S.; Dellinger, B., Formation of PCDD/Fs from oxidation of 2-monochlorophenol over an Fe2O3/silica surface. *Chemosphere* **2012,** *88* (3), 371-376.

59.   Sun, Q.; Altarawneh, M.; Dlugogorski, B. Z.; Kennedy, E. M.; Mackie, J. C., Catalytic effect of CuO and other transition metal oxides in formation of dioxins: theoretical investigation of reaction between 2, 4, 5-trichlorophenol and CuO. *Environmental science & technology* **2007,** *41* (16), 5708-5715.

60.   Altwicker, E. R., Some laboratory experimental designs for obtaining dynamic property data on dioxins. *Science of the total environment* **1991,** *104* (1-2), 47-72.

61.   Lomnicki, S.; Dellinger, B., Formation of PCDD/F from the pyrolysis of 2-chlorophenol on the surface of dispersed copper oxide particles. *Proceedings of the Combustion Institute* **2002,** *29* (2), 2463-2468.

62.   Pope 3rd, C., Epidemiology of fine particulate air pollution and human health: biologic mechanisms and who's at risk? *Environmental health perspectives* **2000,** *108* (Suppl 4), 713.

63.   Diabate, S.; Muelhopt, S.; Paur, H.-R.; Krug, H. F., The response of a co-culture lung model to fine and ultrafine particles of incinerator fly ash at the air-liquid interface. *Alternatives to laboratory animals: ATLA* **2008,** *36* (3), 285-298.

64.   Borm, P. J., Toxicity and occupational health hazards of coal fly ash (CFA). A review of data and comparison to coal mine dust. *The Annals of occupational hygiene* **1997,** *41* (6), 659-676.

65.   Mubeen, I.; Buekens, A.; Chen, Z.; Lu, S.; Yan, J., De novo formation of dioxins from milled model fly ash. *Environmental Science and Pollution Research* **2017,** *24* (23), 19031-19043.

66.   Wilhelm, J.; Stieglitz, L.; Dinjus, E.; Will, R., Mechanistic studies on the role of PAHs and related compounds in PCDD/F formation on model fly ashes. *Chemosphere* **2001,** *42* (5-7), 797-802.

67.   Hell, K.; Stieglitz, L.; Altwicker, E.; Addink, R.; Will, R., Reactions of 2, 4, 6-trichlorophenol on model fly ash: oxidation to CO and CO2, condensation to PCDD/F and conversion into related compounds. *Chemosphere* **2001,** *42* (5-7), 697-702.

68.   Bertazzi, P. A.; Bernucci, I.; Brambilla, G.; Consonni, D.; Pesatori, A. C., The Seveso studies on early and long-term effects of dioxin exposure: a review. *Environmental Health Perspectives* **1998,** *106* (Suppl 2), 625.

69.   Deziel, N.; Nuckols, J.; Colt, J.; De Roos, A.; Pronk, A.; Gourley, C.; Severson, R.; Cozen, W.; Cerhan, J. R.; Hartge, P., Determinants of polychlorinated dibenzo-p-dioxins and polychlorinated dibenzofurans in house dust samples from four areas of the United States. *Science of the Total Environment* **2012,** *433*, 516-522.

70.   Huwe, J.; Archer, J., Dioxin congener patterns in commercial catfish from the United States and the indication of mineral clays as the potential source. *Food Additives & Contaminants: Part A* **2013,** *30* (2), 331-338.

71.   Organization, W. H., Exposure to dioxins and dioxin-like substances: a major public health concern. *Geneve: WHO* **2010**.

CHAPTER 2 RESEARCH HYPOTHESES AND OBJECTIVES

2.1 Research Hypotheses

Although metal-mediated PCDD/F formation has been studied extensively, [1-4] most of the studies were focused on the effect of single metal chloride or oxide. In the MSWI, fly ash is a complex mixture of components whose concentration can vary widely based on incinerator feedstock. How those components react to each other in terms of PCDD/Fs formation? Some synergistic or inhibitive effect might exist. How does the change of the metal content affect the PCDD/F output? Those questions need to be addressed. Iron and copper are the most commonly transition metals in combustion systems, thus it is important to understand their cooperative effect in terms of PCDD/F formation. The synergy effect between iron and copper has been applied into many fields. A novel nanostructured Fe-Cu binary oxide was synthesized for efficiently removing arsenic from water. [5] Schuchardt's study showed copper oxide exhibits a synergistic effect on iron oxide supported silica for the oxidation of cyclohexane at room temperature. [6] Yang investigated the synergy between iron ore and copper ore as oxygen carriers in chemical-looping combustion and the mixture of iron ore and copper ore are expected to address simultaneously reactivity, recyclability, cost and environmental concerns of oxygen carriers. [7] Rossi prepared iron-copper composite catalysts to study the efficiecy in the Fenton Heterogeneous Process regarding organic charge removal and biodegradability enhancement. [8] For PCDD/F formation, Liao used different mixture of $CuCl_2$ and Fe_2O_3 for de novo synthesis of PCDD/F but no synegistic effects were observed. [9]

Iron oxide, which is redox-active, is almost always at the highest concentration of all transition metals in combustion systems. It could mediate or catalyze the formation of PCDD/Fs. However, the relationship between iron content in the fly ash and the yield of PCDD/Fs is not clear. Is it possible that different content of iron oxide form various nanoclusters on the surface of silica, which will affect the formation of the EPRFs, thus the yield of dioxins? At present, there is hardly a quantitative link between fly ash physical properties/chemical reactivity and PCDD/F yield.

My research hypotheses are (1) In the fly ash, synergy between iron and copper affects the formation, yield and emission of PCDD/Fs; (2) The concentration of iron in fly ash and, even the morphology and size of the iron oxide clusters affect PCDD/Fs formation and yield.

2.2 Research Objectives

With this research the detailed insight into the following mechanistic questions will be obtained: (1) Does a cooperative effect between Fe_2O_3 and CuO exist and contribute to the PCDD/F yields? (2) How is the metal state change before and after reaction? (3) Which intermediates play a key part in the PCDD/F formation? (4) How could the metal content and morphology affect PCDD/F yield?

The research objectives are to understand which components of a multiple-catalyst system contribute to PCDD/F congener profile formation and which contribute to yield. Knowing the roles of each metal will lead to better models for PCDD/F formation prediction. In addition, to understand the relationship between the content of Fe_2O_3 in the fly ash and total yield of PCDD/Fs.

2.3 References

1.   Ryu, J.-Y.; Mulholland, J. A., Metal-mediated chlorinated dibenzo-p-dioxin (CDD) and dibenzofuran (CDF) formation from phenols. *Chemosphere* **2005,** *58* (7), 977-988.

2.   Öberg, T.; Bergbäck, B.; Filipsson, M., Catalytic effects by metal oxides on the formation and degradation of chlorinated aromatic compounds in fly ash. *Chemosphere* **2008,** *71* (6), 1135-1143.

3.   Chin, Y.-T.; Lin, C.; Chang-Chien, G.-P.; Wang, Y.-M., PCDD/F formation catalyzed by the metal chlorides and chlorinated aromatic compounds in fly ash. *Aerosol Air Qual. Res* **2012,** *12* (2), 228-236.

4.   Kiruri, L. W.; Khachatryan, L.; Dellinger, B.; Lomnicki, S., Effect of copper oxide concentration on the formation and persistency of environmentally persistent free radicals (EPFRs) in particulates. *Environmental science & technology* **2014,** *48* (4), 2212-2217.

5.   Zhang, G.; Ren, Z.; Zhang, X.; Chen, J., Nanostructured iron (III)-copper (II) binary oxide: a novel adsorbent for enhanced arsenic removal from aqueous solutions. *Water research* **2013,** *47* (12), 4022-4031.

6.   Schuchardt, U.; Pereira, R.; Krähembühl, C. E.; Rufo, M.; Buffon, R., Synergistic effect of iron and copper oxides supported on silica in the room temperature oxidation of cyclohexane. *Applied Catalysis A: General* **1995,** *131* (1), 135-141.

7.   Yang, W.; Zhao, H.; Wang, K.; Zheng, C., Synergistic effects of mixtures of iron ores and copper ores as oxygen carriers in chemical-looping combustion. *Proceedings of the Combustion Institute* **2015,** *35* (3), 2811-2818.

8.   Rossi, A. F.; Martins, R. C.; Quinta-Ferreira, R. M., Composition effect of iron–copper composite catalysts in the Fenton heterogeneous process efficiency and cooxidation synergy assessment. *Industrial & Engineering Chemistry Research* **2014,** *53* (40), 15369-15373.

9.   Liao, J.; Buekens, A.; Olie, K.; Yang, J.; Chen, T.; Li, X., Iron and copper catalysis of PCDD/F formation. *Environmental Science and Pollution Research* **2016,** *23* (3), 2415-2425.

CHAPTER 3 EXPERIMENTAL

3.1 Fly Ash Surrogate Synthesis

The incipient wetness method was used to prepare the mixed oxide fly ash surrogates. An aqueous solution of copper (II) nitrate and iron (III) nitrate was introduced into silica gel powder (Aldrich, grade 923, 100−200 mesh size) in the appropriate amount for incipient wetness to occur. Various ratios of Fe^{3+}/Cu^{2+} were used to produce 1% Fe_2O_3/4% CuO, 2.5% Fe_2O_3/2.5% CuO and 4% Fe_2O_3/1% CuO on silica (by weight). The samples were rotated on Rotavap for 24 h at room temperature, dried 12 h at 120°C, and calcined in air for 7 h at 450°C. Figure 3.1 depicts the procedure.

The same procedure was applied for the synthesis of 1 %, 2.5 %, 4% and 5 % Fe_2O_3 fly ash surrogates, respectively by introducing appropriate amount of iron (III) nitrate aqueous solution into silica gel powder. After rotatory evaporation and calcination, Fe_2O_3 model fly ashes with different iron content were obtained. Table 3.1 lists the composition of fly ash surrogate samples.
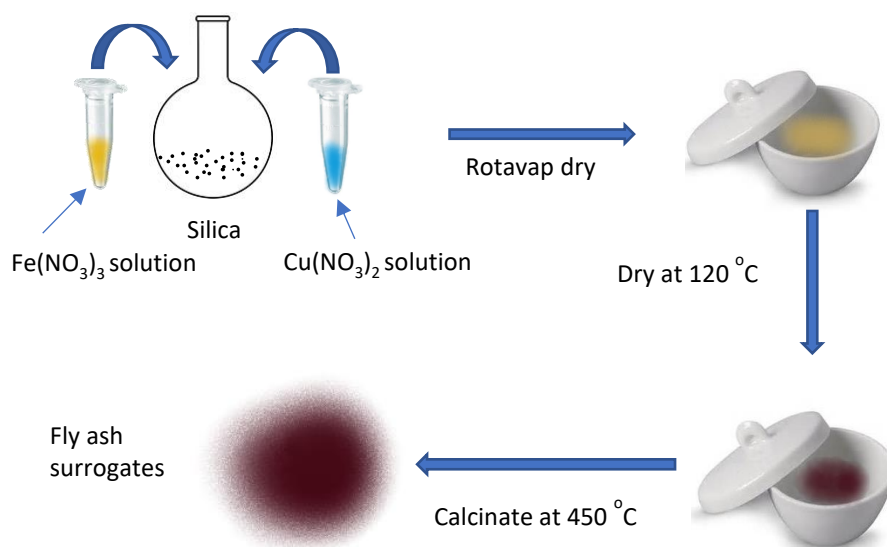
Figure 3.1. Incipient Wetness Synthesis of Fly Ash Surrogates

Table 3.1. Synthesized and Studied Fly Ash Surrogate Samples							
Samples	% w/w				Ratio		
	Fe_2O_3	CuO	Fe	Cu	Fe_2O_3: CuO (% w/w)	Fe: Cu (% w/w)	Fe: Cu (mole ratio)
Fe_2O_3-CuO/SiO$_2$	1 2.5 4	4 2.5 1	0.7 1.75 2.8	3.2 2 0.8	0.25 1 4	0.22 0.88 3.5	0.25 1 4
Fe_2O_3/SiO$_2$* CuO/SiO$_2$*	5 0	0 5	3.5 -	- 4			
	Fe_2O_3		Fe				
Fe_2O_3/ SiO$_2$	1 2.5 4		0.7 1.75 2.8		–		
Fe_2O_3/SiO$_2$*	5		3.5				
*: Reference samples studied before and used for comparison							

3.2 System for Thermal Diagnostic Studies

The thermal degradation of organic materials is a complex process as temperature, carrier gas, and catalyst are all involved in the process and affect the organic material's degradation behavior. [1] Conducting the extensive range of thermal diagnostic studies requires flexible experimentation and instrumentation. Rubey and Grant [2] described the detailed design aspects of the system for thermal diagnostic studies (STDS) to flexibility and versatility for conducting a broad range of thermal related studies in 1988. Since then, STDS has been widely applied for investigating the degradation behavior and decomposition products of organic materials in thermal and combustion processes. [3-4]

Our customized STDS [5] consists of four basic components to operate as an integrated functional system: a thermal couple console, two GC ovens and a Mass Spec detector. The diagram for STDS is shown in Figure 3.2.
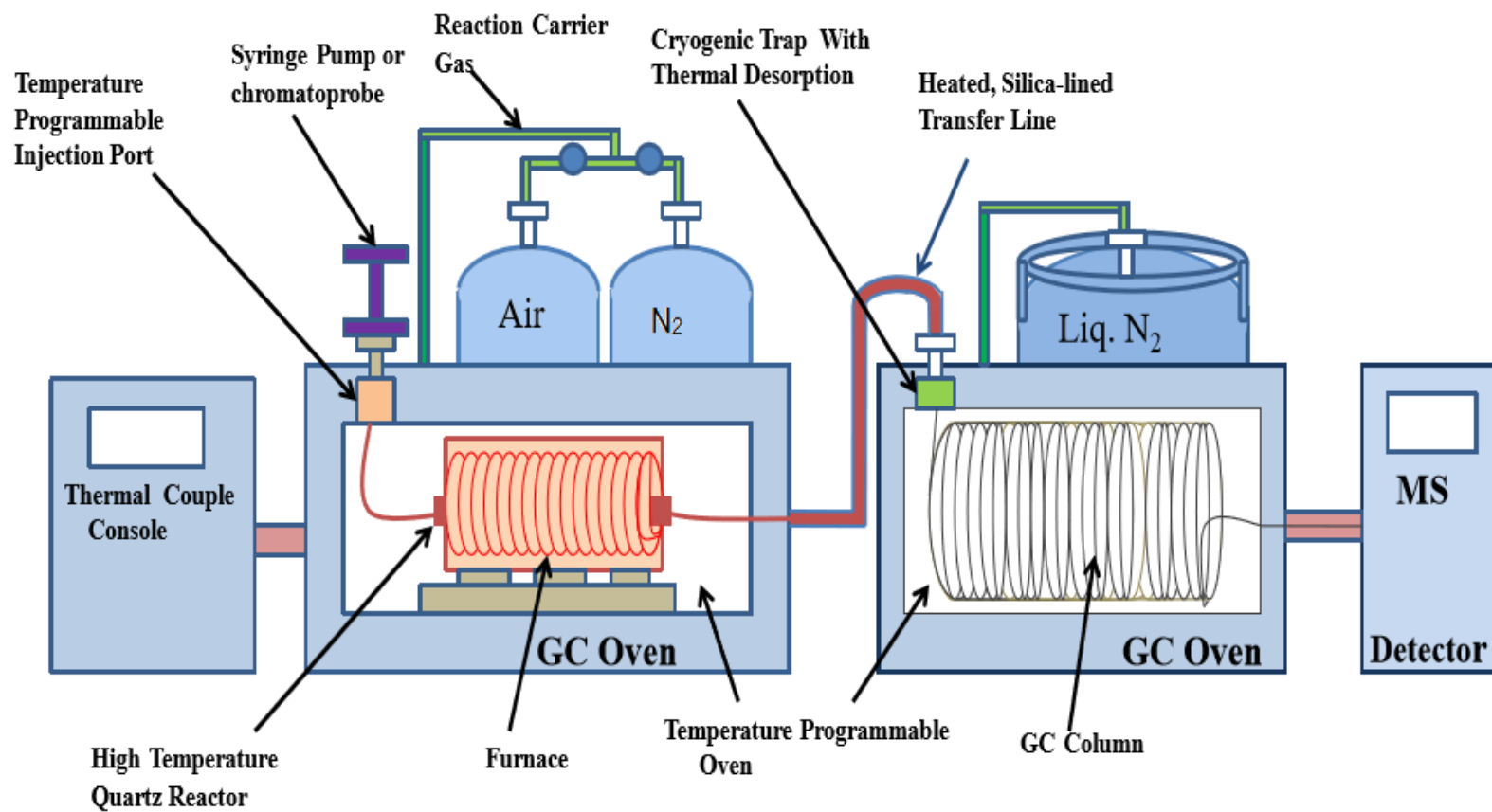
Figure 3.2. System for Thermal Diagnostic Studies (adapted from [5])

3.3 PCDD/F Formation Studies

The STDS was used to investigate the surface-mediated reactions of 2-monochlorophenol (2-MCP), which is a known PCDD/F precursor, over a Fe_2O_3/CuO/Silica or Fe_2O_3/Silica surface. Briefly, a thermal reactor (4.0 mm i.d. fused silica reactor) is set in a high-temperature furnace housed within an isothermal oven that facilitates precise temperature control over all transfer lines to and from the reactor (180 ^{o}C). A GC-MS system was interfaced in-line with a thermal reactor for analysis of combustion products.

A small amount of catalyst (40 mg) was placed between quartz wool plugs in the thermal reactor. To avoid condensation of the reaction products, all transfer lines were maintained at a constant temperature of 180 °C. Prior to each experiment, the catalyst was oxidized in situ at 450 °C for 1 h under an air flow of 5 cc/min to oxidize the surface of the fly ash surrogate. 2-MCP (Aldrich) was introduced into the flow stream by a digital syringe pump (KD Scientific, model-100) through a GC injection port maintained at 185 °C. Two carrier gases were used: air (~21% O_2) for oxidation experiments and pure nitrogen for pyrolytic experiments. The rate of injection was set to maintain a constant gas phase concentration of 50 ppm of 2-MCP with a residence time of 0. 2 s. Reaction temperatures range from 200 to 550 °C. In between runs the transfer lines were baked out at 210 ^{o}C in air flow and blank run was performed to check for trace residue of products.

The products from the reaction were analyzed using an in-line Varian CP-3800 GC system. A 30 m, 0.25 mm i.d., 0.25 μm film thickness column was used (HP-5MS) for product separation. The temperature was held at -60 °C for the reaction period followed

by a ramp from -60 to 300 at a rate of 10 °C min^{-1}. Detection and quantification of the

products were obtained on a Varian Saturn 2000 mass spectrometer, which was operated

in full-scan mode from 15 to 450 amu for the duration of the GC run. Identification of the

eluting compounds was done based on the mass spectrum of the eluent and the retention

time comparison to a standard. The amount of the formed products was calculated based

on the calibration curves using respective standard solutions. The following standards

were used for the calibration of PCDD/F products based on the peak area in the

chromatogram: dibenzofuran   (DF),   2-chlorodibenzo-*p*-dioxin   (MCDD),   4-

chlorodibenzofuran (MCDF), 2,7-/2,8-dichlorodibenzo-*p*-dioxin (DCDD). For the selected

PCDD/F compounds, calibration was based on the MS response to the similar

compounds: The calibration curve for DCDD was used to calculate DCDF,

trichlorodibenzo-*p*-dioxin (TriCDD) and tetrachlorodibenzo-p-dioxin (TetraCDD). The

yields of the products were calculated by use of the expression:

$$Y = \frac{[PROD] \times A}{[2-MCP]_0} \times 100\% \quad [1]$$

where [PROD] is the concentration of specific product formed (in moles), $[2\text{-}MCP]_0$ is the

initial concentration of 2-MCP (in moles), and A is the molar stoichiometric factor.

Quantitative standards were used to calibrate the MS response for all products. Total

yield of the PCDD/F for each temperature is defined as:

$$Y_T = \sum Y_{PROD} \quad [2]$$

where PROD is: DD, DF, MCDD, DCDD, DCDF, TriCDD and TetraCDD. PCDD/F ratio

was calculated based on the average integrated yields of PCDD and PCDF (average of

the total PCDD or PCDF yields within the entire temperature range 200-550 °C). All

experimental data represent an average of triplicate or more runs. Between each experiment a reactant/product transport analysis was performed.

3.4 EPFRs Formation and Analysis

A custom-made vacuum exposure system was built to perform the EPFRs formation experiment. [6] The diagram of the system is shown in Figure 2.3. It includes a vacuum pump, a pressure gauge, a vacuum exposure chamber, a high temperature ceramic heater, a dosing pot and two EPR-extraction cells.

The vacuum pump can evacuate to lower pressure down to 10^{-2} torr to ensure the appropriate vacuum for the formation and stabilization of the EPFRs. A digital pressure gauge (Varian, eyesys convector, model L973633200220) is used to monitor the pressure of the whole system. The dosing pot was attached to the vacuum exposure chamber, within which is the chemical to be dosed. The EPR-extraction cells can be easily detached from the dosing exposure chamber after dosing. The vacuum exposure glass chamber is covered with heating ropes (Omegalux®, model FGR) that connected to a variable AC temperature controller (Electrothermal, model MC240X1) that control the temperature of the whole chamber to about 80 $^{\circ}$C. Above the heating ropes, the vacuum exposure glass chamber is covered with aluminum foil to prevent the organic precursor from condensing. A liquid nitrogen thermos is placed in-between the vacuum pumps and the vacuum exposure chamber to trap excess physisorbed species so as to prevent excess physisorbed species from reaching the vacuum pumps.

EPFR formation was studied by exposing both $CuO/Fe_2O_3/SiO_2$ and Fe_2O_3/SiO_2 particles to 2-MCP precursor vapors, respectively. Before 2-MCP's exposure, the particles were heated in situ at 450 °C for 1 h to remove organics on the surface. After

that, these particles were exposed to the 2-MCP vapors at 230 °C in the customized vacuum exposure chamber for 6 min under vapor.

After exposure, samples stayed under vacuum for 1 h to remove excess non-chemisorbed adsorbate at 10^{-2} Torr. Still under vacuum conditions, the dosed particles
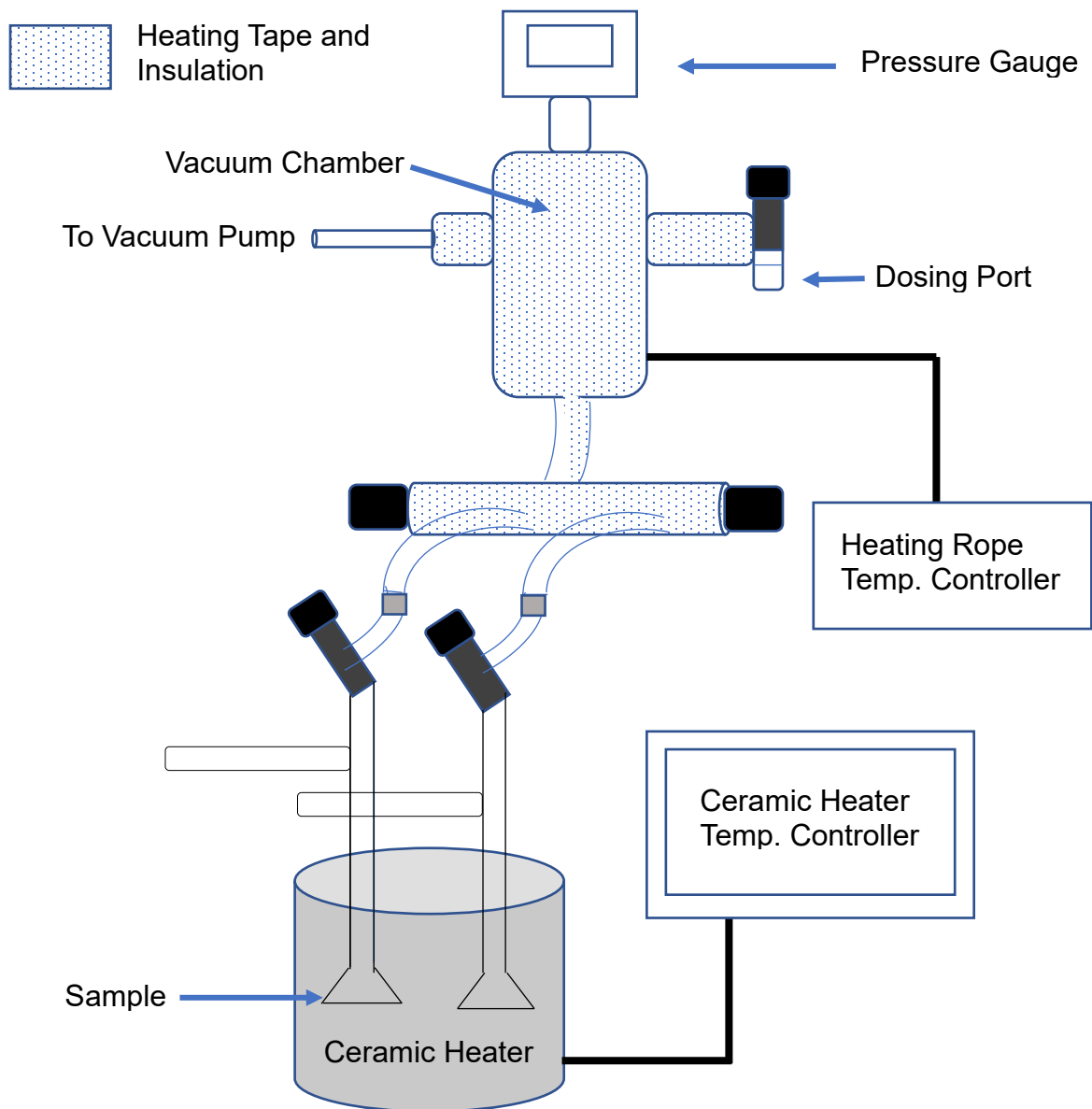
Figure 3.3. Diagram of Dosing System for EPFRs Formation (adapted from [6])

were cooled to room temperature before EPR spectra were recorded. EPR spectra were recorded in a Suprasil EPR tube at room temperature using a computer-controlled Bruker EMX 10/2.7 EPR spectrometer. Instrument parameters were as follows: center field, 3470 G; sweep width, 100 G; microwave frequency, 9.7 GHz; microwave power, 2.0 mW; modulation frequency, 4.0 G; modulation amplitude, 4.0 G; receiver gain, 3.54×10^4; time constant, 41.0 ms; and three scans. Radical concentration was calculated using the 2,2-diphenyl-1-picrylhydrazyl (DPPH) standard due to the similarity between the spectral profiles of DPPH and the radicals formed on $CuO/Fe_2O_3/Silica$ and $Fe_2O_3/Silica$.

3.5 Characterization of Fly Ash Surrogate

3.5.1 XPS analysis

To evaluate the oxidation state and coordination of the active metal centers of surrogate samples, X-ray Photoelectron Spectroscopy (XPS) measurements were carried out using a Kratos Axis-165 Auger/XPS system. A survey scan and high-resolution individual elemental scans were performed on the surrogate surface of each mixed oxide catalyst with the mono Al x-ray source at a beam current of 15 mA and anode high tension of 15KV.

All survey scans were performed at binding energy range of 0-1200 eV with pass energy of 160 eV; High-resolution scans of all the elements were performed with pass energy of 40 eV. Composition quantification results were based on the high-resolution elemental scans before and after PCDD/F formation reactions.

All spectra were fit using X-ray Photoelectron Spectroscopy Tools (XPST) version 1.1, a curve fitting software package for Igor (Igor Pro 6.3.4.1). Peaks were identified using the NIST X-ray Photoelectron Spectroscopy Database version 4.1. Copper

reduction was determined by calculating the ratio of Cu^{2+} 2p3/2 peak areas and Cu^{1+} 2p3/2 peak areas.

3.5.2 TEM-EDAX Measurements

The morphology of the Fe_2O_3 fly ash surrogates was characterized using TEM (JEOL 2011 TEM) with an acceleration voltage of 200 kV. Five (5) µL of a diluted suspension of sample was deposited on a Lacey (300-mesh carbon-coated copper) grid. The material was allowed to dry overnight. The distribution of nanocrystal dimensions was obtained from the analysis of TEM images using Gatan Microscopy Suite, Digital Micrograph software. About 80 nanocrystals were randomly selected and the length and of each were measured using the ruler tool. EDS testing was conducted by EDAX TEAM.

3.5.3 XRD analysis

Powder X-ray diffraction (XRD) measurements were conducted on 1 %, 2.5 %, 4 % and 5 % Fe_2O_3 synthetic fly ash using a PANalytical Empyrea X-ray diffractometer with Cu Kα radiation. XRD Data were collected at a constant scanning rate of 2°/min. Data was processed by PANalytical high score plus software.

3.6 References

1.   Ross, B.; Naikwadi, K.; Karasek, F., Effect of temperature, carrier gas and precursor structure on PCDD and PCDF formed from precursors by catalytic activity of MSW incinerator fly ash. *Chemosphere* **1989,** *19* (1-6), 291-298.

2.   Rubey, W. A.; Grant, R. A., Design aspects of a modular instrumentation system for thermal diagnostic studies. *Review of scientific instruments* **1988,** *59* (2), 265-269.

3.   Pitzer, E. W., Analyses of oxidative decomposition products of tricresylphosphates using a system for thermal diagnostic studies (STDS). *Journal of chromatographic science* **1993,** *31* (11), 474-476.

4.   Striebich, R.; Rubey, W., A system for thermal diagnostic studies. *American Laboratory* **1990,** *22* (1), 64-&.

5.   Nganai, S. K., iron (III) oxide and copper (II) oxide mediated formation of PCDD/Fs from thermal degradation of 2-MCP and 1,2-DCBz

LSU Doctoral Dissertations. 381. **2010**, 41.

6.   dela Cruz, A. L. N.; Gehling, W.; Lomnicki, S.; Cook, R.; Dellinger, B., Detection of environmentally persistent free radicals at a superfund wood treating site. *Environmental science & technology* **2011,** *45* (15), 6356-6365.

CHAPTER 4 RESULTS*

4.1 Thermal Degradation of 2-Monochlorophenol over $1\%Fe_2O_3/4\%CuO/SiO_2$

4.1.1 Pyrolytic Conditions

The temperature dependence of the surface-mediated pyrolysis of 2-MCP over $1\%Fe_2O_3/4\%CuO/SiO_2$ and the yields of major organic products are presented below. 95% of 2-MCP already degraded at 200 °C, with 5% of the initial reactant remaining undestroyed. (Figure 4.1). Chlorophenols and chlorobenzenes were the major aromatic products. The maximum yields of 2,4-and 2,6-dichlorophenol (2,4-+2,6-DCP) were 0.02% at 250 °C (Figure 4.1). Chlorobenzenes were detected at 300-450 °C. The maximum yields of monochlorobenzene (MCBz) and 1,2-dichlorobenzene (1,2-DCBz) were 0.01% and 0.002% at 300 °C (Figure 4.2).

Compared to chlorophenols and chlorobenzenes, significant amounts of PCDD/F were produced at 200-250 °C on pyrolysis of 2-MCP over $1\%Fe_2O_3/4\%CuO/SiO_2$ (Figure 4.3). The observed dioxin products were: 1-chloro-dibenzo-*p*-dioxin (1-MCDD), 2,7+2,8-dichlorodibenzo-*p*-dioxin (2,7+2,8 - DCDD) and 4,6- dichlorodibenzofuran (4,6-DCDF) with the yields of MCDD > DCDD > DCDF. The maximum yields of 1-MCDD, 2,7+2,8-DCDD and 4,6-DCDF were 0.55 %, 0.15% and 0.14% at 250 °C, respectively. Trace amount of trichlorodibenzo-*p*-dioxin (TriCDD), dibenzo-*p*-dioxin (DD) and dibenzofuran (DF) were also detected.

---

*Portions of this chapter reprinted by permission of Elsevier, Journal of Chemosphere
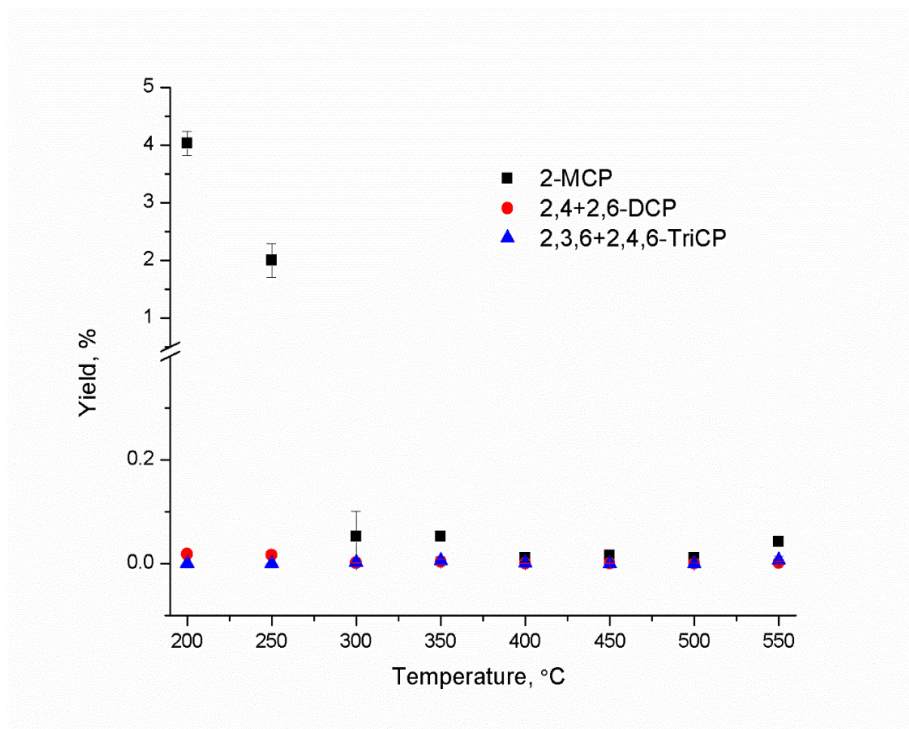
Figure 4.1. Chlorophenol Yields and Precursor Conversion from Pyrolysis of 2-MCP over 1%Fe$_2$O$_3$ /4%CuO/SiO$_2$
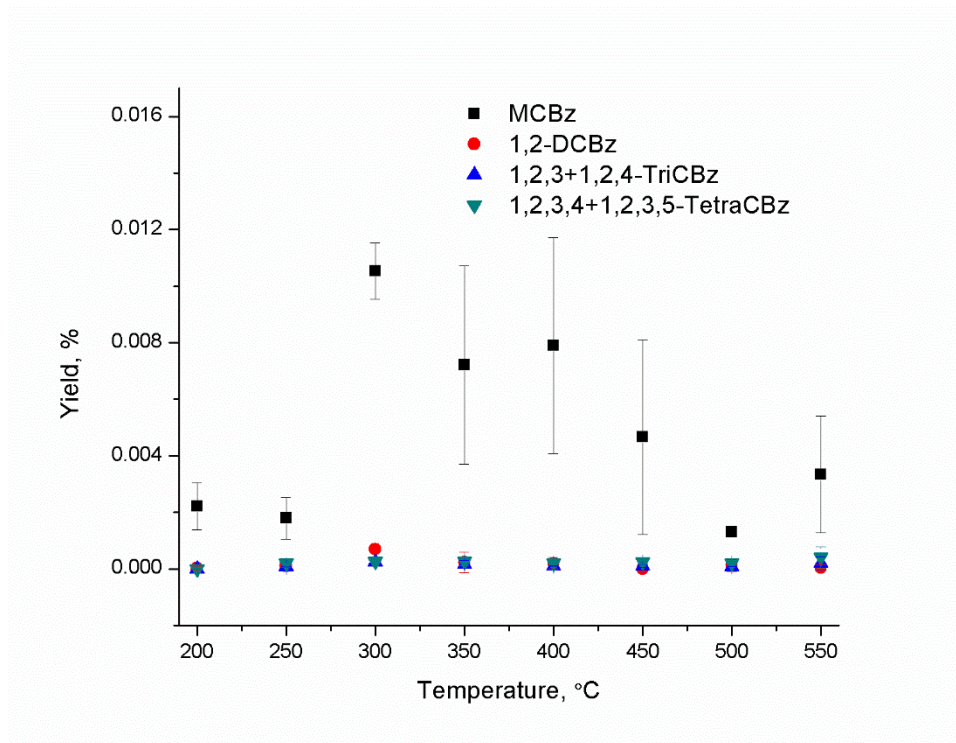
Figure 4.2. Chlorobenzene Yields from Pyrolysis of 2-MCP over 1%Fe$_2$O$_3$ 4%CuO/SiO$_2$
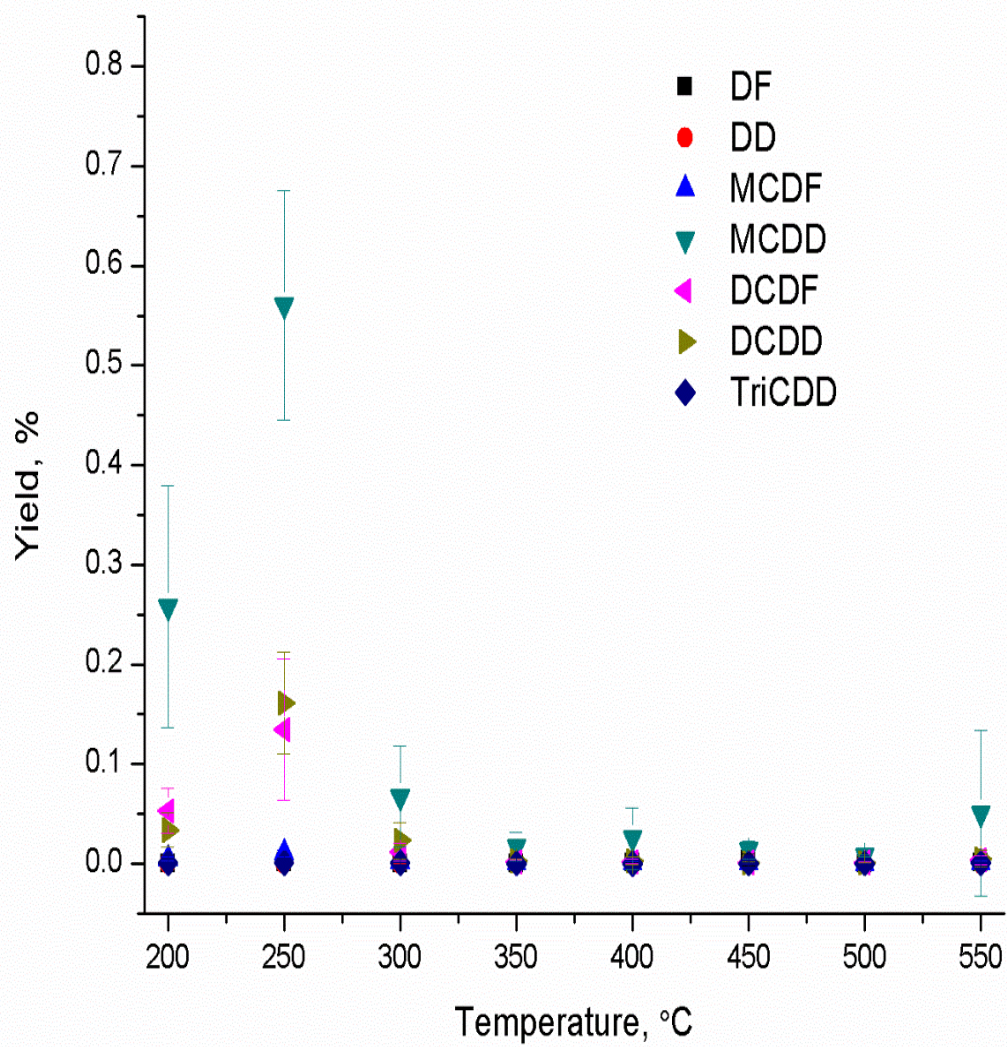
Figure 4.3. Major PCDD/F Yields from Pyrolysis of 2-MCP over 1%Fe_2O_3 /4%CuO/SiO_2

Table 4.1. Dioxin and Non-Dioxin Products and Percent Yields from Pyrolysis of 2-Monochlorophenol over 1% Fe_2O_3/4%CuO/SiO_2

Products	Reaction Temperature (°C)							
	200	250	300	350	400	450	500	550
Monochlorobenzene	2.11E-03	1.79E-03	10.5E-03	7.21E-03	7.89E-03	4.66E-03	1.30E-03	3.34E-03
2-Monochlorophenol	403E-03	200E-03	51.8E-03	52.3E-03	10.8E-03	15.5E-03	10.7E-03	41.7E-03
1,2-Dichlorobenzene	0.04E-03	0.11E-03	0.69E-03	0.23E-03	0.20E-03	bdl	0.12E-03	0.05E-03
2,4+2,6-Dichlorophenol	18.1E-03	16.3E-03	1.34E-03	3.70E-03	0.55E-03	0.38E-03	0.46E-03	1.62E-03
1,2,3+1,2,4-Trichlorobenzene	bdl	0.07E-03	0.25E-03	0.15E-03	0.10E-03	0.10E-03	0.08E-03	0.21E-03
1,2,3,4+1,2,3,5-Tetrachlorobenzene	bdl	0.19E-03	0.26E-03	0.26E-03	0.20E-03	0.23E-03	0.20E-03	0.41E-03
2,3,6+2,4,6-Trichlorophenol	bdl	bdl	1.60E-03	5.39E-03	1.03E-03	bdl	0.05E-03	6.54E-03
Pentachlorobenzene	bdl	0.27E-03	0.30E-03	0.34E-03	0.27E-03	0.31E-03	0.27E-03	0.47E-03
Hexachlorobenzene	bdl	bdl	bdl	0.11E-03	bdl	bdl	bdl	0.44E-03
Dibenzofuran	0.27E-03	0.58E-03	0.30E-03	0.30E-03	0.57E-03	4.32E-03	0.24E-03	1.22E-03
Dibenzo-*p*-dioxin	0.15 E-03	0.54E-03	0.06E-03	0.02E-03	0.03E-03	0.14E-03	bdl	0.06E-03
4-Monochlorodibenzofuran	4.70E-03	10.4E-03	1.90E-03	0.62E-03	0.95E-03	1.10E-03	0.28E-03	1.13E-03
1-Monochlorodibenzondioxin	258E-03	560E-03	67.1E-03	16.9E-03	25.2E-03	13.4E-03	7.98E-03	50.3E-03
4,6-Dichlorodibenzofuran	53.0E-03	135E-03	11.5E-03	2.02E-03	2.11E-03	1.36E-03	1.40E-03	3.50E-03
2,7-Dichlorodibenzodioxin	33.7E-03	161E-03	23.4E-03	2.61E-03	2.88E-03	1.11E-03	0.66E-03	5.08E-03
1,3,7-Trichlorodibenzodioxin	0.85E-03	0.89E-03	0.86E-03	0.29E-03	bdl	0.50E-03	0.29E-03	0.73E-03
Total PCDD/F	0.35	0.87	0.11	0.02	0.03	0.02	0.01	0.06
bdl-Below Detection Limit								

4.1.2 Oxidative Conditions

The temperature dependence of the surface-mediated oxidation of 2-MCP over $1\%Fe_2O_3/4\%CuO/SiO_2$ and the yields of major organic products are presented below. Complete degradation of 2-MCP occurred as low as 200 °C (Figure 4.4). Chlorophenols and chlorobenzenes were the major aromatic products. The maximum yields of 2,4-+2,6-DCP and 2,3,6+2,4,6-trichlorophenol (2,3,6+2,4,6-TriCP) were 0.05% and 0.07% at 250 °C (Figure 4.4). The amount of 2,4-+2,6-DCP was 2.5 times of which under pyrolysis. The maximum yields of MCBz were 0.005% at 250 °C (Figure 4.5), which was only half of that under pyrolysis. Trace amount of 1,2-DCBz, 1,2,3 + 1,2,4-trichlorobenzene (1,2,3 + 1,2,4-TriCBz) were also detected.

Compared to chlorophenols and chlorobenzenes, comparable amount of PCDD/F were produced at 200-250 °C on oxidation of 2-MCP over $1\%Fe_2O_3/4\%CuO/SiO_2$ (Figure 4.6). The observed dioxin products were: 1-MCDD, 2,7+2,8-DCDD and TriCDD with the yields of 1-MCDD > DCDD > TriCDD. The maximum yields of 1-MCDD and DCDD were 0.04% and 0.03% at 275 and 250 °C, respectively. There was almost none of PCDFs observed.
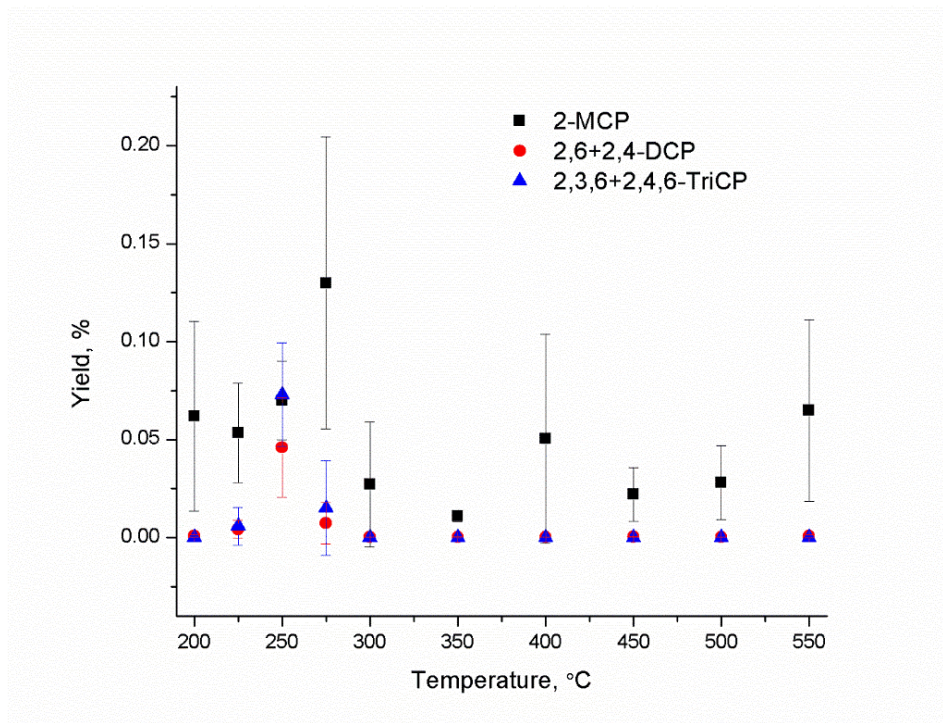
Figure 4.4. Chlorophenol Yields and Precursor Conversion from Oxidation of 2-MCP over 1%Fe_2O_3 /4%CuO/SiO_2
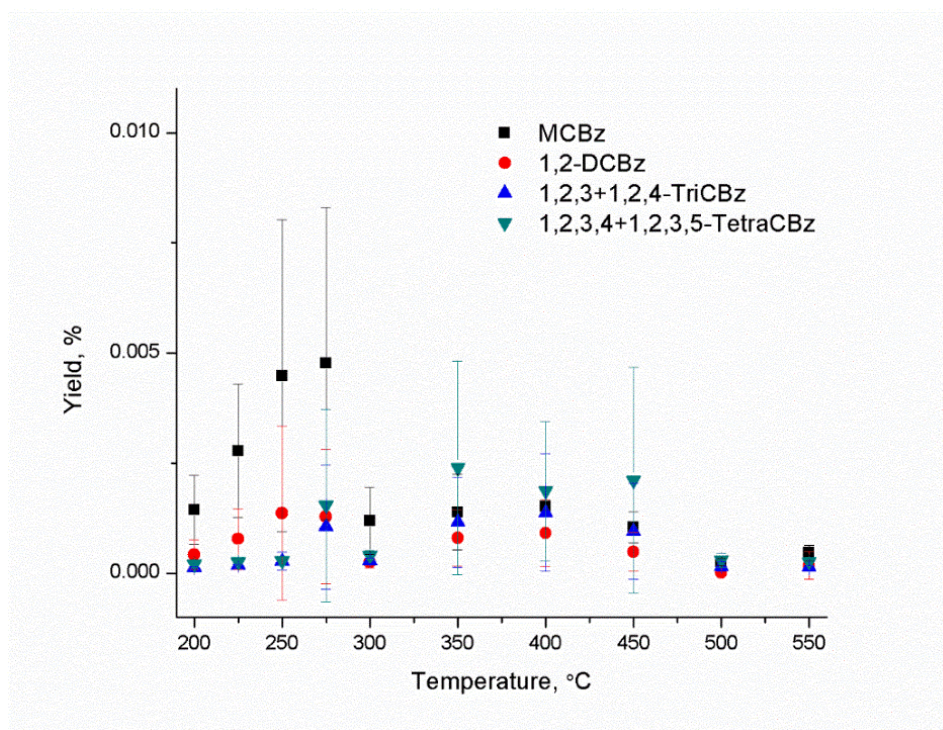
Figure 4.5. Chlorobenzene Yields from Oxidation of 2-MCP over 1%Fe_2O_3 4%CuO/SiO_2
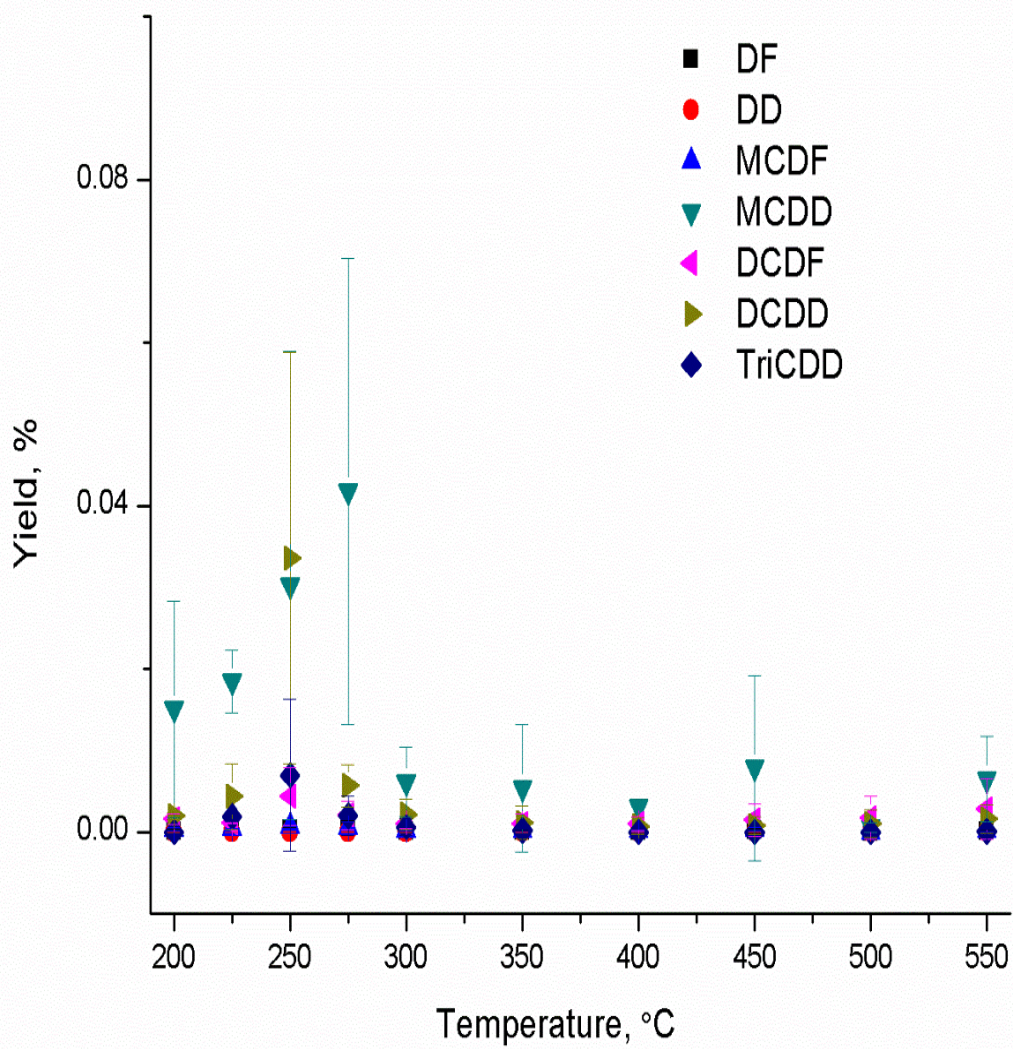
Figure 4.6. Major PCDD/F Yields from Oxidation of 2-MCP over 1%Fe_2O_3 4%CuO/SiO_2

Table 4.2. Dioxin and Non-Dioxin Products and Percent Yields from Oxidation of 2-Monochlorophenol over 1% Fe_2O_3/4%CuO/SiO_2

Products	Reaction Temperature (°C)							
	200	250	300	350	400	450	500	550
Monochlorobenzene	1.44E-03	4.48E-03	1.19E-03	1.39E-03	1.52E-03	1.05E-03	0.25E-03	0.46E-03
2-Monochlorophenol	62.1E-03	70.0E-03	27.1E-03	10.9E-03	50.5E-03	22.1E-03	28.1E-03	65.0E-03
1,2-Dichlorobenzene	0.42E-03	1.36E-03	0.24E-03	0.80E-03	0.91E-03	0.49E-03	0.01E-03	0.18E-03
2,4+2,6-Dichlorophenol	0.96E-03	46.1E-03	0.36E-03	0.40E-03	0.40E-03	0.52E-03	0.33E-03	0.80E-03
1,2,3+1,2,4-Trichlorobenzene	0.13E-03	0.28E-03	0.29E-03	1.16E-03	1.37E-03	0.95E-03	0.15E-03	0.14E-03
1,2,3,4+1,2,3,5-Tetrachlorobenzene	0.21E-03	0.28E-03	0.40E-03	2.40E-03	1.86E-03	2.11E-03	0.30E-03	0.25E-03
2,3,6+2,4,6-Trichlorophenol	bdl	73.0E-03	bdl	bdl	bdl	bdl	bdl	bdl
Pentachlorobenzene	0.27E-03	0.30E-03	0.31E-03	1.27E-03	1.13E-03	1.22E-03	0.39E-03	0.33E-03
Hexachlorobenzene	0.26E-03	Bdl	bdl	1.42E-03	1.45E-03	2.11E-03	0.28E-03	bdl
Dibenzofuran	0.12E-03	0.37E-03	0.11E-03	0.07E-03	0.09E-03	0.15E-03	bdl	0.06E-03
Dibenzo-*p*-dioxin	bdl	0.01E-03	bdl	bdl	bdl	bdl	bdl	bdl
4-Monochlorodibenzofuran	0.37E-03	0.64E-03	0.26E-03	0.26E-03	0.19E-03	0.32E-03	bdl	0.22E-03
1-Monochlorodibenzondioxin	15.0E-03	30.2E-03	6.13E-03	5.38E-03	3.10E-03	7.85E-03	0.58E-03	6.48E-03
4,6-Dichlorodibenzofuran	1.61E-03	4.37E-03	1.05E-03	1.00E-03	1.05E-03	1.49E-03	1.76E-03	2.86E-03
2,7-Dichlorodibenzodioxin	1.95E-03	33.6E-03	2.16E-03	1.16E-03	0.73E-03	0.80E-03	1.03E-03	1.62E-03
1,3,7-Trichlorodibenzodioxin	bdl	6.97E-03	0.61E-03	0.17E-03	bdl	bdl	bdl	0.09E-03
2,3,7,8-Tetrachlorodibenzodioxin	bdl	0.49E-03	bdl	0.12E-03	bdl	bdl	bdl	0.23E-03
Total PCDD/F	0.02	0.08	0.01	0.008	0.005	0.01	0.003	0.011
bdl-Below Detection Limit								

4.2 Thermal Degradation of 2-Monochlorophenol over 2.5%Fe$_2$O$_3$ /2.5%CuO/SiO$_2$

4.2.1 Pyrolytic Conditions

The temperature dependence of the surface-mediated pyrolysis of 2-MCP over 2.5%Fe$_2$O$_3$/2.5%CuO/SiO$_2$ and the yields of major organic products are presented below. 85% of the 2-MCP decomposed at 200 °C and almost complete destroyed by 250 °C (Figure 4.7). Chlorophenols and chlorobenzenes were the major aromatic products. The maximum yields of 2,4-+2,6-DCP and 2,3,6+2,4,6-TriCP were 0.01% and 0.05% at 200 °C and 250 °C (Figure 4.7). The maximum yields of MCBz were 0.06% at 400 °C (Figure 4.8).

Compared to chlorophenols and chlorobenzenes, huge amount of PCDD/F were produced at 300 °C on pyrolysis of 2-MCP over 2.5%Fe$_2$O$_3$/2.5%CuO/SiO$_2$ (Figure 4.9). The observed dioxin products were: 1-MCDD, 2,7+2,8-DCDD and 4,6-DCDF with the yields of 1-MCDD > DCDF > DCDD. The maximum yields of 1-MCDD, DCDF and DCDD were 4.4%, 0.75% and 0.6% at 300 °C, respectively.

Compared to the PCDD/F produced from 1%Fe$_2$O$_3$ 4%CuO/SiO$_2$, the highest yield of congener 1-MCDD at 250 °C was 0.55%. This same load amount of metal oxide fly ash surrogate generates almost 10-fold of dioxin yield, which was 4.4%. We can assume there is synergistic effect between iron and copper oxides which contributes the formation of significant amount of PCDD/F.
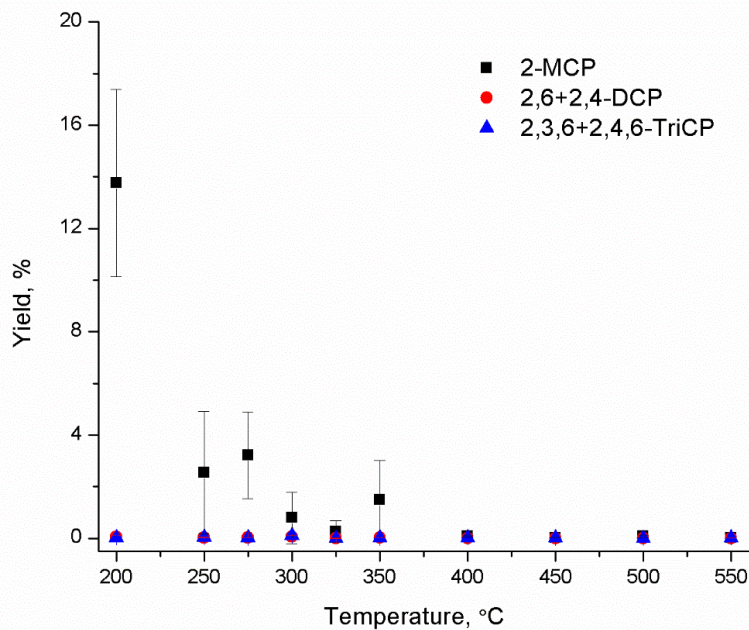
Figure 4.7. Chlorophenol Yields and Precursor Conversion from Pyrolysis of 2-MCP over 2.5%Fe_2O_3 /2.5%CuO/SiO_2
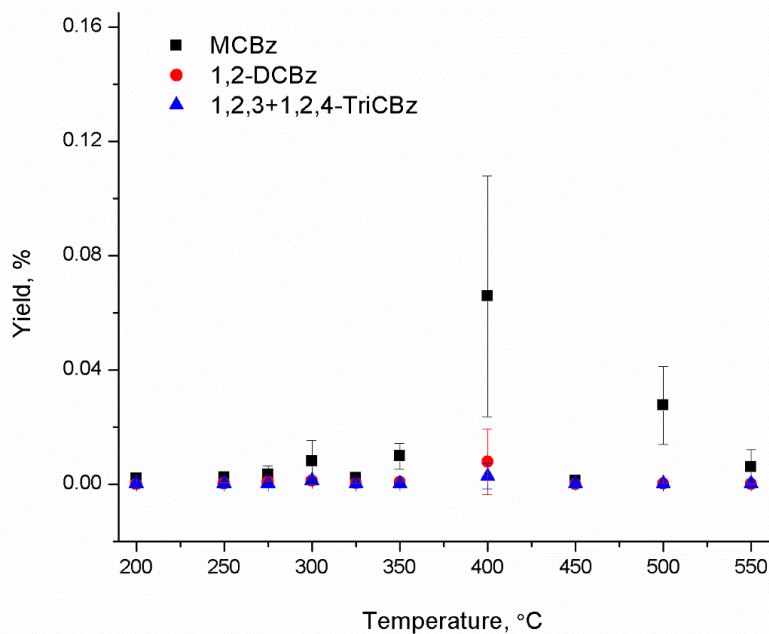
Figure 4.8. Chlorobenzene Yields from Pyrolysis of 2-MCP over 2.5%Fe_2O_3 /2.5%CuO/SiO_2
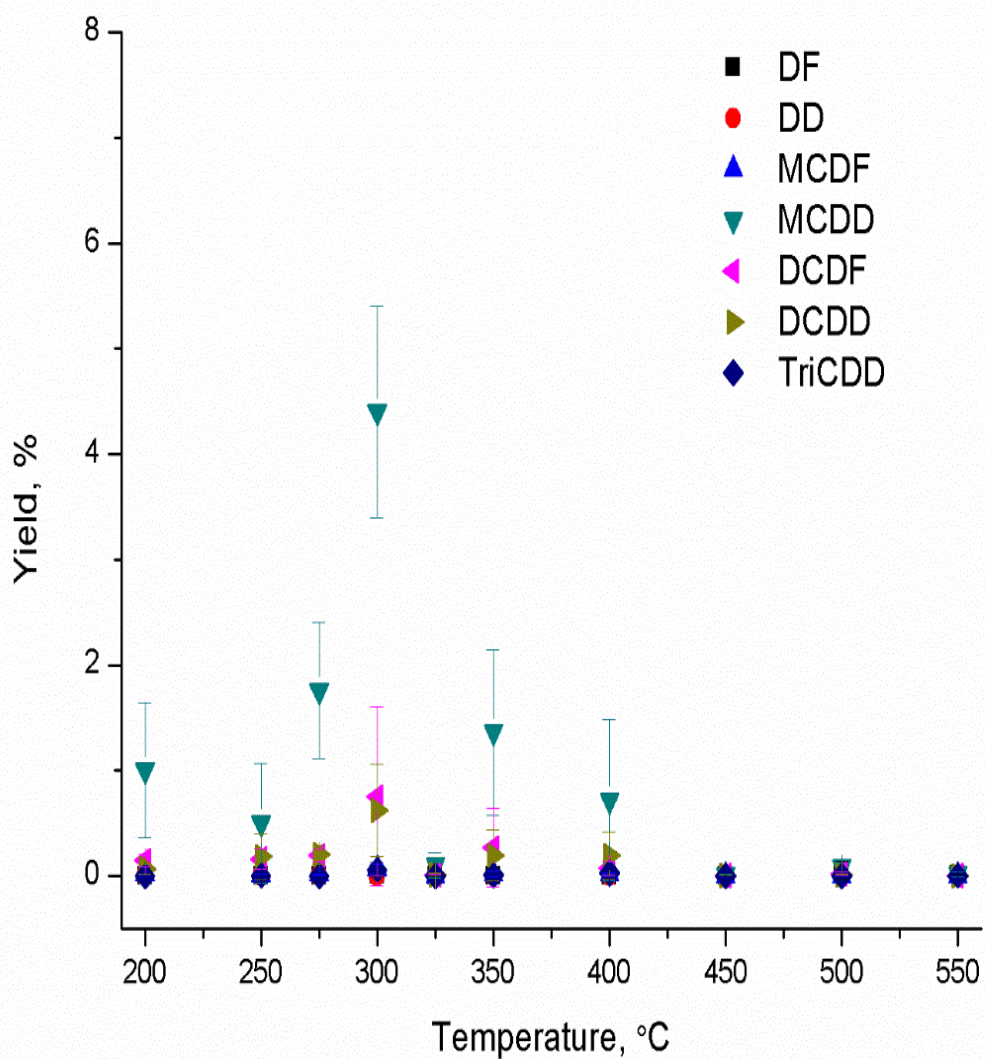
Figure 4.9. Major PCDD/F Yields from Pyrolysis of 2-MCP over 2.5%Fe_2O_3 2.5%CuO/SiO_2

Table 4.3. Dioxin and Non-Dioxin Products and Percent Yields from Pyrolysis of 2-Monochlorophenol over 2.5% Fe_2O_3/2.5%CuO/SiO_2

Products	Reaction Temperature (°C)							
	200	250	300	350	400	450	500	550
Monochlorobenzene	1.96E-03	2.43E-03	8.03E-03	9.80E-03	65.8E-03	1.26E-03	27.6E-03	5.95E-03
2-Monochlorophenol	14	2.6	790E-03	1.5	85.2E-03	21.6E-03	70.6E-03	17.0E-03
1,2-Dichlorobenzene	0.02E-03	0.24E-03	1.18E-03	0.67E-03	7.90E-03	bdl	0.16E-03	0.10E-03
2,4+2,6-Dichlorophenol	61.6E-03	26.1E-03	61.3E-03	18.8E-03	4.64E-03	0.73E-03	1.93E-03	1.17E-03
1,2,3+1,2,4-Trichlorobenzene	0.10E-03	0.11E-03	1.11E-03	0.21E-03	2.82E-03	0.21E-03	0.09E-03	0.13E-03
1,2,3,4+1,2,3,5-Tetrachlorobenzene	0.24E-03	0.24E-03	1.34E-03	0.30E-03	1.68E-03	0.50E-03	0.20E-03	0.27E-03
2,3,6+2,4,6-Trichlorophenol	17.8E-03	29.9E-03	93.6E-03	6.98E-03	18.6E-03	2.53E-03	0.79E-03	14.6E-03
Pentachlorobenzene	0.31E-03	0.38E-03	1.19E-03	0.38E-03	0.96E-03	0.69E-03	0.27E-03	0.38E-03
Hexachlorobenzene	0.55E-03	0.39E-03	2.51E-03	0.38E-03	0.63E-03	1.15E-03	bdl	0.40E-03
Dibenzofuran	0.46E-03	0.60E-03	5.46E-03	1.66E-03	4.72E-03	3.59E-03	51.5E-03	7.08E-03
Dibenzo-*p*-dioxin	0.44E-03	0.32E-03	3.18E-03	1.99E-03	0.87E-03	0.03E-03	1.01E-03	0.08E-03
4-Monochlorodibenzofuran	14.7E-03	8.15E-03	63.3E-03	22.8E-03	15.1E-03	0.76E-03	4.05E-03	0.82E-03
1-Monochlorodibenzondioxin	100E-02	503E-03	440E-02	136E-02	719E-03	9.53E-03	81.1E-03	17.5E-03
4,6-Dichlorodibenzofuran	147E-03	162E-03	753E-03	271E-03	75.3E-03	3.59E-03	23.1E-03	3.79E-03
2,7-Dichlorodibenzodioxin	69.1E-03	183E-03	623E-03	197E-03	196E-03	3.13E-03	11.3E-03	2.45E-03
1,3,7-Trichlorodibenzodioxin	0.46E-03	4.82E-03	60.0E-03	5.23E-03	27.0E-03	1.51E-03	0.27E-03	3.10E-03
2,3,7,8-Tetrachlorodibenzodioxin	bdl	0.24E-03	13.8E-03	0.07E-03	2.34E-03	bdl	bdl	3.73E-03
Total PCDD/F	1.23	0.86	5.92	1.86	1.04	0.02	0.17	0.04
bdl-Below Detection Limit								

4.2.2 Oxidative Conditions

The temperature dependence of the surface-mediated oxidation of 2-MCP over 2.5%Fe_2O_3/2.5%CuO/SiO_2 and the yields of major organic products are presented below. Almost complete degradation of 2-MCP occurred at 200 °C (Figure 4.10). Chlorophenols and chlorobenzenes were the major aromatic products. The maximum yields of 2,4-+2,6-DCP were 0.004% at 250 °C (Figure 4.10). The maximum yields of MCBz, DCBz and TriCBz were 0.004%, 0.004% at 350 °C and 0.006% at 400 °C (Figure 4.11).

Compared to chlorophenols and chlorobenzenes, significant amount of PCDD/F were produced at 250 °C on oxidation of 2-MCP over 2.5%Fe_2O_3/2.5%CuO/SiO_2 (Figure 4.12). The observed dioxin products were: 1-MCDD, 2,7+2,8-DCDD, TriCDD and 4,6-DCDF with the yields of DCDD > DCDF > TriCDD > MCDD. Their maximum yields were 0.03%, 0.02%, 0.015% and 0.013% at 250 °C, respectively.

Synergy of iron and copper also worked under oxidation conditions but produced a completely different result. Instead of producing large amount of PCDD/F, the synergistic catalytic effect between iron and copper disrupted the precursor 2-MCP quickly as low as 200 °C. Therefore, less amount of surface condensation of adsorbed phenolic species was left for the subsequent formation of PCDD/F.
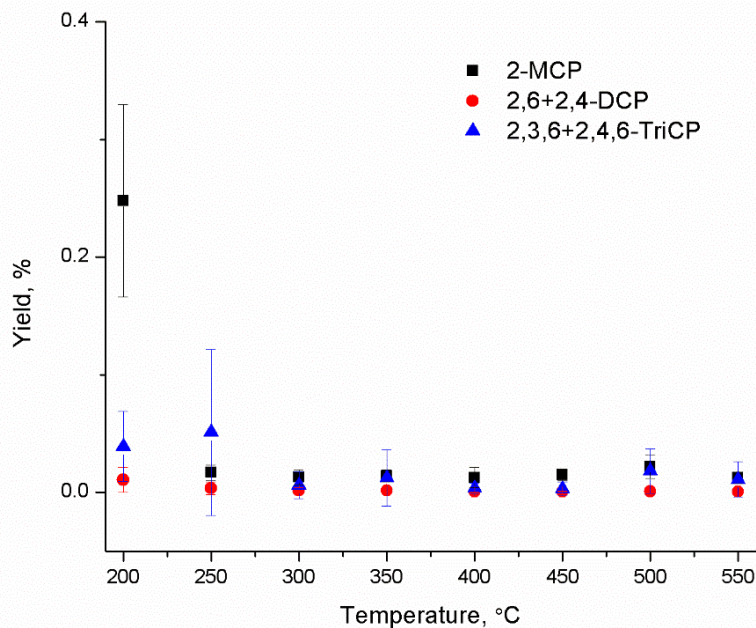
Figure 4.10. Chlorophenol Yields and Precursor Conversion from Oxidation of 2-MCP over 2.5%Fe_2O_3 /2.5%CuO/SiO_2
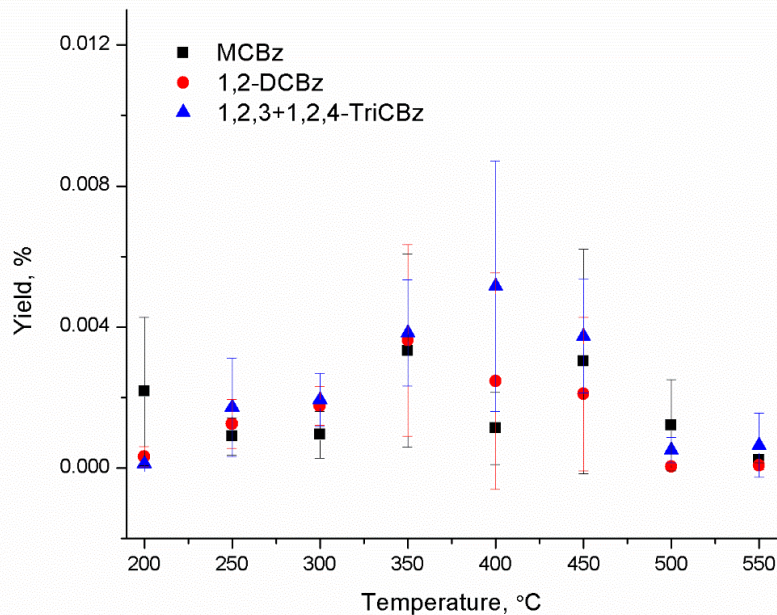
Figure 4.11. Chlorobenzene Yields from Oxidation of 2-MCP over 2.5%Fe_2O_3 /2.5%CuO/SiO_2
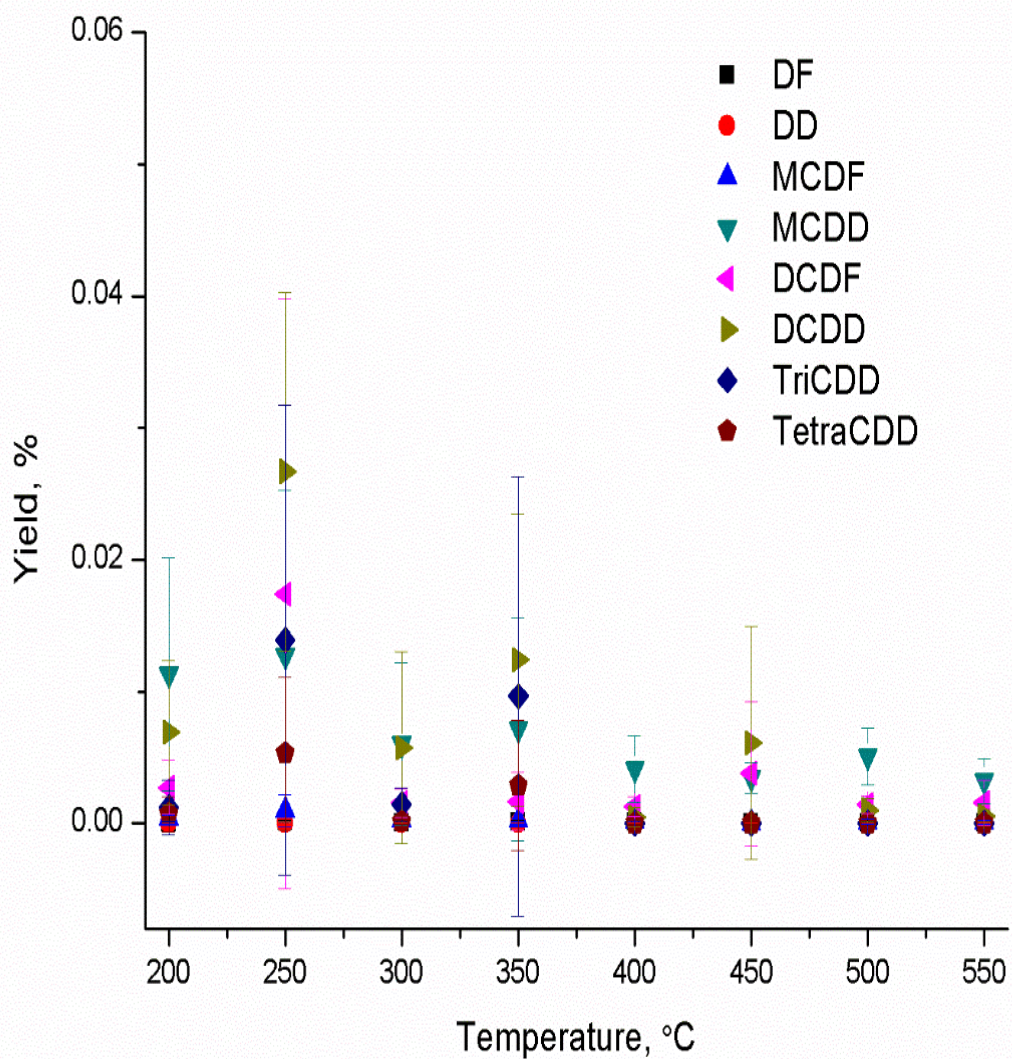
Figure 4.12. Major PCDD/F Yields from Oxidation of 2-MCP over 2.5%Fe_2O_3 2.5%CuO/SiO_2

Table 4.4. Dioxin and Non-Dioxin Products and Percent Yields from Oxidation of 2-Monochlorophenol over 2.5% Fe_2O_3/2.5%CuO/SiO_2

Products	Reaction Temperature (°C)							
	200	250	300	350	400	450	500	550
Monochlorobenzene	2.17E-03	0.90E-03	0.94E-03	3.33E-03	1.12E-03	3.02E-03	1.21E-03	0.23E-03
2-Monochlorophenol	248E-03	16.7E-03	12.9E-03	14.0E-03	12.6E-03	14.8E-03	21.7E-03	12.3E-03
1,2-Dichlorobenzene	0.32E-03	1.25E-03	1.76E-03	3.62E-03	2.46E-03	2.10E-03	0.04E-03	0.07E-03
2,4+2,6-Dichlorophenol	10.7E-03	3.50E-03	1.67E-03	1.53E-03	0.59 E-03	0.66E-03	0.89E-03	0.57E-03
1,2,3+1,2,4-Trichlorobenzene	0.11E-03	1.72E-03	1.93E-03	3.83E-03	5.16E-03	3.74E-03	0.51E-03	0.64E-03
1,2,3,4+1,2,3,5-Tetrachlorobenzene	0.25E-03	3.08E-03	2.28E-03	6.22E-03	11.0E-03	6.90E-03	1.67E-03	1.81E-03
2,3,6+2,4,6-Trichlorophenol	39.1E-03	5.11E-02	6.17E-03	12.5 E-03	3.46E-03	3.22E-03	18.1E-03	11.0E-03
Pentachlorobenzene	0.33E-03	1.80E-03	0.72E-03	2.05E-03	5.49E-03	3.77E-03	2.81E-03	2.44E-03
Hexachlorobenzene	0.71E-03	8.16E-03	0.32E-03	1.94E-03	8.17E-03	7.27E-03	9.98E-03	bdl
Dibenzofuran	0.04E-03	0.13E-03	bdl	0.10E-03	0.08 E-03	bdl	0.04E-03	0.04E-03
Dibenzo-*p*-dioxin	bdl	bdl	bdl	bdl	bdl	bdl	bdl	bdl
4-Monochlorodibenzofuran	0.39E-03	0.95E-03	0.23E-03	0.26E-03	0.16 E-03	bdl	0.12E-03	0.09E-03
1-Monochlorodibenzondioxin	11.3E-03	12.7E-03	6.04E-03	7.12E-03	4.08E-03	3.41E-03	5.06E-03	3.23E-03
4,6-Dichlorodibenzofuran	2.72E-03	17.4E-03	1.54E-03	1.65E-03	1.29E-03	3.78E-03	1.44E-03	1.58E-03
2,7-Dichlorodibenzodioxin	6.89E-03	26.7E-03	5.74E-03	12.4E-03	0.45E-03	6.08E-03	1.00E-03	0.56E-03
1,3,7-Trichlorodibenzodioxin	1.19E-03	13.9E-03	1.43E-03	9.64E-03	bdl	bdl	bdl	bdl
2,3,7,8-Tetrachlorodibenzodioxin	0.68E-03	5.30E-03	0.10E-03	2.86E-03	bdl	bdl	bdl	bdl
Total PCDD/F	0.02	0.08	0.015	0.03	0.006	0.013	0.009	0.006
bdl-Below Detection Limit								

4.3 Thermal Degradation of 2-Monochlorophenol over 4%Fe₂O₃ /1%CuO/SiO₂

4.3.1 Pyrolytic Conditions

The temperature dependence of the surface-mediated pyrolysis of 2-MCP over $4\%Fe_2O_3/1\%CuO/SiO_2$ and the yields of major organic products are presented below. 90% of the 2-MCP degraded at 200 °C and the rest of the 10% almost decomposed completely by 350 °C (Figure 4.13). Chlorophenols and chlorobenzenes were the major aromatic products with chlorophenols observed in greater yields than chlorobenzenes. The maximum yields of 2,4-+2,6-DCP and 2,3,6+2,4,6-TriCP were 0.3% and 2% at 250 °C, which were the highest yields on all the fly ash surrogates (Figure 4.13). The maximum yields of MCBz were 0.07% at 550 °C (Figure 4.14).

Compared to chlorophenols and chlorobenzenes, significant amount of PCDD/F were produced at 275 °C on pyrolysis of 2-MCP over $4\%Fe_2O_3/1\%CuO/SiO_2$ (Figure 4.15). The observed dioxin products were: 1-MCDD, 2,7+2,8-DCDD and 4,6-DCDF with the yields of 1-MCDD > DCDF > DCDD. Their maximum yields were 3.6%, 0.5% and 0.5% at 275 °C, 250 °C, and 300 °C respectively (Figure 4.15).

Compared to the PCDD/F produced from $2.5\%Fe_2O_3/2.5\%CuO/SiO_2$ under pyrolysis, 4.4% of 1-MCDD at 300 °C, the maximum output of 1-MCDD from $4\%Fe_2O_3/1\%CuO/SiO_2$ shifted to 275 °C with the yield of 3.5%.
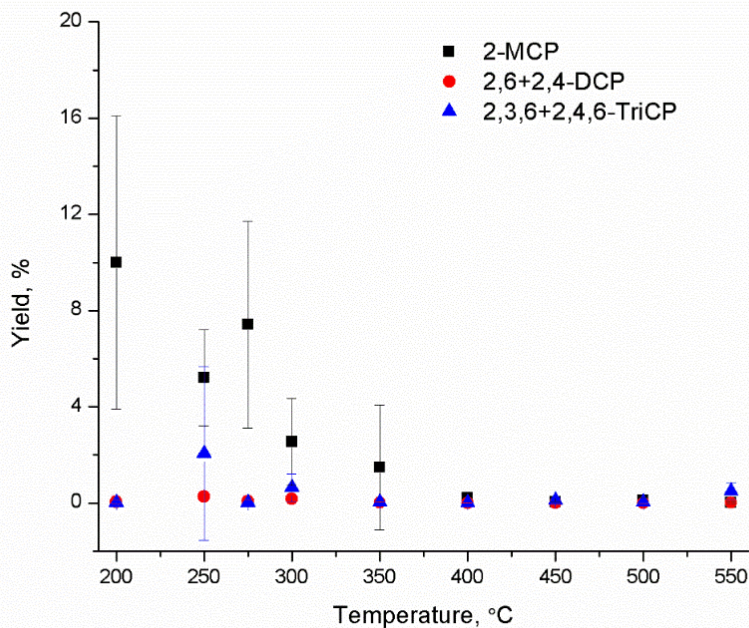
Figure 4.13. Chlorophenol Yields and Precursor Conversion from Pyrolysis of 2-MCP over 4%Fe_2O_3 /1%CuO/SiO_2
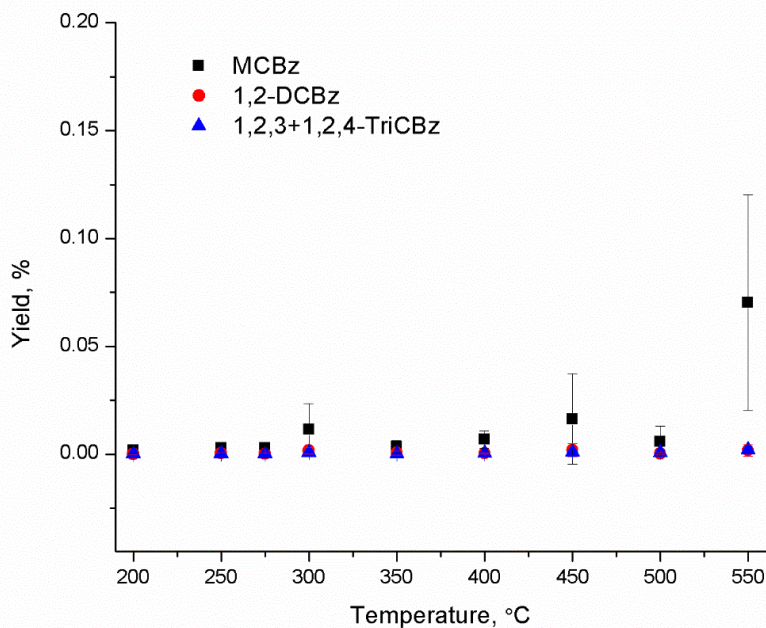
Figure 4.14. Chlorobenzene Yields from Pyrolysis of 2-MCP over 4%Fe_2O_3 /1%CuO/SiO_2
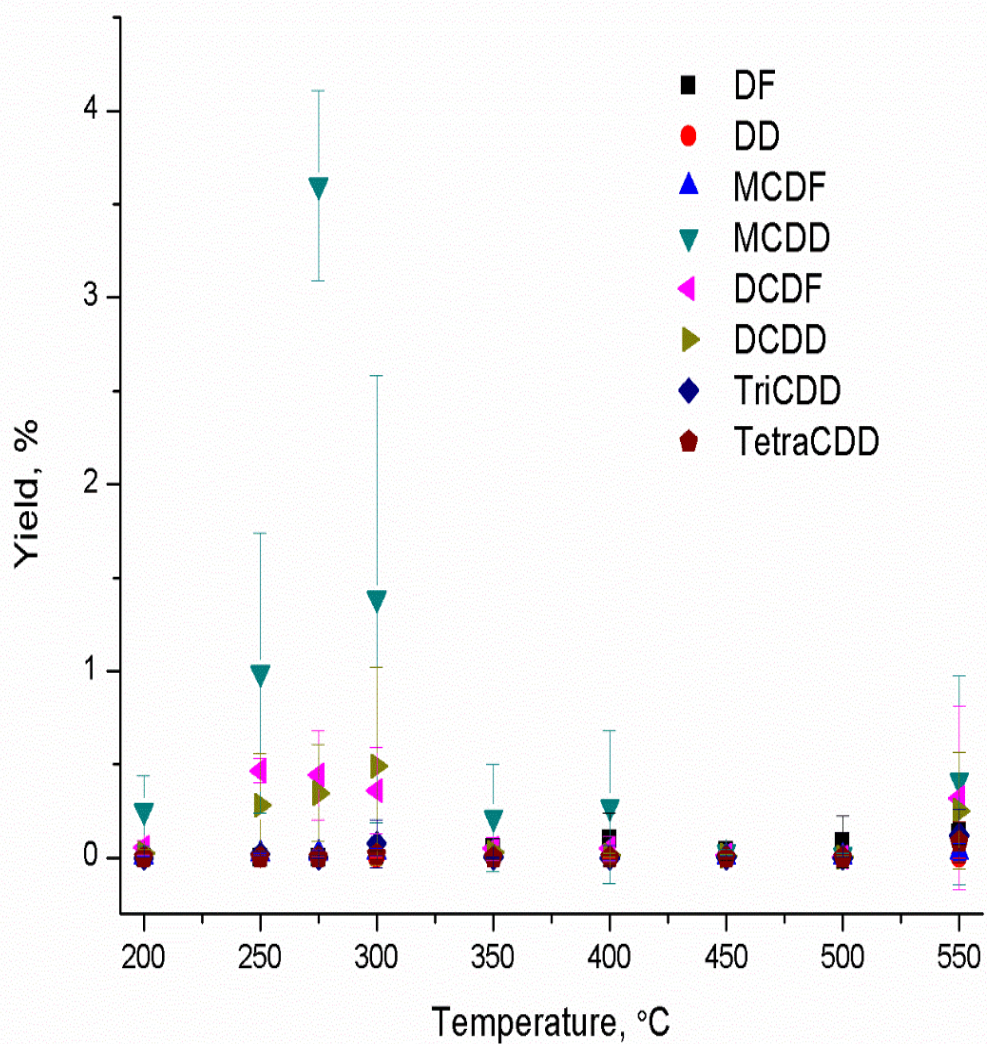
Figure 4.15. Major PCDD/F Yields from Pyrolysis of 2-MCP over 4%Fe_2O_3/ 1%CuO/SiO_2

Products	Reaction Temperature (°C)							
	200	250	300	350	400	450	500	550
Monochlorobenzene	1.90E-03	2.78E-03	11.5E-03	3.44E-03	6.92E-03	16.4E-03	5.87E-03	70.3E-03
2-Monochlorophenol	10	5.2	2.5	1.5	213E-03	34.9 E-03	102 E-03	24.6E-03
1,2-Dichlorobenzene	0.07E-03	0.49E-03	1.63E-03	0.67E-03	0.49 E-03	1.89E-03	0.36 E-03	1.76E-03
2,4+2,6-Dichlorophenol	52.4E-03	271 E-03	169E-03	14.2E-03	2.82E-03	1.03E-03	1.23E-03	14.6E-03
1,2,3+1,2,4-Trichlorobenzene	0.08E-03	0.17E-03	0.73E-03	0.17E-03	0.39E-03	0.97E-03	0.78 E-03	2.15E-03
1,2,3,4+1,2,3,5-Tetrachlorobenzene	0.23E-03	0.60E-03	0.97E-03	0.40E-03	1.09E-03	2.02E-03	1.65E-03	8.05E-03
2,3,6+2,4,6-Trichlorophenol	22.3E-03	206E-02	649E-03	45.7E-03	17.6E-03	108 E-03	30.5 E-03	506E-03
Pentachlorobenzene	0.47E-03	2.18E-03	1.68E-03	0.99E-03	1.91E-03	6.76E-03	2.39E-03	31.1E-03
Hexachlorobenzene	2.80E-03	17.1E-03	8.48E-03	3.04E-03	5.21E-03	35.3E-03	6.92E-03	181E-03
Dibenzofuran	0.72E-03	0.81E-03	11.7E-03	48.6E-03	98.7E-03	36.5E-03	84.2 E-03	130E-03
Dibenzo-*p*-dioxin	0.10E-03	0.50E-03	1.17E-03	0.46E-03	1.15E-03	0.25E-03	0.38 E-03	0.07E-03
4-Monochlorodibenzofuran	4.30E-03	17.7E-03	27.7E-03	30.0E-03	25.8E-03	5.99E-03	2.84E-03	31.3E-03
1-Monochlorodibenzondioxin	249E-03	988E-03	139E-02	213E-03	272E-03	29.9E-03	13.7E-03	414E-03
4,6-Dichlorodibenzofuran	55.1E-03	467E-03	360 E-03	49.1E-03	48.3E-03	11.6E-03	4.51E-03	319E-03
2,7-Dichlorodibenzodioxin	22.9E-03	280E-03	489 E-03	28.3E-03	13.3E-03	11.0E-03	3.20E-03	252E-03
1,3,7-Trichlorodibenzodioxin	0.76E-03	16.7E-03	74.7E-03	1.27E-03	bdl	2.92E-03	0.50E-03	120E-03
2,3,7,8-Tetrachlorodibenzodioxin	0.14E-03	1.72E-03	13.3E-03	bdl	bdl	0.67E-03	0.27E-03	84.3E-03
Total PCDD/F	0.33	1.77	2.37	0.37	0.46	0.10	0.11	1.35
bdl-Below Detection Limit								

Table 4.5. Dioxin and Non-Dioxin Products and Percent Yields from Pyrolysis of 2-Monochlorophenol over 4% Fe_2O_3/1%CuO/SiO_2

4.3.2 Oxidative Conditions

The temperature dependence of the surface-mediated oxidation of 2-MCP over 4%Fe_2O_3/1%CuO/SiO_2 and the yields of major organic products are presented below. Complete degradation of the 2-MCP already occurred at 200 °C (Figure 4.16). Chlorophenols and chlorobenzenes were the major aromatic products with chlorophenols observed in greater yields than chlorobenzenes. The maximum yields of 2,4-+2,6-DCP and 2,3,6+2,4,6-TriCP were 0.04% and 0.22% at 250 °C (Figure 4.16). The maximum yields of 1,2,3,4+1,2,3,5-tetrachlorobenzene (TetraCBz) were 0.014% at 350 °C, the maximum yields of MCB, DCBz and TriCBz were all 0.006% at 350 °C (Figure 4.17).

Compared to chlorophenols, similar amount of PCDD/F were produced at 250 °C on oxidation of 2-MCP over 4%Fe_2O_3/1%CuO/SiO_2 (Figure 4.18). The observed dioxin products were: 1-MCDD, 2,7+2,8-DCDD, TriCDD and 4,6-DCDF with the yields of DCDD >1-MCDD > TriCDD > DCDF. Their maximum yields were 0.22%, 0.12%,0.08% and 0.03% at 250 °C respectively (Figure 4.18). 0.05% of TetraCDD was also detected at 200°C.
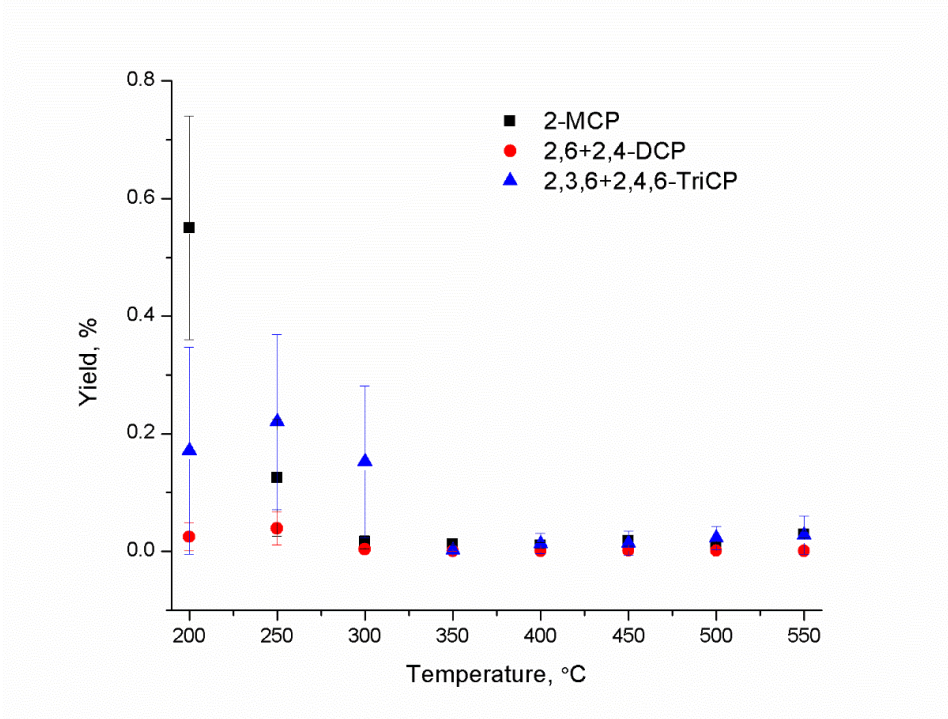
Figure 4.16. Chlorophenol Yields and Precursor conversion from Oxidation of 2-MCP over $4\%Fe_2O_3 /1\%CuO/SiO_2$
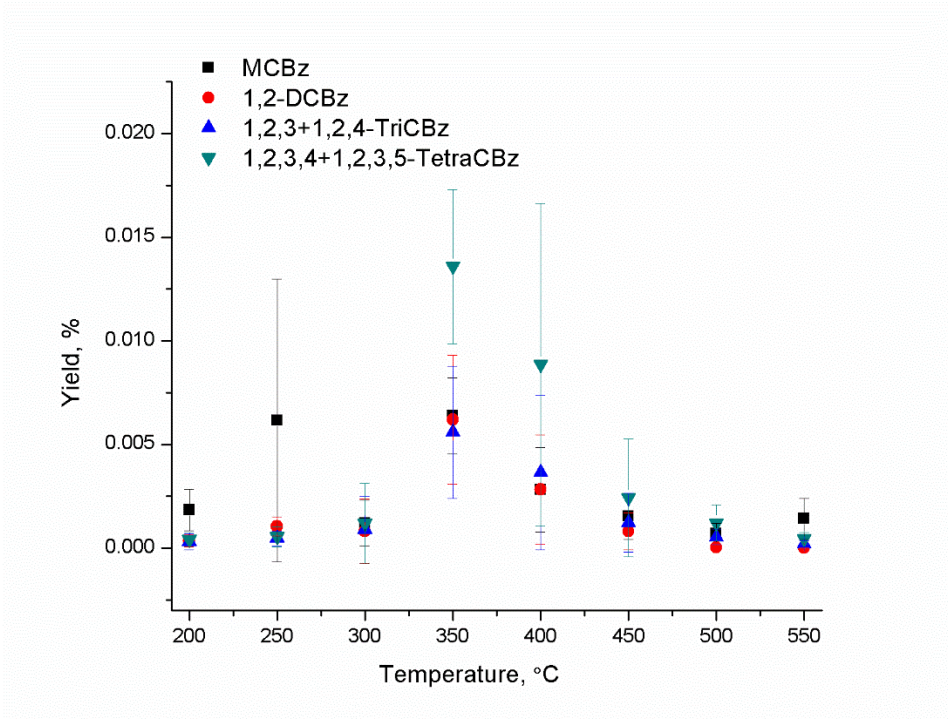
Figure 4.17. Chlorobenzene Yields from Oxidation of 2-MCP over $4\%Fe_2O_3 /1\%CuO/SiO_2$
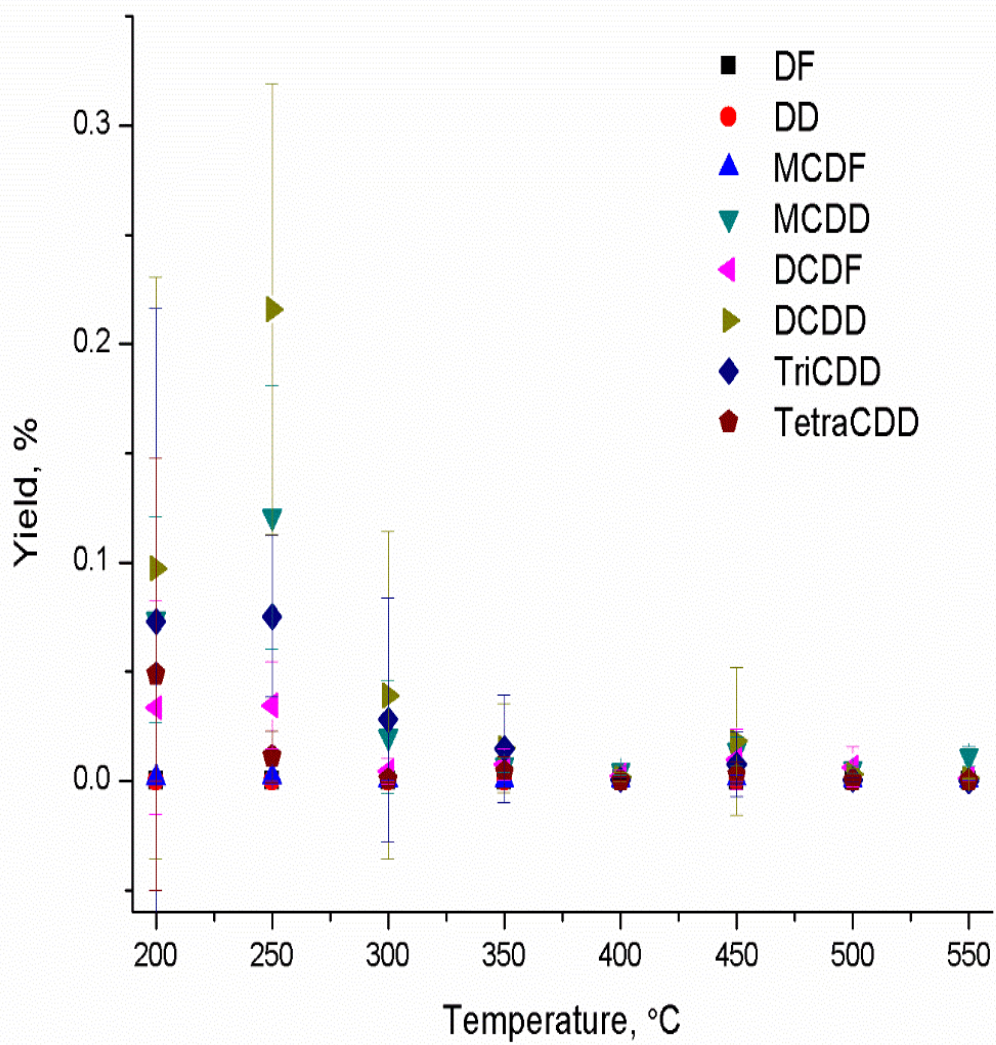
Figure 4.18. Major PCDD/F Yields from Oxidation of 2-MCP over 4%Fe_2O_3 1%CuO/SiO_2

Table 4.6. Dioxin and Non-Dioxin Products and Percent Yields from Oxidation of 2-Monochlorophenol over 4% Fe_2O_3/1%CuO/SiO_2

Products	Reaction Temperature (°C)							
	200	250	300	350	400	450	500	550
Monochlorobenzene	1.85E-03	6.15E-03	1.21E-03	6.38E-03	2.82E-03	1.54E-03	0.70E-03	1.41E-03
2-Monochlorophenol	550E-03	125E-03	15.4E-03	12.4E-03	10.1E-03	17.8E-03	8.79E-03	28.7E-03
1,2-Dichlorobenzene	0.36E-03	1.05E-03	0.81E-03	6.20E-03	2.83E-03	0.82E-03	0.03E-03	0.01E-03
2,4+2,6-Dichlorophenol	24.5E-03	39.0E-03	3.82E-03	0.72E-03	0.80E-03	1.86E-03	1.03E-03	0.77E-03
1,2,3+1,2,4-Trichlorobenzene	0.31E-03	0.47E-03	0.89E-03	5.59E-03	3.67E-03	1.23E-03	0.54 E-03	0.21E-03
1,2,3,4+1,2,3,5-Tetrachlorobenzene	0.42E-03	0.56E-03	1.20E-03	13.6 E-03	8.86E-03	2.43E-03	1.21E-03	0.46E-03
2,3,6+2,4,6-Trichlorophenol	171E-03	220E-03	152 E-03	2.37E-03	13.1E-03	1.41E-02	23.0E-03	27.7E-03
Pentachlorobenzene	0.67E-03	0.46E-03	0.66E-03	5.25E-03	6.42E-03	1.70E-03	1.11E-03	0.78E-03
Hexachlorobenzene	6.87E-03	2.55E-03	1.58E-03	7.92E-03	11.1E-03	2.66E-03	1.20E-03	8.00E-03
Dibenzofuran	0.09E-03	0.03E-03	0.03E-03	0.06 E-03	0.34E-03	0.07E-03	0.13E-03	bdl
Dibenzo-*p*-dioxin	bdl	0.01E-03	bdl	bdl	bdl	bdl	bdl	bdl
4-Monochlorodibenzofuran	1.17E-03	1.81E-03	0.38E-03	0.24E-03	0.30E-03	1.25E-03	0.27E-03	0.34E-03
1-Monochlorodibenzondioxin	74.0E-03	121E-03	20.0E-03	6.96E-03	4.57E-03	13.7E-03	5.19E-03	11.2E-03
4,6-Dichlorodibenzofuran	33.6E-03	34.6E-03	4.39E-03	7.54E-03	2.31E-03	9.82E-03	6.29E-03	1.12E-03
2,7-Dichlorodibenzodioxin	97.3E-03	216E-03	39.1E-03	15.0E-03	1.84E-03	18.2E-03	3.07E-03	1.08E-03
1,3,7-Trichlorodibenzodioxin	72.9E-03	75.3E-03	28.0E-03	14.8E-03	0.55E-03	7.42E-03	0.54E-03	bdl
2,3,7,8-Tetrachlorodibenzodioxin	48.8E-03	11.1E-03	0.47E-03	4.07E-03	0.19E-03	2.97E-03	0.19E-03	bdl
Total PCDD/F	0.33	0.46	0.09	0.05	0.01	0.05	0.02	0.01
bdl-Below Detection Limit								

4.4 Thermal Degradation of 2-Monochlorophenol over 1%Fe$_2$O$_3$/SiO$_2$

4.4.1 Pyrolytic Conditions

The temperature dependence of the surface-mediated pyrolysis of 2-MCP over 1%Fe$_2$O$_3$/SiO$_2$ and the yields of major organic products are presented below. Significant catalytic degradation of 2-MCP occurred at 200 °C, with 20% of the initial reactant remaining undestroyed. Rapid decomposition was observed at above 300 °C, achieving almost complete degradation of 2-MCP by 400 °C (Figure 4.19). Chlorophenols and chlorobenzenes were the major aromatic products, with maximum yield of 0.04% of 2,4 and 2,6-DCP at 350 °C, 0.03 % of MCBz at 550 °C (Figure 4.19 and Figure 4.20). 2-chloro-1-benzofuran (CBF) and 5,7-dichlorobenzofuran (DCBF) were also observed with the maximum yields of 0.03 % and 0.001% at 400 °C, respectively (Figure 4.21). The observed dioxin products were: DD, DF, 1-MCDD, 4-MCDF and 4,6-DCDF. The maximum yields of 4-MCDF and 4,6-DCDF were at 400 and 275 °C, respectively whereas DD and 1-MCDD exhibited maximum yields at 350 °C (Figure 4.22).
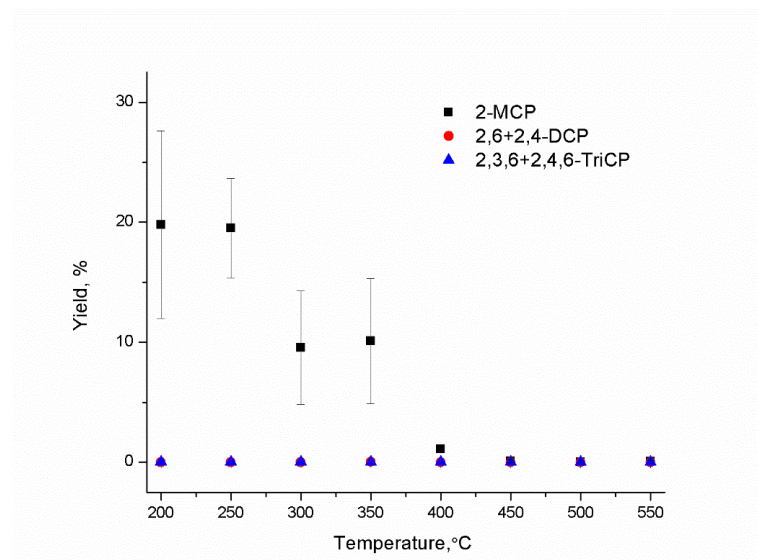
Figure 4.19. Chlorophenol Yields and Precursor Conversion from Pyrolysis of 2-MCP over 1% Fe$_2$O$_3$/SiO$_2$
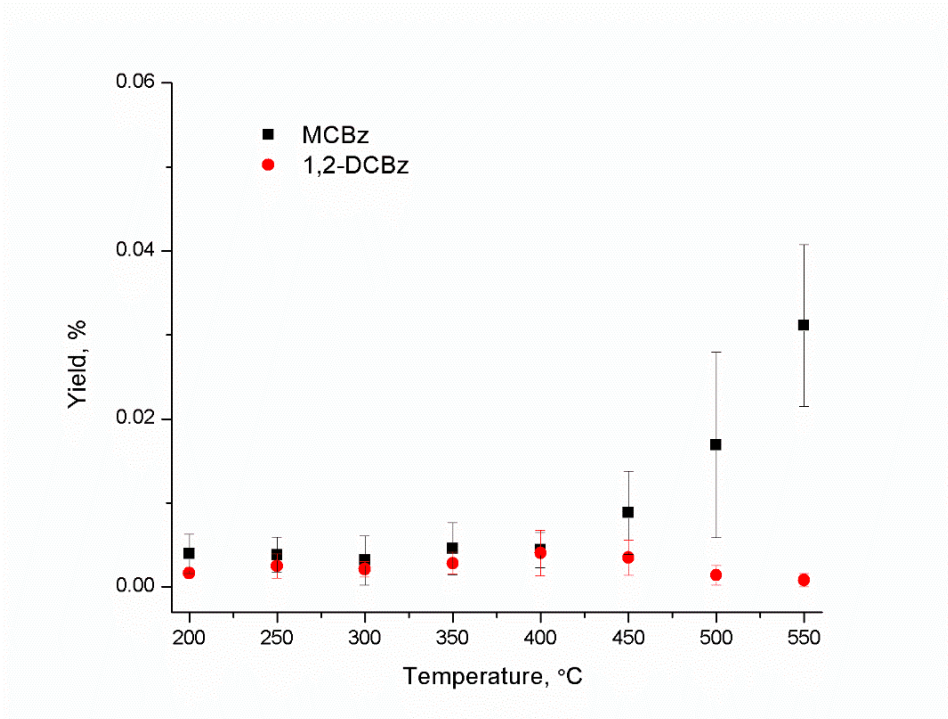
Figure 4.20. Chlorobenzene Yields from Pyrolysis of 2-MCP over 1% Fe_2O_3/SiO_2
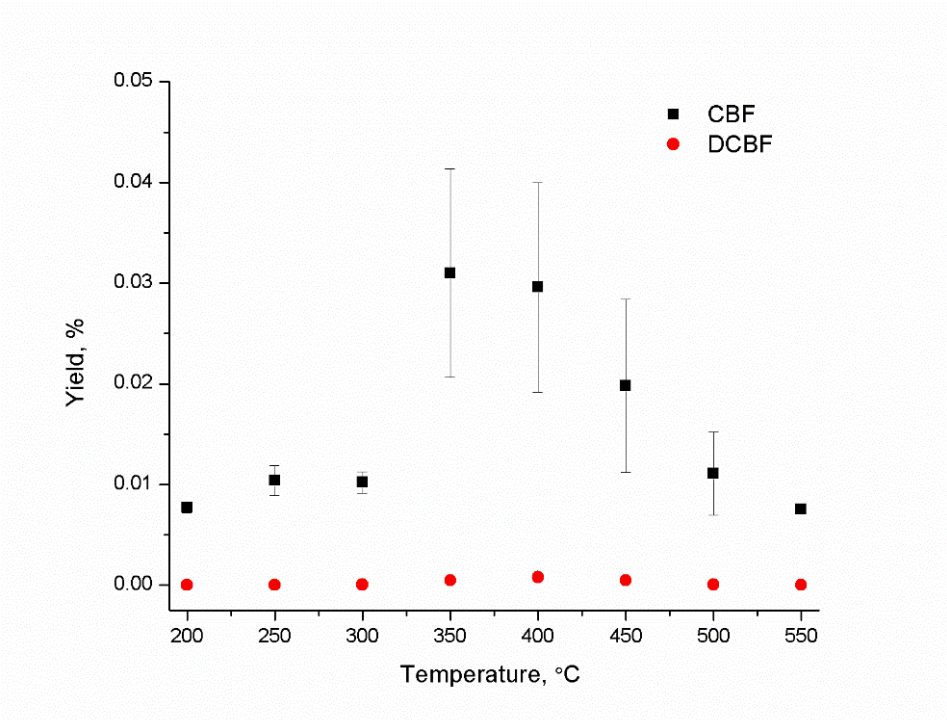
Figure 4.21. Chlorobenzofuran Yields from Pyrolysis of 2-MCP over 1% Fe_2O_3/SiO_2
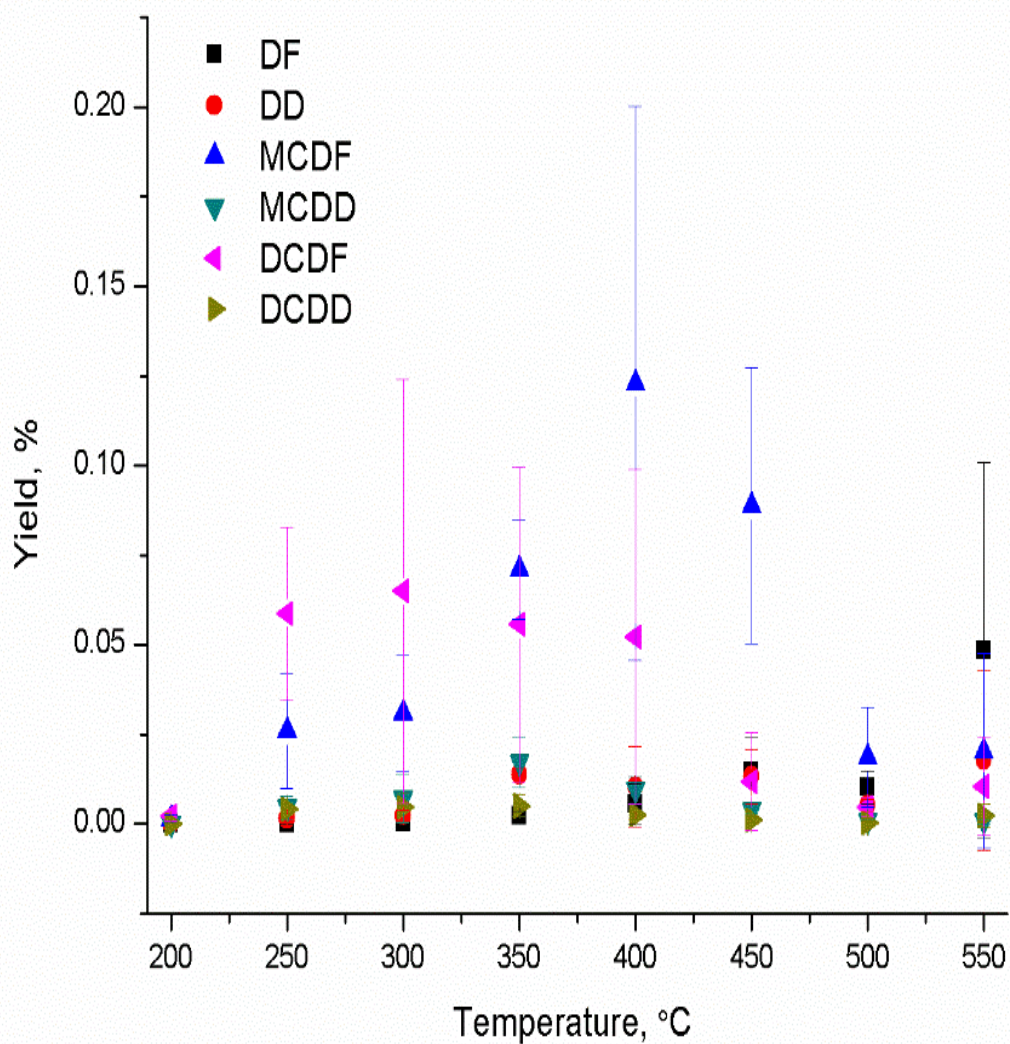
Figure 4.22. Major PCDD/F Yields from Pyrolysis of 2-MCP over 1% Fe_2O_3/SiO_2

Table 4.7. Dioxin and Non-Dioxin Products and Percent Yields from Pyrolysis of 2-Monochlorophenol over 1% Fe_2O_3/SiO_2 surface

Products	Reaction Temperature (°C)							
	200	250	300	350	400	450	500	550
Monochlorobenzene	3.97E-03	3.83E-03	3.16E-03	4.55E-03	4.41E-03	8.84E-03	16.9E-03	31.1E-03
2-Monochlorophenol	20	19	10.6	10.3	10	95.2E-03	33.8E-03	65.8E-03
1,2-Dichlorobenzene	1.64E-03	2.49E-03	2.11E-03	2.82E-03	4.04E-03	3.49E-03	1.39E-03	0.82E-03
2,4+2,6-Dichlorophenol	3.03E-03	8.52E-03	7.48E-03	35.4E-03	6.20E-03	0.84E-03	0.27E-03	1.08E-03
1,2,3+1,2,4-Trichlorobenzene	bdl	0.01E-03	bdl	0.02E-03	0.04E-03	0.05E-03	0.02E-03	0.01E-03
3-Chloro-1-benzofuran	7.71E-03	10.4E-03	10.2E-03	31.0E-03	29.6E-03	19.8E-03	11.1E-03	7.50E-03
5,7-Dichlorobenzofuran	bdl	0.01E-03	0.04E-03	0.48E-03	0.78E-03	0.47E-03	0.03E-03	0.01E-03
2,3,6+2,4,6-Trichlorophenol	0.12E-03	0.19E-03	0.16E-03	0.40E-03	0.29E-03	0.27E-03	0.14E-03	0.60E-03
Dibenzofuran	0.04E-03	0.15E-03	0.35E-03	2.36E-03	5.56E-03	14.6E-03	10.2E-03	48.5E-03
Dibenzo-p-dioxin	0.04E-03	1.59E-03	2.31E-03	13.9E-03	10.5E-03	13.3E-03	5.29E-03	17.8E-03
4-Monochlorodibenzofuran	1.59E-03	26.0E-03	31.0E-03	71.0E-03	123E-03	88.8E-03	18.6E-03	20.4E-03
1-Monochlorodibenzondioxin	0.06E-03	4.60E-03	7.14E-03	17.3E-03	9.59E-03	3.91E-03	0.81E-03	0.77E-03
4,6-Dichlorodibenzofuran	2.21E-03	58.8E-03	65.0E-03	55.7E-03	52.3E-03	11.7E-03	4.78E-03	10.6E-03
2,7-Dichlorodibenzodioxin	0.13E-03	4.08E-03	4.66E-03	5.13E-03	2.58E-03	1.09E-03	0.23E-03	2.38E-03
1,3,7-Trichlorodibenzodioxin	0.01E-03	0.07E-03	0.24E-03	0.08E-03	0.02E-03	0.02E-03	0.01E-03	0.10E-03
Total PCDD/F	4.08E-03	0.10	0.11	0.17	0.20	0.13	0.04	0.1
bdl-Below Detection Limit								

4.4.2 Oxidative Conditions

The temperature dependence of the surface-mediated oxidation of 2-MCP over $1\%Fe_2O_3/SiO_2$ and the yields of major organic products are presented below. At the lowest temperature we studied of 200 °C, 85% of the 2-MCP undergoes surface mediated decomposition, above 200 °C, the reaction rapidly accelerates resulting in almost complete degradation of 2-MCP by 400 °C. The main products were chlorophenols, chlorobenzenes, PCDD/Fs, and chlorobenzofurans. Chlorophenols have higher yields than chlorobenzenes, with the maximum yields of 0.06% for 2,4- and 2,6-dichlorophenols at lower temperature region (200-250 °C). Chlorobenzene products are all trace amount, dichlorobenzene has the maximum yield of 0.015% at 350 °C and monochlorobenzene (MCBz) has a constant yield of 0.006% across the temperature range from 200-450 °C. 1,2,4- and 1,2,3-trichlorobeneze (TriCBz) has the maximum yield of 0.002% at 450 °C. Figure 4.23 and Figure 4.24 depicts the yields of chlorophenols and chlorobenzenes respectively from the oxidation of 2-MCP over $1\%Fe_2O_3/SiO_2$ surface.

In addition to PCDD/Fs, single benzene ring compounds including chlorobenezenefuran (CBF) and dichlorobenezenefuran (DCBF) are also produced from oxidation of 2-MCP over $1\%Fe_2O_3/SiO_2$ surface. As shown in Figure 4.25, CBF and DCBF have the maximum yields of 0.012% and 0.004% at 350 °C, respectively.

Compared to chlorobenzenes and chlorophenols, significant amounts of PCDD/Fs were produced at 350 °C, with the maximum yield of 0.11% of 4,6-DCDF and the maximum yield of 0.03% for both 1- MCDD and DCDD (Figure 4.26).
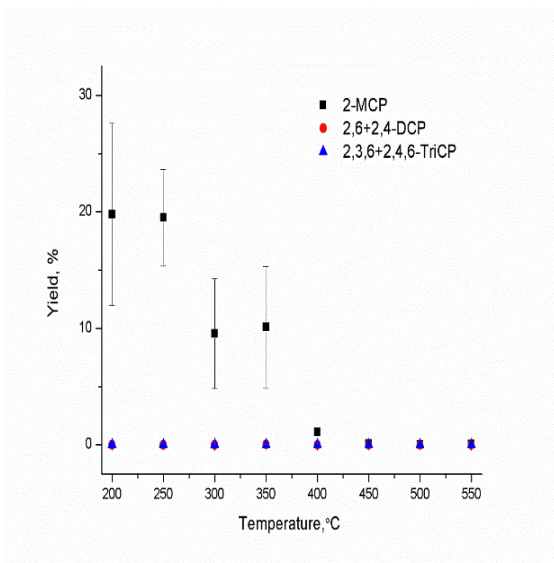
Figure 4.23. Chlorophenol Yields and Precursor Conversion from Oxidation of 2-MCP over 1% Fe_2O_3/SiO_2
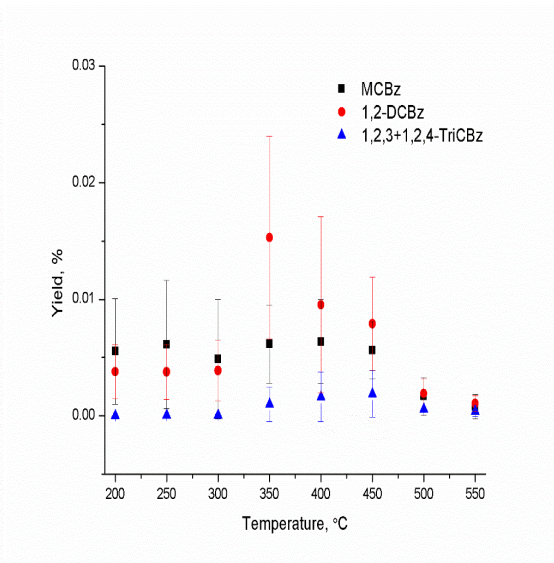
Figure 4.24. Chlorobenzenes Yield from Oxidation of 2-MCP over 1% Fe_2O_3/SiO_2
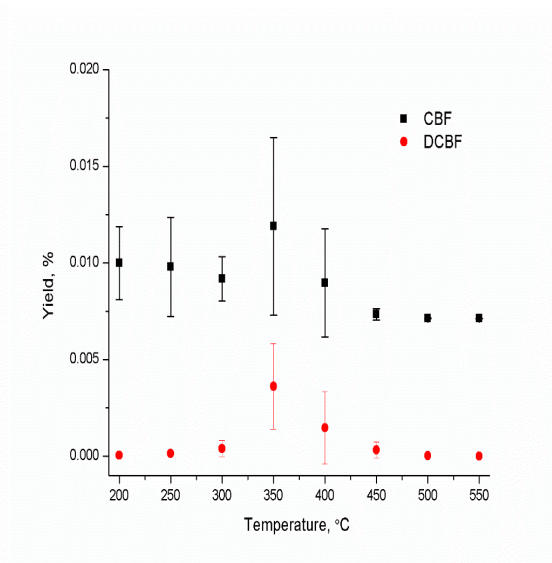
Figure 4.25. Major PCDD/F Yields from Oxidation of 2-MCP over 1% Fe_2O_3/SiO_2
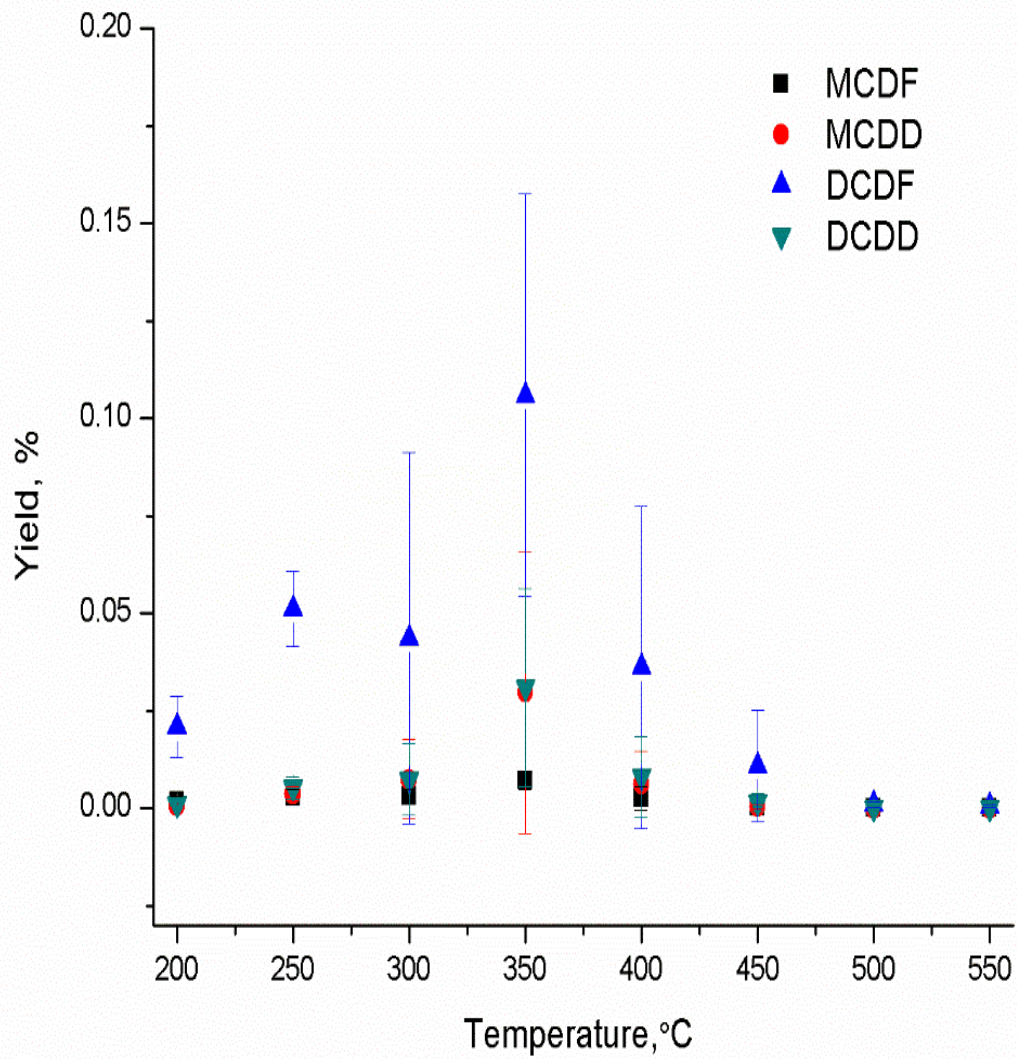
Figure 4.26. Major PCDD/F Yield from Oxidation of 2-MCP over 1% Fe_2O_3/SiO_2

Table 4.8. Dioxin and Non-Dioxin Products and Percent Yields from Oxidation of 2-Monochlorophenol over 1% Fe_2O_3/SiO_2 Surface

Products	Reaction Temperature (°C)							
	200	250	300	350	400	450	500	550
Monochlorobenzene	5.53E-03	6.12E-03	4.86E-03	6.15E-03	6.36E-03	5.64E-03	1.68E-03	0.78E-03
2-Monochlorophenol	15	3.2	2.5	794E-03	70.9E-03	68.5E-03	84.9E-03	95.6E-03
1,2-Dichlorobenzene	3.79E-03	3.76E-03	3.88E-03	15.3E-03	9.52E-03	7.89E-03	1.92E-03	1.05E-03
2,4+2,6-Dichlorophenol	64.7E-03	62.0E-03	32.4E-03	37.2E-03	5.45E-03	0.38E-03	0.97E-03	0.41E-03
1,2,3+1,2,4-Trichlorobenzene	0.02E-03	0.04E-03	0.06E-03	1.01E-03	1.62E-03	1.89E-03	0.57E-03	0.40E-03
3-Chloro-1-benzofuran	10.0E-03	9.80E-03	9.18E-03	11.9E-03	8.97E-03	7.35E-03	7.14E-03	7.13E-03
5,7-Dichlorobenzofuran	0.05E-03	0.14E-03	0.39E-03	3.62E-03	1.47E-03	0.32E-03	0.02E-03	bdl
1,2,3,4+1,2,3,5-Tetrachlorobenzene	bdl	bdl	bdl	0.07E-03	0.13E-03	0.16E-03	0.10E-03	0.11E-03
2,3,6+2,4,6-Trichlorophenol	2.49E-03	3.28E-03	3.32E-03	8.85E-03	1.49E-03	0.44E-03	0.94E-03	0.52E-03
Dibenzofuran	0.02E-03	0.02E-03	0.05E-03	0.03E-03	0.01E-03	0.01E-03	0.01E-03	0.02E-03
Dibenzo-*p*-dioxin	0.04E-03	0.07E-03	1.37E-04	0.36E-03	0.14E-03	bdl	bdl	bdl
4-Monochlorodibenzofuran	1.91E-03	2.99E-03	3.03E-03	7.20E-03	2.73E-03	0.49E-03	0.06E-03	bdl
1-Monochlorodibenzondioxin	0.68E-03	3.71E-03	7.46E-03	29.7E-03	6.24E-03	0.54E-03	0.03E-03	bdl
4,6-Dichlorodibenzofuran	20.9E-03	51.2E-03	43.7E-03	106E-03	36.2E-03	11.0E-03	1.01E-03	0.54E-03
2,7-Dichlorodibenzodioxin	1.09E-03	5.31E-03	7.43E-03	31.1E-03	8.12E-03	1.63E-03	0.07E-03	0.04E-03
1,3,7-Trichlorodibenzodioxin	0.67E-03	0.57E-03	0.96E-03	4.54E-03	1.16E-03	0.26E-03	0.05E-03	bdl
2,3,7,8-Tetrachlorodibenzodioxin	0.01E-03	0.01E-03	0.03E-03	0.20E-03	bdl	bdl	bdl	bdl
Total PCDD/F	0.03	0.06	0.06	0.18	0.05	0.014	1.23E-03	0.6E-03
bdl-Below Detection Limit								

4.5 Thermal Degradation of 2-Monochlorophenol over 2.5%Fe$_2$O$_3$/SiO$_2$

4.5.1 Pyrolytic Conditions

The temperature dependence of the surface-mediated pyrolysis of 2-MCP over 2.5%Fe$_2$O$_3$/SiO$_2$ and the yields of major organic products are presented below. The catalytic degradation of 2-MCP occurred at 200 °C. Compared with the 80% of 2-MCP degradation on 1%Fe$_2$O$_3$/SiO$_2$ surface, only 60% of the initial reactant were destroyed at 200 °C. Rapid decomposition reaction followed above 300 °C, achieving almost complete degradation of 2-MCP by 400 °C (Figure 4.27). Chlorophenols and chlorobenzenes were the major aromatic products; the yields of chlorophenol were greater than chlorobenzenes. The maximum yield of 2,4 and 2,6-DCP were observed at 300 °C with the value of 0.05%. The maximum yield of MCB and DCBz were 0.016% and 0.006% at 400 and 350 °C, respectively (Figure 4.28).

The maximum yields of CBF and DCBF were 0.03 % and 0.002% at 350 °C, respectively (Figure 4.29).

Compared to chlorophenols and chlorobenzenes, significant amount of PCDD/F were produced on pyrolysis of 2-MCP on 2.5%Fe$_2$O$_3$/SiO$_2$ (Figure 3.30). The observed dioxin products were: DD, DF, 1-MCDD, 4-MCDF and 4,6-DCDF with the yields of 4,6-DCDF> 4-MCDF > 1-MCDD > DCDD > DF > DD. The maximum yields of 4,6-DCDF and 4-MCDF were at 250 and 300 °C, respectively whereas 1-MCDD and DCDD exhibited maximum yields at 300 °C. The maximum yields of 4,6-DCDF and 4-MCDF were 0.22% and 0.14%, respectively.
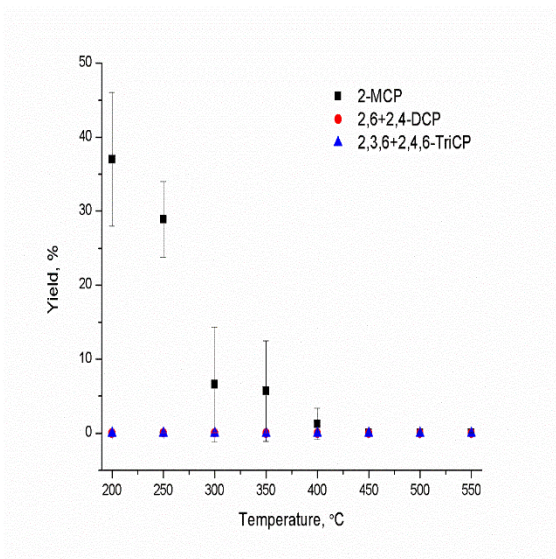
Figure 4.27. Chlorophenol Yields and Precursor Conversion from Pyrolysis of 2-MCP over 2.5% Fe_2O_3/SiO_2
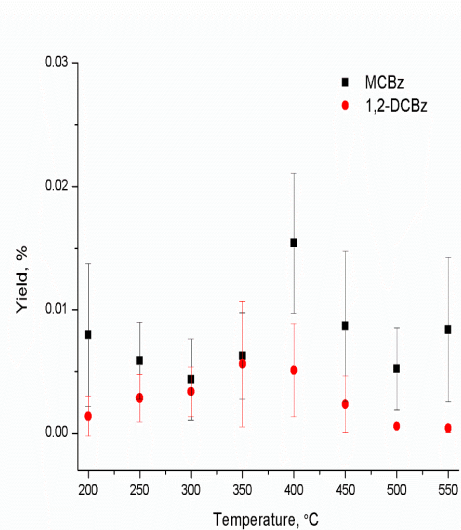
Figure 4.28. Chlorobenzene Yields from Pyrolysis of 2-MCP over 2.5% Fe_2O_3/SiO_2
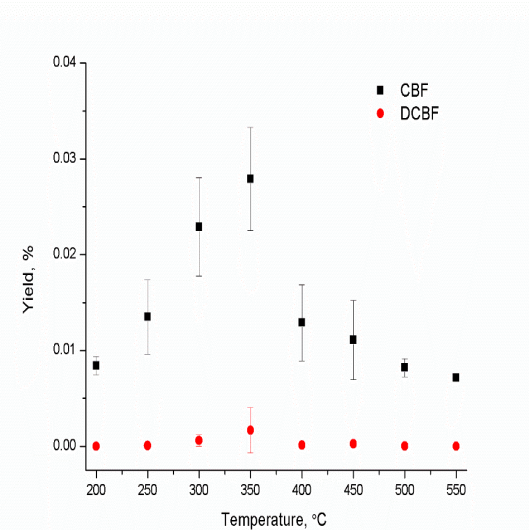
Figure 4.29. Chlorobenzofuran Yields from Pyrolysis of 2-MCP over 2.5% Fe_2O_3/SiO_2
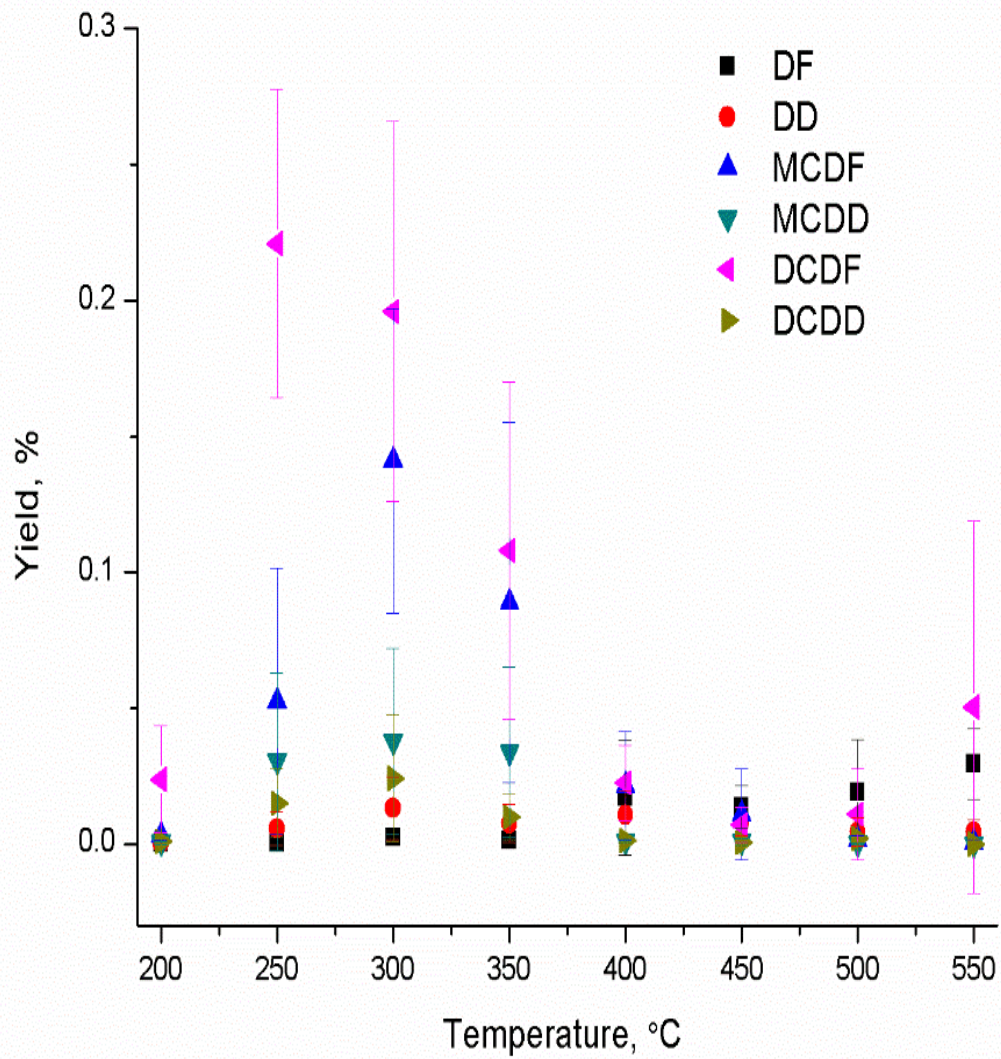
Figure 4.30. Major PCDD/F Yields from Pyrolysis of 2-MCP over 2.5% Fe_2O_3/SiO_2

Products	Reaction Temperature (°C)							
	200	250	300	350	400	450	500	550
Monochlorobenzene	7.96E-03	5.88E-03	4.36E-03	6.27E-03	15.4E-03	8.66E-03	5.22E-03	8.39E-03
2-Monochlorophenol	37	29	6.6	5.7	1.3	38.0E-03	29.8E-03	46.8E-03
1,2-Dichlorobenzene	1.38E-03	2.86E-03	3.37E-03	5.62E-03	5.11E-03	2.35E-03	0.57E-03	0.40E-03
2,4+2,6-Dichlorophenol	6.36E-03	33.8E-03	41.9E-03	12.1E-03	0.14E-03	0.22E-03	0.10E-03	0.36E-03
1,2,3+1,2,4-Trichlorobenzene	0.02E-03	0.03E-03	0.03E-03	0.03E-03	bdl	0.02E-03	0.01E-03	0.04E-03
3-Chloro-1-benzofuran	8.42E-03	13.5E-03	22.9E-03	27.9E-03	12.9E-03	11.1E-03	8.21E-03	7.16E-03
5,7-Dichlorobenzofuran	0.01E-03	0.06E-03	0.61E-03	1.67E-03	0.12E-03	0.25E-03	0.04E-03	bdl
2,3,6+2,4,6-Trichlorophenol	0.25E-03	0.33E-03	0.81E-03	0.85E-03	0.04E-03	0.09E-03	0.09E-03	0.17E-03
Dibenzofuran	0.06E-03	0.22E-03	2.34E-03	1.27E-03	17.1E-03	13.5E-03	18.8E-03	29.4E-03
Dibenzo-*p*-dioxin	0.18E-03	5.58E-03	13.3E-03	7.57E-03	10.6E-03	8.27E-03	4.36E-03	4.43E-03
4-Monochlorodibenzofuran	3.16E-03	52.6E-03	141E-03	88.9E-03	21.5E-03	10.9E-03	1.71E-03	0.72E-03
1-Monochlorodibenzondioxin	0.51E-03	30.5E-03	37.7E-03	33.9E-03	0.91E-03	0.83E-03	0.07E-03	0.05E-03
4,6-Dichlorodibenzofuran	23.8E-03	221E-03	196E-03	108E-03	22.5E-03	6.98E-03	11.0E-03	50.5E-03
2,7-Dichlorodibenzodioxin	0.96E-03	15.1E-03	24.2E-03	9.95E-03	1.31E-03	0.57E-03	2.12E-03	0.04E-03
1,3,7-Trichlorodibenzodioxin	0.05E-03	0.20E-03	0.46E-03	0.12E-03	bdl	bdl	bdl	bdl
Total PCDD/F	0.03	0.33	0.42	0.25	0.07	0.04	0.04	0.09
bdl-Below Detection Limit								

Table 4.9. Dioxin and Non-Dioxin Products and Percent Yields from Pyrolysis of 2-Monochlorophenol over 2.5% Fe_2O_3/SiO_2 surface

4.5.2 Oxidative Conditions

The temperature dependence of the surface-mediated oxidation of 2-MCP over 2.5%Fe_2O_3/SiO_2 and the yields of major organic products are presented below. The catalytic degradation of 2-MCP occurred at 200 °C. Compared with only 60% of 2-MCP degraded on 2.5%Fe_2O_3/SiO_2 at 200 °C under pyrolysis, 85% of the 2-MCP were destroyed under oxidation. Then decomposition reaction accelerated above 200 °C, with almost complete degradation of 2-MCP by 350 °C (Figure 4.31). Chlorophenols and chlorobenzenes were the major aromatic products; the yields of chlorophenol were greater than chlorobenzenes. The maximum yield of 2,4 and 2,6-DCP were observed at 250 °C with the value of 0.07%. The maximum yield of MCB and DCBz were 0.01% at 350 °C (Figure 4.32).

The maximum yields of CBF and DCBF were 0.01 % and 0.001% at 300 °C, respectively (Figure 4.33).

Under oxidation conditions, comparable amount of PCDD/F were produced on 2.5%Fe_2O_3/SiO_2 (Figure 4.34). The observed dioxin products were: 1-MCDD, 4-MCDF and 4,6-DCDF, DCDD with the yields of 4,6-DCDF > DCDD > 1-MCDD > 4-MCDF. The maximum yields of 4,6-DCDF were at 250 °C with a value of 0.09%, 1-MCDD and DCDD exhibited maximum yields at 300 °C. with the value of 0.02% and 0.01%, respectively.
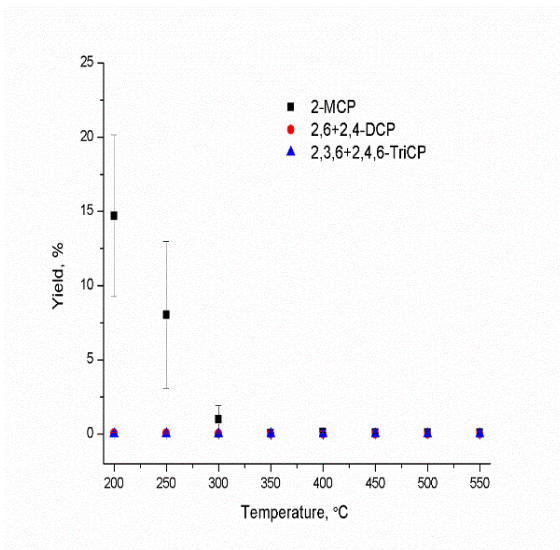
Figure 4.31. Chlorophenol Yields and Precursor Conversion from Oxidation of 2-MCP over 2.5% Fe_2O_3/SiO_2
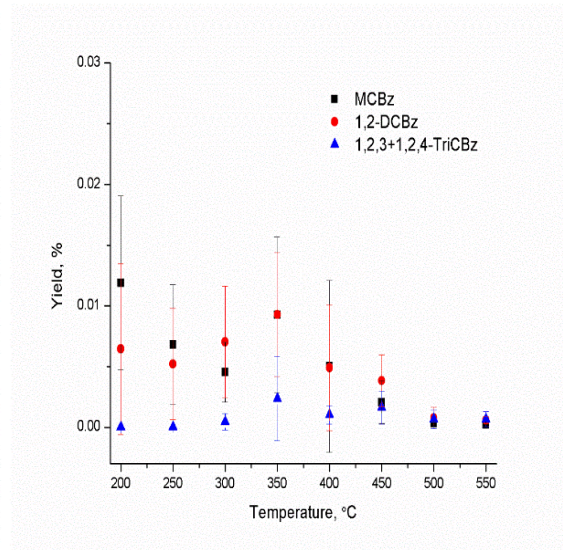
Figure 4.32. Chlorobenzene Yields from Oxidation of 2-MCP over 2.5% Fe_2O_3/SiO_2
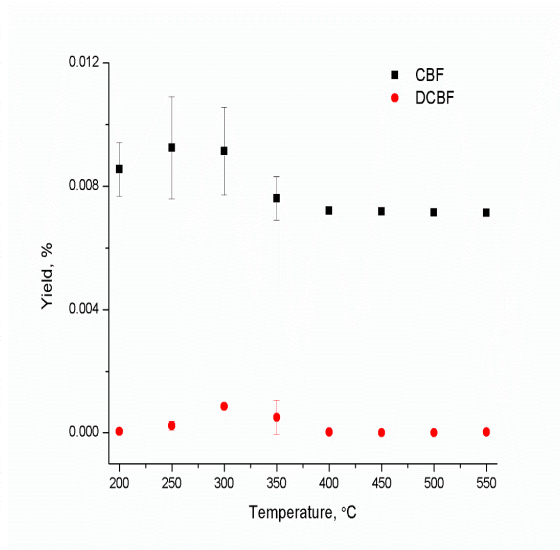
Figure 4.33. Chlorobenzofuran Yields from Oxidation of 2-MCP over 2.5% Fe_2O_3/SiO_2

74
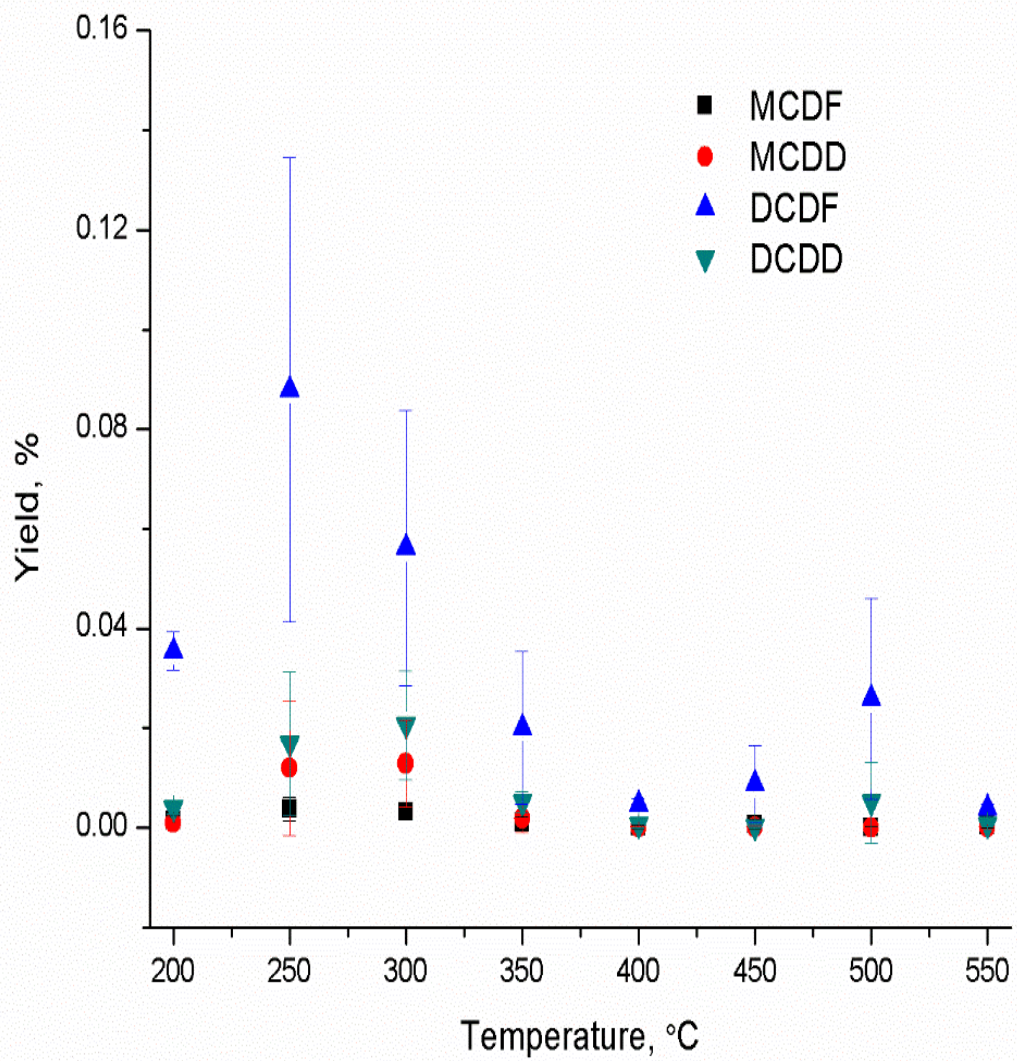
Figure 4.34. Major PCDD/F Yields from Oxidation of 2-MCP over 2.5% Fe_2O_3/SiO_2

Table 4.10. Dioxin and Non-Dioxin Products and Percent Yields from Oxidation of 2-Monochlorophenol over 2.5% Fe$_2$O$_3$/SiO$_2$								
Products	Reaction Temperature (°C)							
	200	250	300	350	400	450	500	550
Monochlorobenzene	11.9E-03	6.79E-03	4.54E-03	9.26E-03	5.02E-03	2.05E-03	0.31E-03	0.19E-03
2-Monochlorophenol	15	8.0	977E-03	37.0E-03	106E-03	78.5E-03	94.2E-03	89.9E-03
1,2-Dichlorobenzene	6.45E-03	5.21E-03	7.03E-03	9.28E-03	4.91E-03	3.84E-03	0.77E-03	0.60E-03
2,4+2,6-Dichlorophenol	55.2E-03	65.3E-03	33.8E-03	2.37E-03	1.18E-03	1.05E-03	0.19E-03	0.48E-03
1,2,3+1,2,4-Trichlorobenzene	bdl	0.04E-03	0.46E-03	2.38E-03	1.04E-03	1.63E-03	0.66E-03	0.68E-03
3-Chloro-1-benzofuran	8.55E-03	9.25E-03	9.14E-03	7.61E-03	7.20E-03	7.18E-03	7.15E-03	7.14E-03
5,7-Dichlorobenzofuran	0.05 E-03	0.24E-03	0.86E-03	0.50E-03	0.03E-03	bdl	bdl	0.03 E-03
1,2,3,4+1,2,3,5-Tetrachlorobenzene	bdl	bdl	0.04E-03	0.24E-03	0.11E-03	0.18E-03	0.07E-03	0.33E-03
2,3,6+2,4,6-Trichlorophenol	2.58E-03	3.94E-03	3.24E-03	0.83E-03	0.50E-03	0.79E-03	0.30E-03	0.85E-03
Dibenzofuran	0.02E-03	0.03E-03	0.03E-03	0.03E-03	0.03E-03	0.03E-03	0.02E-03	0.01E-03
Dibenzo-*p*-dioxin	0.05E-03	0.18E-03	0.12E-03	0.04E-03	0.02E-03	0.02E-03	bdl	0.02E-03
4-Monochlorodibenzofuran	1.33E-03	3.72E-03	3.25E-03	1.00E-03	0.26E-03	0.70E-03	0.08E-03	0.40E-03
1-Monochlorodibenzondioxin	1.04E-03	12.0E-03	12.9E-03	1.88E-03	0.10E-03	0.16E-03	0.07E-03	0.18E-03
4,6-Dichlorodibenzofuran	35.5E-03	88.0E-03	56.2E-03	20.1E-03	4.72E-03	8.81E-03	25.9E-03	3.95E-03
2,7-Dichlorodibenzodioxin	4.06E-03	16.9E-03	20.6E-03	5.21E-03	0.66E-03	0.29E-03	5.07E-03	0.63E-03
1,3,7-Trichlorodibenzodioxin	0.63E-03	1.00E-03	2.00E-03	0.62E-03	0.03E-03	0.03E-03	0.01E-03	0.03E-03
Total PCDD/F	0.04	0.12	0.095	0.03	5.82E-03	0.01	0.03	5.22E-03
bdl-Below Detection Limit								

4.6 Thermal Degradation of 2-Monochlorophenol over 4%Fe_2O_3/SiO_2

4.6.1 Pyrolytic Conditions

The temperature dependence of the surface-mediated pyrolysis of 2-MCP over 4%Fe_2O_3/SiO_2 and the yields of major organic products are presented below. The catalytic degradation of 2-MCP occurred at 200 °C, 80% of the 2-MCP were destroyed. Then decomposition reaction accelerated above 200 °C, with almost complete degradation of 2-MCP by 350 °C (Figure 4.35). Chlorophenols and chlorobenzenes were the major aromatic products; the yields of chlorophenol were greater than chlorobenzenes. The maximum yield of 2,4 and 2,6-DCP were observed at 250 °C with the value of 0.05%. The maximum yield of MCB and DCBz were 0.0035% and 0.0025% at 350 °C and 300 °C (Figure 4.36).

The maximum yields of CBF and DCBF were 0.025 % and 0.002% at 350 °C, respectively (Figure 4.37).

Significant amount of PCDD/F were produced on pyrolysis of 2-MCP over 4%Fe_2O_3/SiO_2 (Figure 4.38). The observed dioxin products were: 1-MCDD, 4-MCDF and 4,6-DCDF, DCDD with the yields of 4,6-DCDF > 4-MCDF > 1-MCDD > DCDD. The maximum yields of 4,6-DCDF were at 250 °C with a value of 0.27%, 4-MCDF and 1-MCDD exhibited maximum yields at 300 °C. with the value of 0.12% and 0.06%, respectively.

77
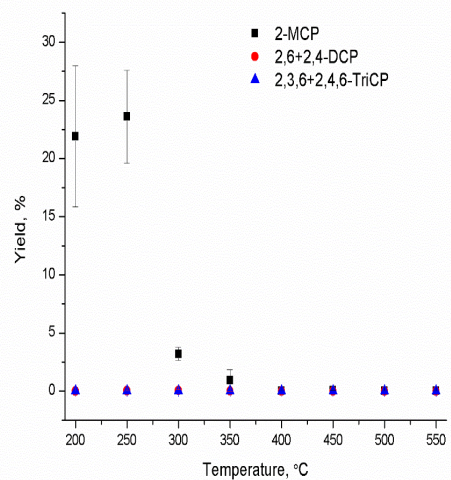
Figure 4.35. Chlorophenol Yields and Precursor Conversion from Pyrolysis of 2-MCP over 4% Fe_2O_3/SiO_2
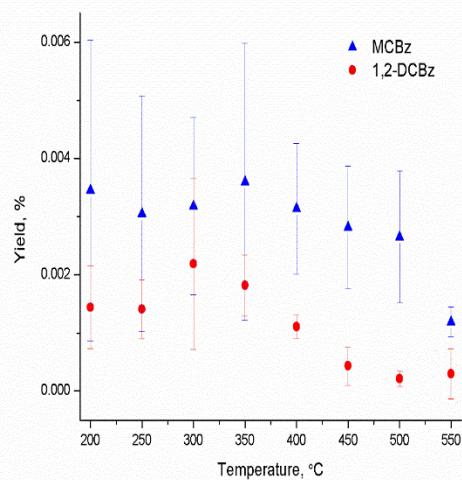
Figure 4.36. Chlorobenzene Yields from Pyrolysis of 2-MCP over 4% Fe_2O_3/SiO_2
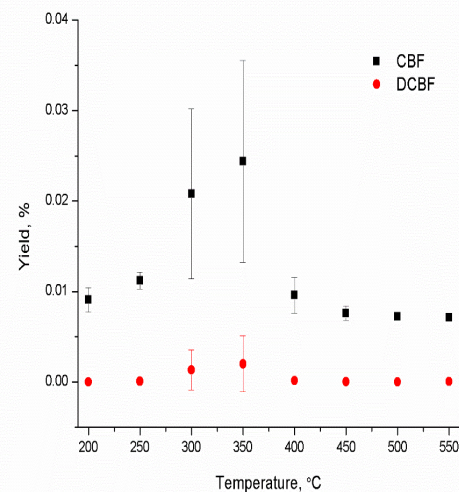
Figure 4.37. Chlorobenzofuran Yields from Pyrolysis of 2-MCP over 4% Fe_2O_3/SiO_2
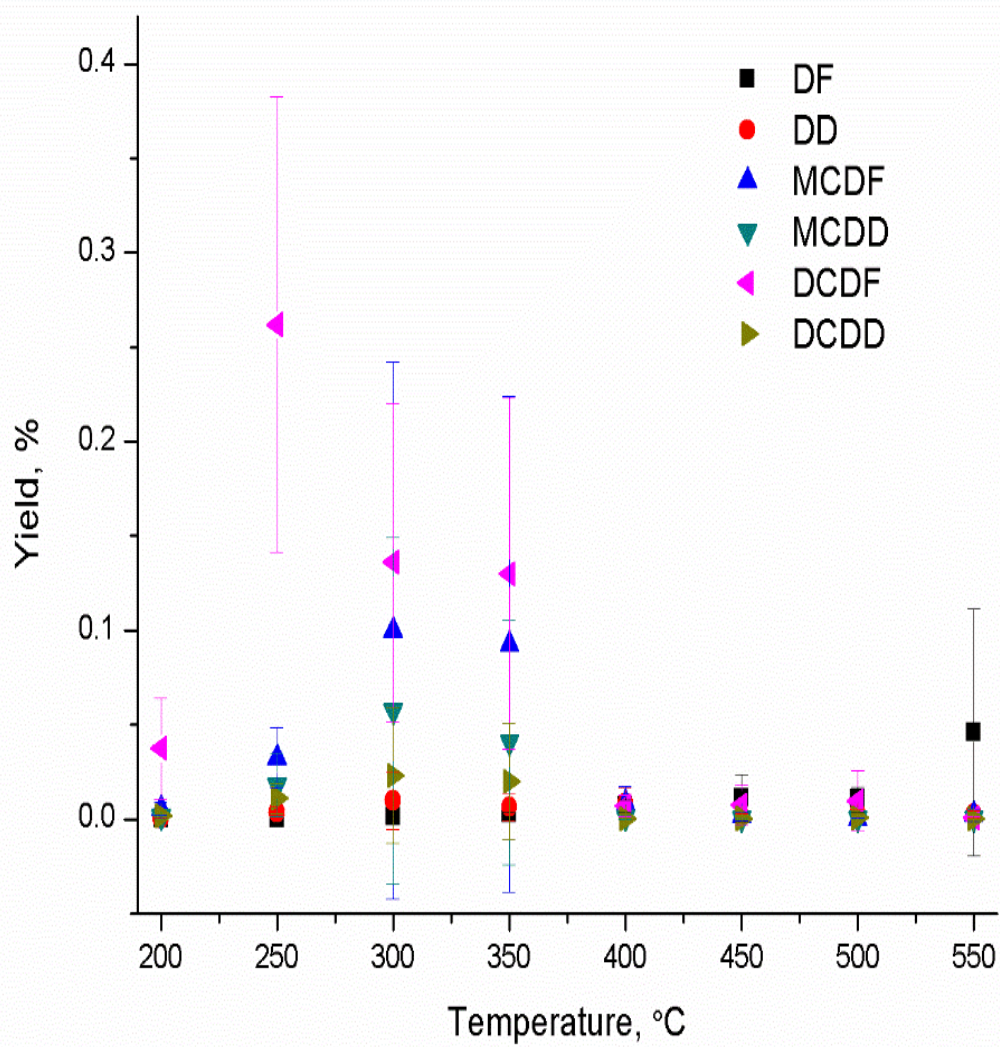
Figure 4.38. Major PCDD/F Yields from Pyrolysis of 2-MCP over 4% Fe_2O_3/SiO_2

Table 4.11. Dioxin and Non-Dioxin Products and Percent Yields from Pyrolysis of 2-Monochlorophenol over 4% Fe_2O_3/SiO_2 surface

Products	Reaction Temperature (°C)							
	200	250	300	350	400	450	500	550
Monochlorobenzene	3.45E-03	3.05E-03	3.18E-03	3.60E-03	3.14E-03	2.82E-03	2.65E-03	1.19E-03
2-Monochlorophenol	22	21	3.2	933E-03	30.7E-03	52.1E-03	34.6E-03	29.9E-03
1,2-Dichlorobenzene	1.44E-03	1.41E-03	2.19E-03	1.82E-03	1.11E-03	0.43E-03	0.21E-03	0.30E-03
2,4+2,6-Dichlorophenol	6.73E-03	32.8E-03	52.5E-03	9.49E-03	0.17E-03	0.19E-03	0.18E-03	0.35E-03
1,2,3+1,2,4-Trichlorobenzene	bdl	bdl	0.03E-03	0.04E-03	0.01E-03	bdl	0.03E-03	0.05E-03
3-Chloro-1-benzofuran	9.08E-03	11.2E-03	20.8E-03	24.4E-03	9.58E-03	7.60E-03	7.21E-03	7.14E-03
5,7-Dichlorobenzofuran	0.01E-03	0.09E-03	1.34E-03	2.01E-03	0.15E-03	0.02E-03	0.02E-03	0.04E-03
2,3,6+2,4,6-Trichlorophenol	0.11E-03	0.27E-03	1.84E-03	2.32E-03	0.04E-03	0.06E-03	0.07E-03	0.21E-03
Dibenzofuran	0.06E-03	0.14E-03	1.17E-03	2.68E-03	7.01E-03	11.0E-03	10.5E-03	45.9E-03
Dibenzo-*p*-dioxin	0.36E-03	3.53E-03	9.77E-03	6.46E-03	8.69E-03	1.88E-03	3.13E-03	2.58E-03
4-Monochlorodibenzofuran	5.66E-03	32.4E-03	100E-03	92.7E-03	8.54E-03	1.61E-03	0.30E-03	2.13E-03
1-Monochlorodibenzondioxin	1.07E-03	18.1E-03	57.3E-03	40.9E-03	0.79E-03	0.08E-03	0.04E-03	0.04E-03
4,6-Dichlorodibenzofuran	37.4E-03	262E-03	136E-03	130E-03	6.90E-03	7.63E-03	9.67E-03	0.72E-03
2,7-Dichlorodibenzodioxin	1.94E-03	11.0E-03	23.1E-03	20.1E-03	0.35E-03	0.45E-03	0.61E-03	0.21E-03
1,3,7-Trichlorodibenzodioxin	0.02E-03	0.15E-03	0.51E-03	0.60E-03	bdl	bdl	0.02E-03	0.01E-03
Total PCDD/F	0.05	0.33	0.33	0.29	0.03	0.02	0.02	0.05
bdl-Below Detection Limit								

4.6.2 Oxidative Conditions

The temperature dependence of the surface-mediated oxidation of 2-MCP over $4\%Fe_2O_3/SiO_2$ and the yields of major organic products are presented below. The catalytic degradation of 2-MCP occurred at 200 °C, about 80% of the 2-MCP were destroyed. Then decomposition reaction accelerated above 200 °C, with almost complete degradation of 2-MCP by 250 °C whereas under pyrolysis conditions, complete degradation of 2-MCP by 350 °C (Figure 4.39). Trance amounts of chlorophenols and chlorobenzenes were observed. The maximum yield of MCB and DCBz were 0.0035% and 0.003% at 200 °C and 250 °C (Figure 4.40).

The maximum yields of CBF and DCBF were 0.007 % and 0.0003% at 250 °C, respectively (Figure 4.41).

Significant amount of PCDD/F were produced on oxidation of 2-MCP over $4\%Fe_2O_3/SiO_2$ (Figure 4.42). The observed dioxin products were: 1-MCDD, 4-MCDF and 4,6-DCDF, DCDD with the yields of 4,6-DCDF > DCDD > 1-MCDD > 4-MCDF. The maximum yields of 4,6-DCDF and DCDD were at 250 °C with a value of 0.045% and 0.005%, respectively.
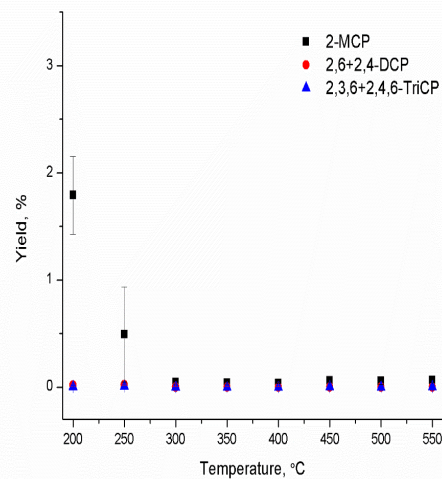
Figure 4.39. Chlorophenol Yields and Precursor Conversion from Oxidation of 2-MCP over 4% Fe_2O_3/SiO_2
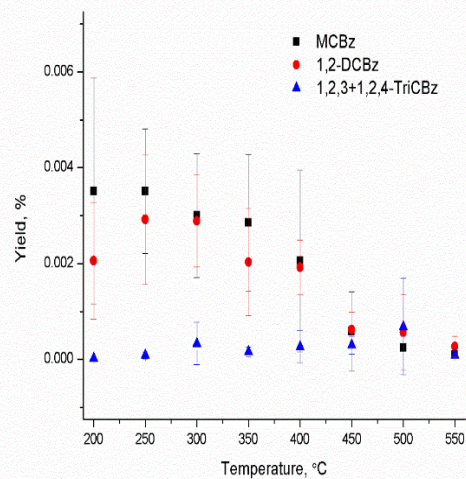
Figure 4.40. Chlorobenzene Yields from Oxidation of 2-MCP over 4% Fe_2O_3/SiO_2
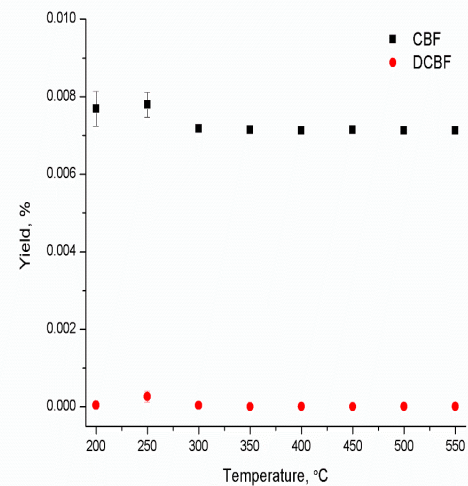
Figure 4.41. Chlorobenzofuran Yields from Oxidation of 2-MCP over 4% Fe_2O_3/SiO_2

82
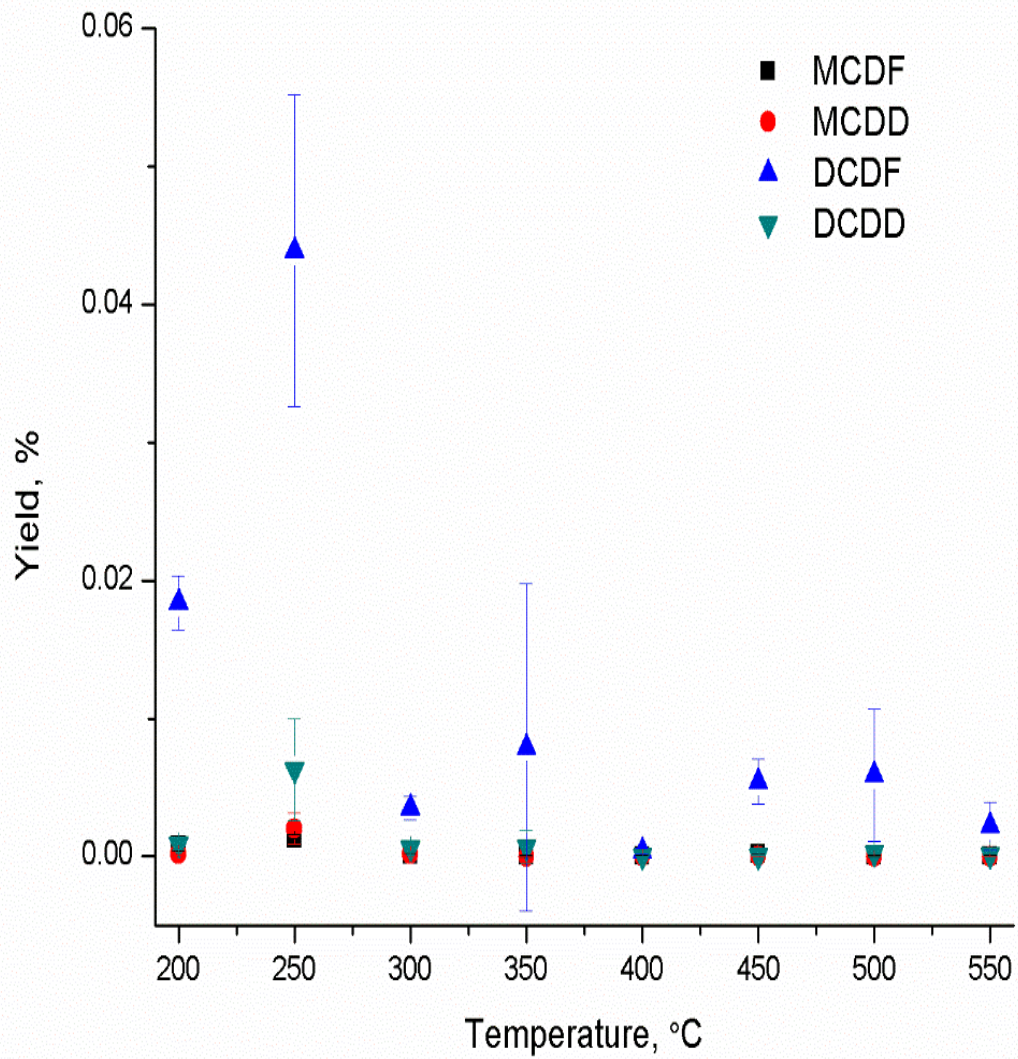
Figure 4.42. Major PCDD/F Yields from Oxidation of 2-MCP over 4% Fe_2O_3/SiO_2

Table 4.12. Dioxin and Non-Dioxin Products and Percent Yields from Oxidation of 2-Monochlorophenol over 4% Fe_2O_3/SiO_2 Surface

Products	Reaction Temperature (°C)							
	200	250	300	350	400	450	500	550
Monochlorobenzene	3.51E-03	3.51E-03	3.00E-03	2.85E-03	2.05E-03	0.58E-03	0.25E-03	0.10E-03
2-Monochlorophenol	1.8	493E-03	45.2E-03	38.5E-03	37.6E-03	62.0E-03	56.3E-03	62.8E-03
1,2-Dichlorobenzene	2.06E-03	2.92E-03	2.89E-03	2.03E-03	1.92E-03	0.62E-03	0.56E-03	0.27E-03
2,4+2,6-Dichlorophenol	18.9E-03	20.8E-03	0.82E-03	0.27E-03	0.27E-03	0.80E-03	0.19E-03	0.48E-03
1,2,3+1,2,4-Trichlorobenzene	0.02E-03	0.08E-03	0.33E-03	0.16E-03	0.26E-03	0.30E-03	0.68E-03	0.09E-03
3-Chloro-1-benzofuran	7.69E-03	7.79E-03	7.17E-03	7.14E-03	7.13E-03	7.14E-03	7.13E-03	7.13E-03
5,7-Dichlorobenzofuran	0.04E-03	0.27E-03	0.04E-03	bdl	bdl	bdl	bdl	bdl
Tetrachlorobenzene	bdl	bdl	0.03E-03	0.01E-03	0.02E-03	0.06E-03	0.09E-03	0.03E-03
2,3,6+2,4,6-Trichlorophenol	1.76E-03	4.62E-03	0.23E-03	0.15E-03	0.23E-03	0.57E-03	0.20E-03	0.45E-03
Dibenzofuran	0.04E-03	0.02E-03	0.01E-03	0.01E-03	0.01E-03	0.01E-03	0.01E-03	0.02E-03
Dibenzo-*p*-dioxin	0.02E-03	0.02E-03	bdl	bdl	bdl	bdl	bdl	bdl
4-Monochlorodibenzofuran	0.78E-03	1.22E-03	0.11E-03	0.05E-03	0.04E-03	0.15E-03	0.03E-03	0.06E-03
1-Monochlorodibenzondioxin	0.19E-03	2.01E-03	0.17E-03	0.01E-03	0.02E-03	0.02E-03	0.01E-03	0.01E-03
4,6-Dichlorodibenzofuran	18.4E-03	43.9E-03	3.52E-03	7.92E-03	0.38E-03	5.44E-03	5.92E-03	2.20E-03
2,7-Dichlorodibenzodioxin	0.88E-03	6.31E-03	0.60E-03	0.70E-03	0.06E-03	0.05E-03	0.28E-03	0.13E-03
1,3,7-Trichlorodibenzodioxin	0.12E-03	0.84E-03	0.07E-03	bdl	bdl	0.02E-03	0.27E-03	0.02E-03
Total PCDD/F	0.02	0.05	4.48E-03	8.69E-03	0.51	5.69	6.52	2.44
bdl-Below Detection Limit								

4.7 EPFRs Formation

The concentration of metals in fly ash vary greatly depending on the incineration facilities and sampling time. The analysis and characterization of transition metals in the fly ashes reveals 0.85-5.02 % iron oxide and 0.09-0.51% copper oxide. [1] The wide distribution of metal concentration raises the question of how the metal concentration affects yields and chemical reactivity of the EPFRs. Kiruri [2] investigated the effect of copper oxide concentration on the formation of EPFRs, instead of a linear correlation between the EPFRs yield and copper content, an exponential decrease in radical density per copper atom was observed between 1% and 5% CuO content for 2-MCP adsorption. Iron oxide is almost the highest concentration transition metal in combustion systems and is known to catalyze PCDD/F formation; it would be interesting to know the effect of iron content on the formation of EPFRs. Figure 4.43 and Figure 4.44 depict the EPFRs' EPR spectra and concentration of EPFRs adsorbed at 230 °C for different Fe_2O_3 content in the model fly ash, respectively. It is shown that with the increasing content of iron oxide in the model fly ash, the EPFRs concentration increased accordingly. Table 4.13 presents g-value, ΔHp-p and concentration of radical signals with changing Fe_2O_3 content in model fly ash. The g values for EPFR species were ~2.00364-2.00433, which came from the mixed of oxygen-centered and carbon-centered free radial species. [3] The surface-mediated precursor mechanism for PCDD/F formation can also be applied to mixed oxides. Indeed, the exposure of mixed metal oxide systems to the vapors of 2-MCP at 230 °C have shown the formation of EPFRs in Figure 4.45 and g-value, ΔHp-p and concentration of radical signals were listed in Table 4.14.
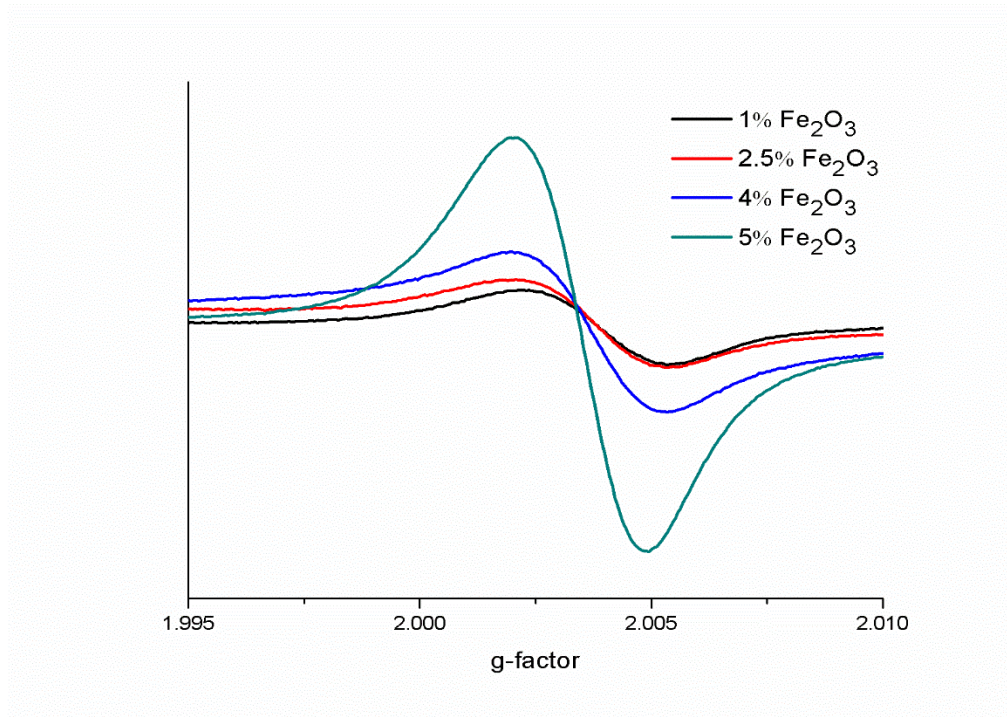
Figure 4.43. Electron Paramagnetic Resonance (EPR) Spectra of Fe_2O_3/Silica Fly Ash Surrogates Dosed with 2-MCP
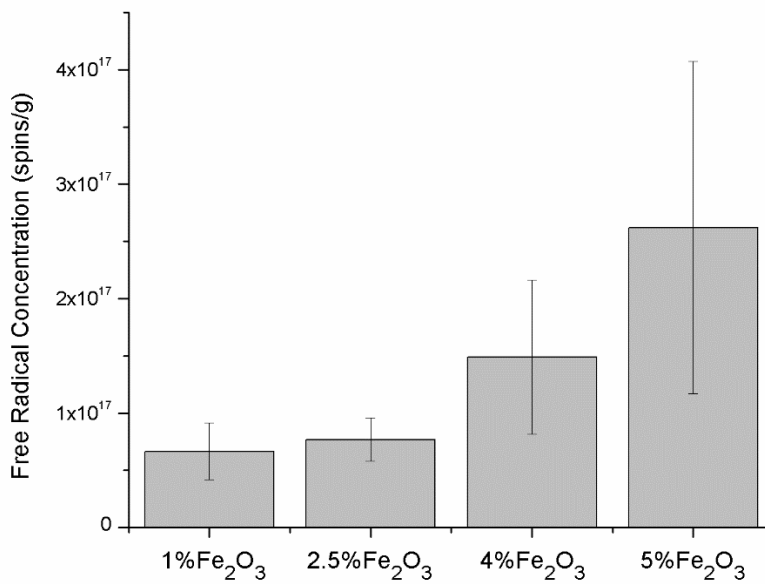
Figure 4.44. EPFRs Concentration from Different Content of Fe_2O_3 in Fly Ash Surrogates

86

Table 4.13. G value, ΔHp-p and Concentration of Radical Signals with Changing Fe_2O_3 Content in Fly Ash Surrogates			
	g factor	ΔHp-p	Spins/g
1% Fe_2O_3	2.0043	6.2	6.7E+16
2.5% Fe_2O_3	2.0041	6.1	7.7E+16
4%Fe_2O_3	2.0036	5.9	15 E+16
5%Fe_2O_3	2.0036	5.7	26 E+16
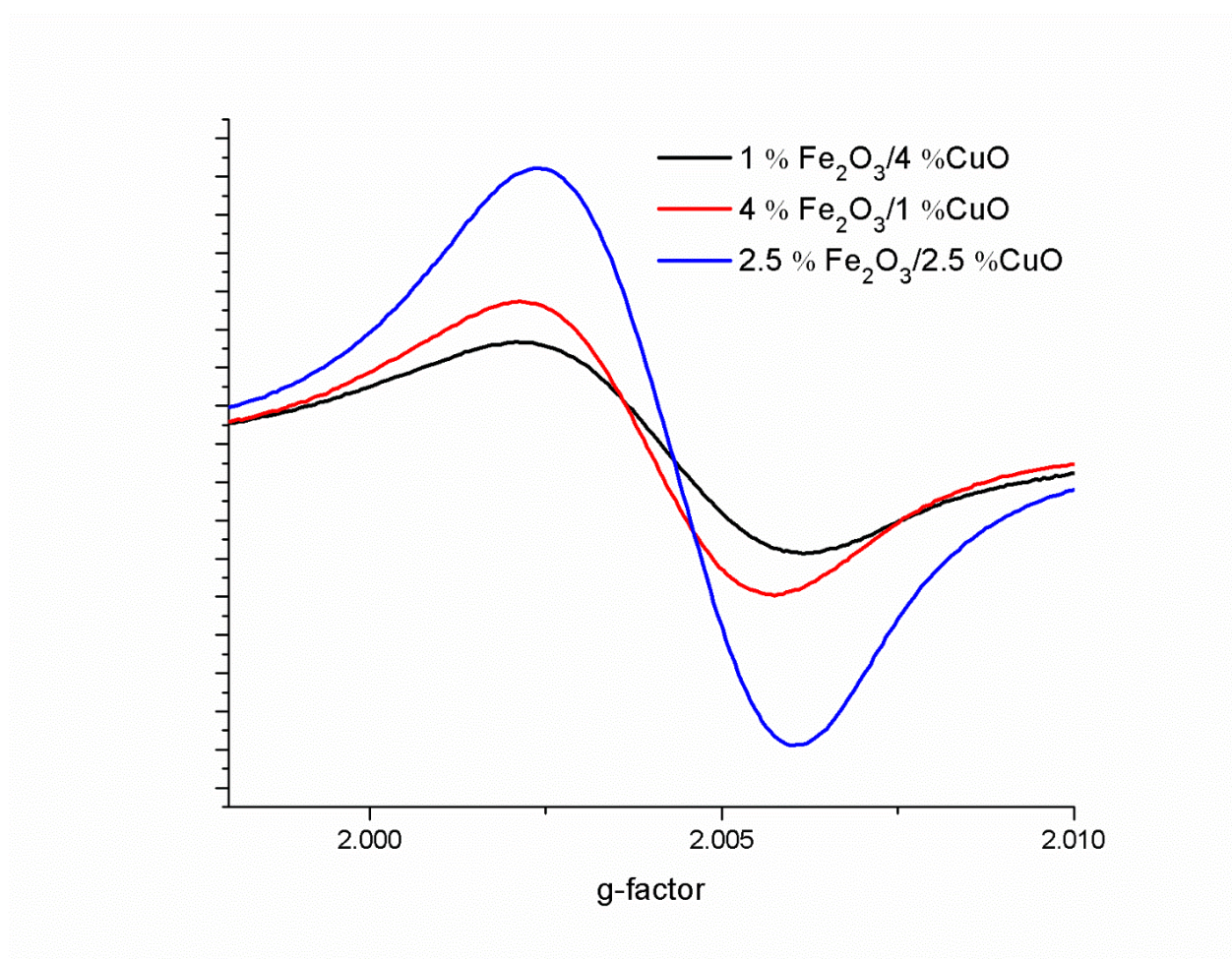
Figure 4.45. EPR Spectra of Fe_2O_3/CuO/Silica Fly Ash Surrogates Dosed with 2-MCP

Table 4.14. EPR Data of Mixed Fe_2O_3/CuO/Silica Fly Ash Surrogates Dosed with 2-MCP			
	g factor	ΔHp-p	Spins/g
4%Fe_2O_3/1%CuO	2.0043	6.3	2.35E+17
	2.0044	6.6	2.10E+17
	2.0044	6.3	4.69E+17
average			3.05E+17
2.5% Fe_2O_3/2.5%CuO	2.0039	6.4	4.40E+17
	2.0040	6.4	4.99E+17
	2.0040	6.5	3.17E+17
average			4.19E+17
1% Fe_2O_3/4%CuO	2.0040	6.0	1.05E+17
	2.0041	7.1	1.50E+17
	2.0041	6.9	1.20E+17
average			1.25E+17

4.8 Characterization of Fly Ash Surrogates

4.8.1 XPS Analysis of Fe_2O_3/CuO/SiO_2

Figure 4.46 and Figure 4.47 present XPS spectra from the fresh and used Fe_2O_3/CuO/SiO_2 fly ash surrogates, respectively. According to NIST X-ray photoelectron spectroscopy database, binding energy for different oxidation state of copper is summarized in table 4.15.

Table 4.15. Binding Energy of Cu $2p_{3/2}$	
Formula	Energy (eV)
Cu	932.2-933.1
Cu_2O	932.2-932.8
CuO	932.7-934.6

As shown in Figure 4.46, among the fresh Fe_2O_3/CuO/SiO_2 fly ash surrogates (before reaction), there is not much difference of binding energy. The peak of Cu $2p_{3/2}$ corresponding to binding energy of 933 eV belong to CuO. After the reaction on the surface of fly ash surrogates (used samples), the peak of Cu $2p_{3/2}$ shifts towards Cu^+. Figure 4.48 presents a comparison of Cu 2p spectra from the catalytic samples after reaction with 2-MCP under pyrolytic conditions. Binding energy absorption peaks were fitted to different oxidation states and speciation of copper and the percent of Cu reduction from +2 to +1 oxidation state were calculated. Addition of Fe_2O_3 into the CuO samples results in gradual increase of the copper reduction. Small addition of iron (1%Fe_2O_3 + 4%CuO) already results in almost double the degree of copper reduction: 79% of the Cu is reduced compared to the 49% reduced in the pure CuO surrogate. In the 1:1 mixture of copper and iron oxides, more than 90% of copper is reduced after reaction. The increased reducibility of copper in mixed oxide systems implies an interaction between iron and copper ions and their direct contact.
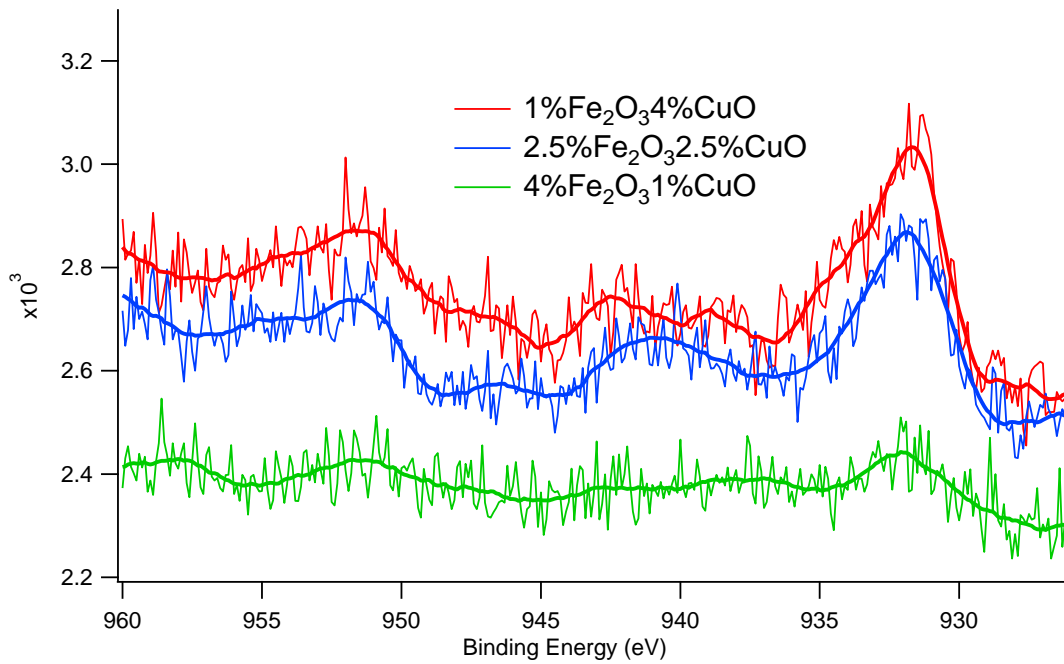
Figure 4.46. XPS Spectra from the Fresh Fe_2O_3/CuO/SiO_2 Fly Ash Surrogates at Cu2p Binding Energy Range
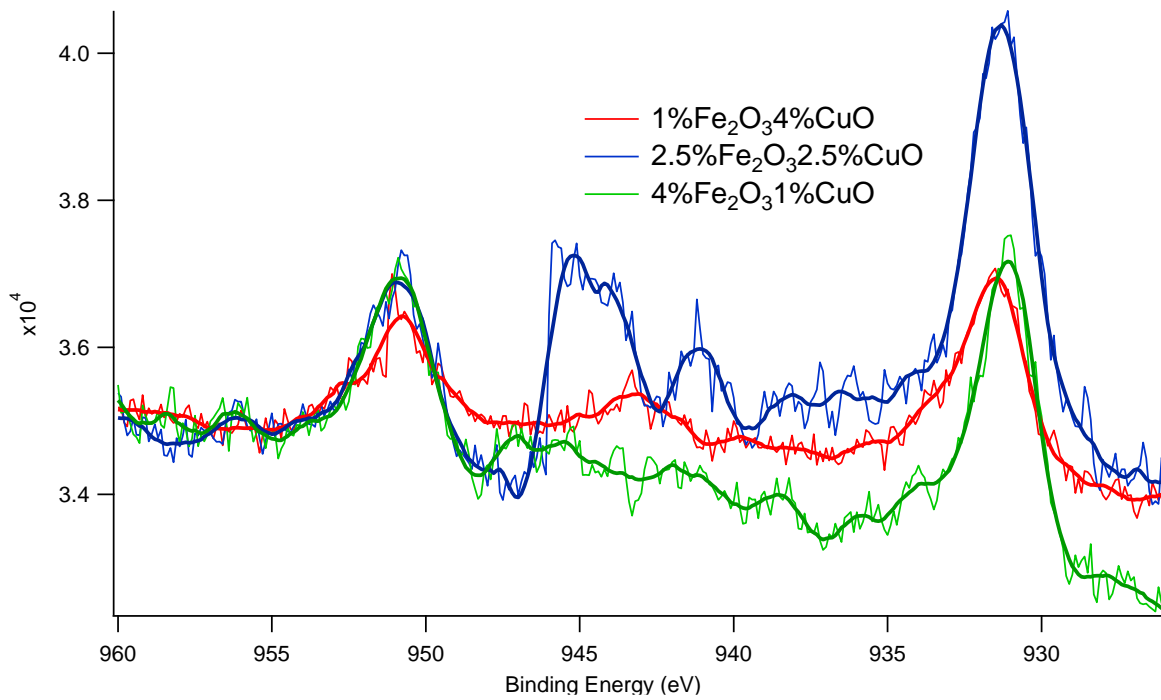
Figure 4.47. XPS Spectra from the Used Fe_2O_3/CuO/SiO_2 Fly Ash Surrogates at Cu2p Binding Energy Range
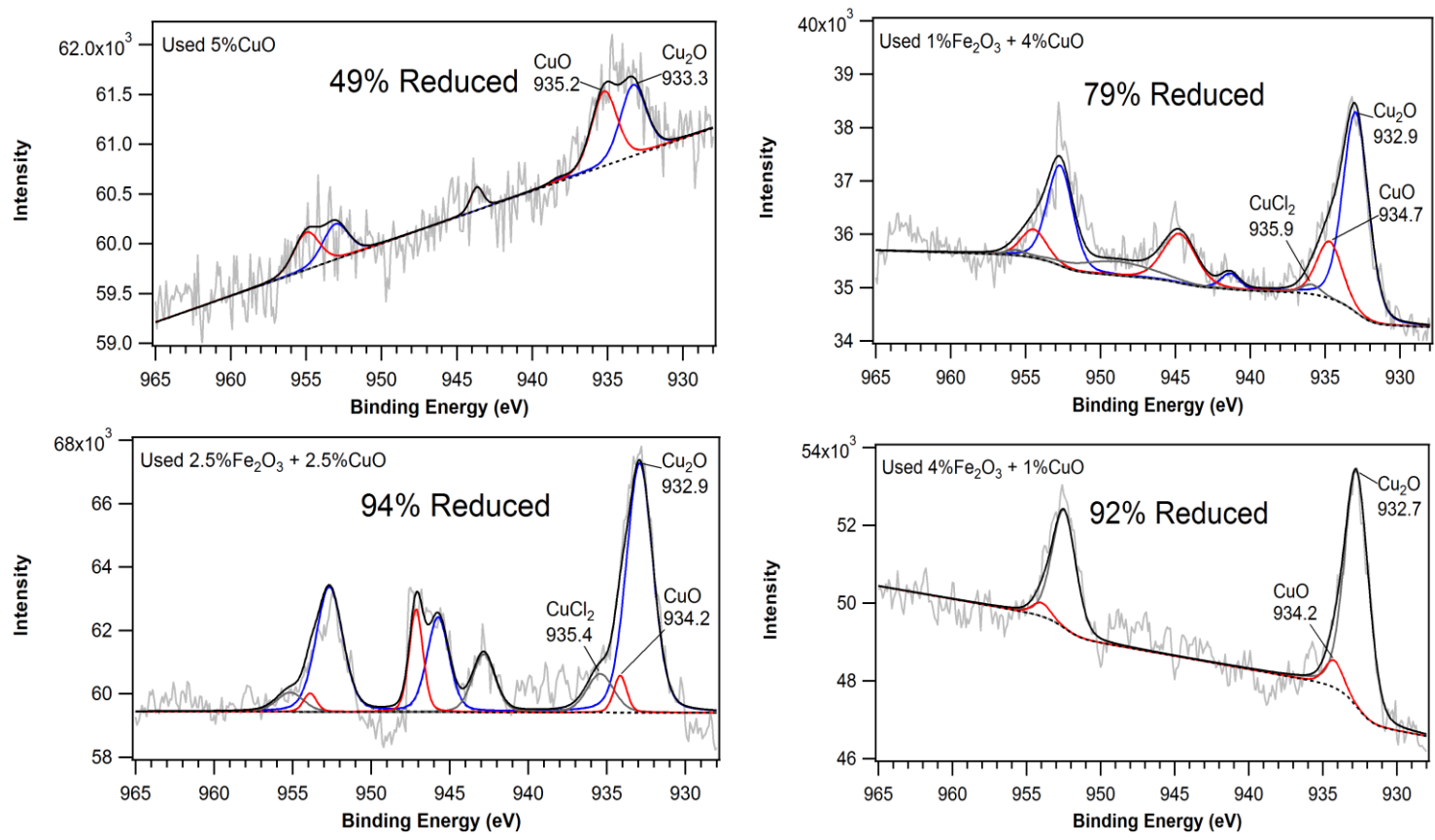
Figure 4.48. High Resolution XPS Spectra of the Cu 2p Binding Energy Region with Fitted Peaks Corresponding to Cu^{2+} and Its Reduced Forms: Cu_2O and $CuCl_2$. The Percent of Reduced Copper after PCDD/F Formation is Emphasized for Each Surrogate

4.8.2 TEM-EDAX Analysis of Fe_2O_3/SiO_2

Figure 4.49 presents Fe_2O_3 nanoclusters' TEM image (top row) and their corresponding diffraction pattern (bottom row). Shown in the high-resolution TEM images , the size of the Fe_2O_3 nanoclusters was <10 nm. With the content of iron increasing in the fly ash surrogates, the nanocluster size is increasing. Simultaneously, the diffraction pattern is changing. Figure 4.50 shows the EDAX analysis results. The appearance of the diffraction pattern can reflect the nature of the crystalline phases in the specimen. For microcrystalline or amorphous systems, the diffraction pattern consists of a series of concentric rings rather than spots/discs. For current Fe_2O_3/silica samples, the electron diffraction pattern is composed of concentric rings. The image on a selected area diffraction pattern from 1% of Fe_2O_3 shows diffuse ring diffraction patterns with no discrete reflections and one or possibly two diffuse rings of maximum intensity, which is typical for amorphous samples. Thus, iron oxide in 1% Fe_2O_3 fly ash surrogate is amorphous with no long-range order in the atomic network. For the material existing as a collection of a large number of crystals, with different geometric orientations, the individual reflections are seen within the rings, observed for samples containing 2.5% to 5% of Fe_2O_3 in fly ash surrogates. Thus, these samples were identified to contain small (nano) crystallites of iron oxide. Fe_2O_3 nanoclusters' size distribution histograms determined from TEM images are shown in Figure 4.51. The particle size of the single cluster ranges from ~3-10 nm. With the increasing content of iron in the model fly ash, the cluster size shifts towards larger diameters. Such clusters were also subject to aggregation, forming larger aggregates with irregular shapes. These aggregates could be identified by EDAX. Due to particles agglomeration, most Fe_2O_3 nanoclusters exist as agglomerates instead of a single cluster.
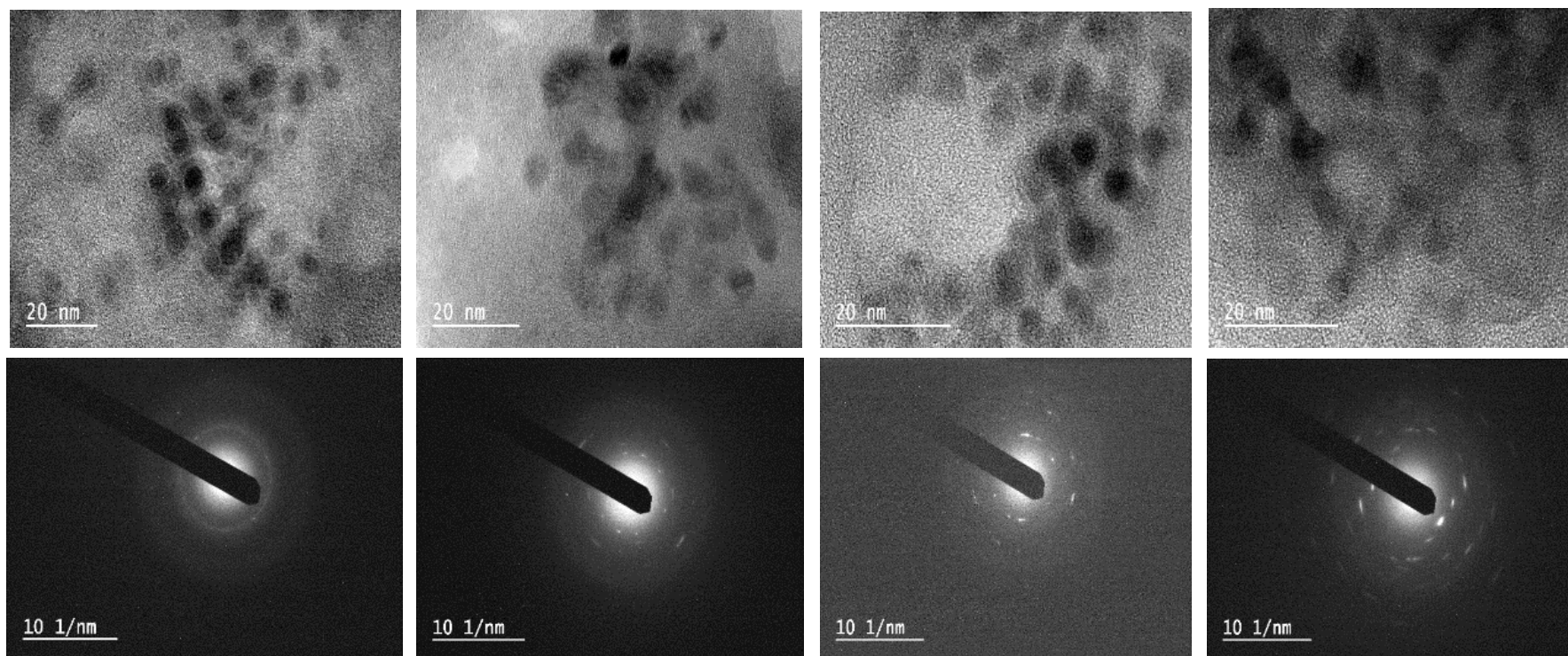
Figure 4.49. TEM Images and Diffraction Patterns of Different Fe_2O_3 Content Fly Ash Surrogates (From Left to Right: 1%, 2.5%, 4% and 5% Fe_2O_3)
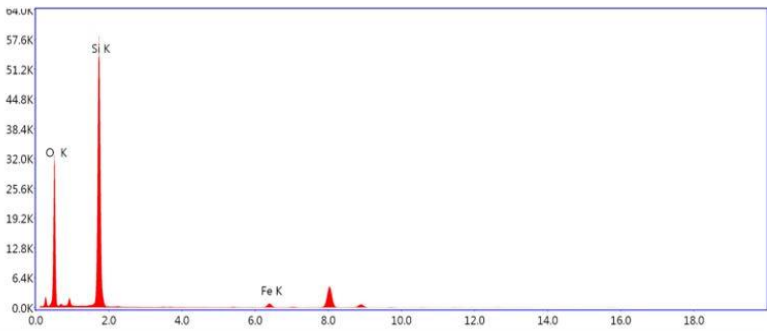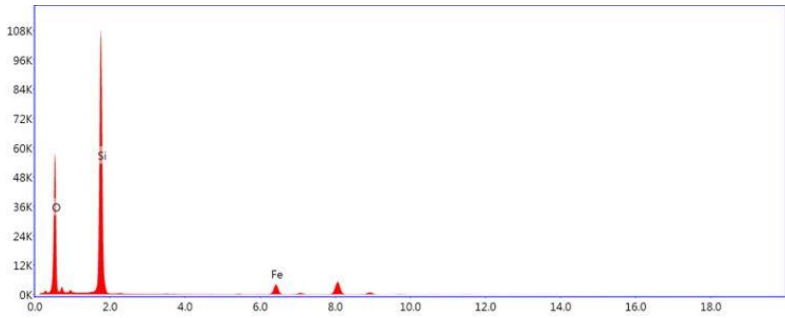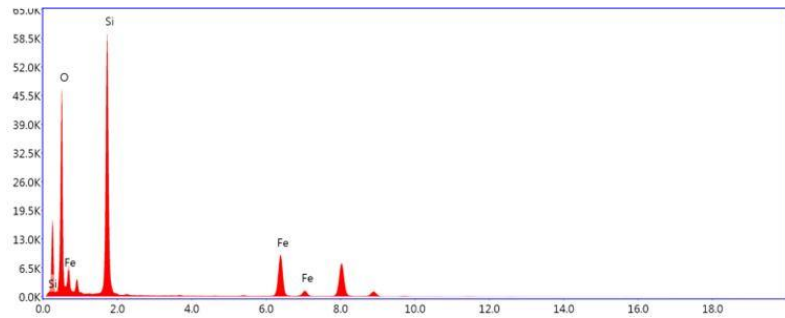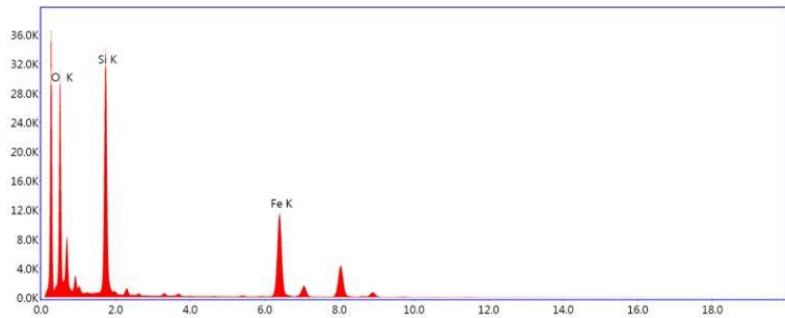
Figure 4.50. EDAX Analysis of Fe_2O_3 Nanoclusters (From Top to Bottom: 1%, 2.5%, 4% and 5% Fe_2O_3)
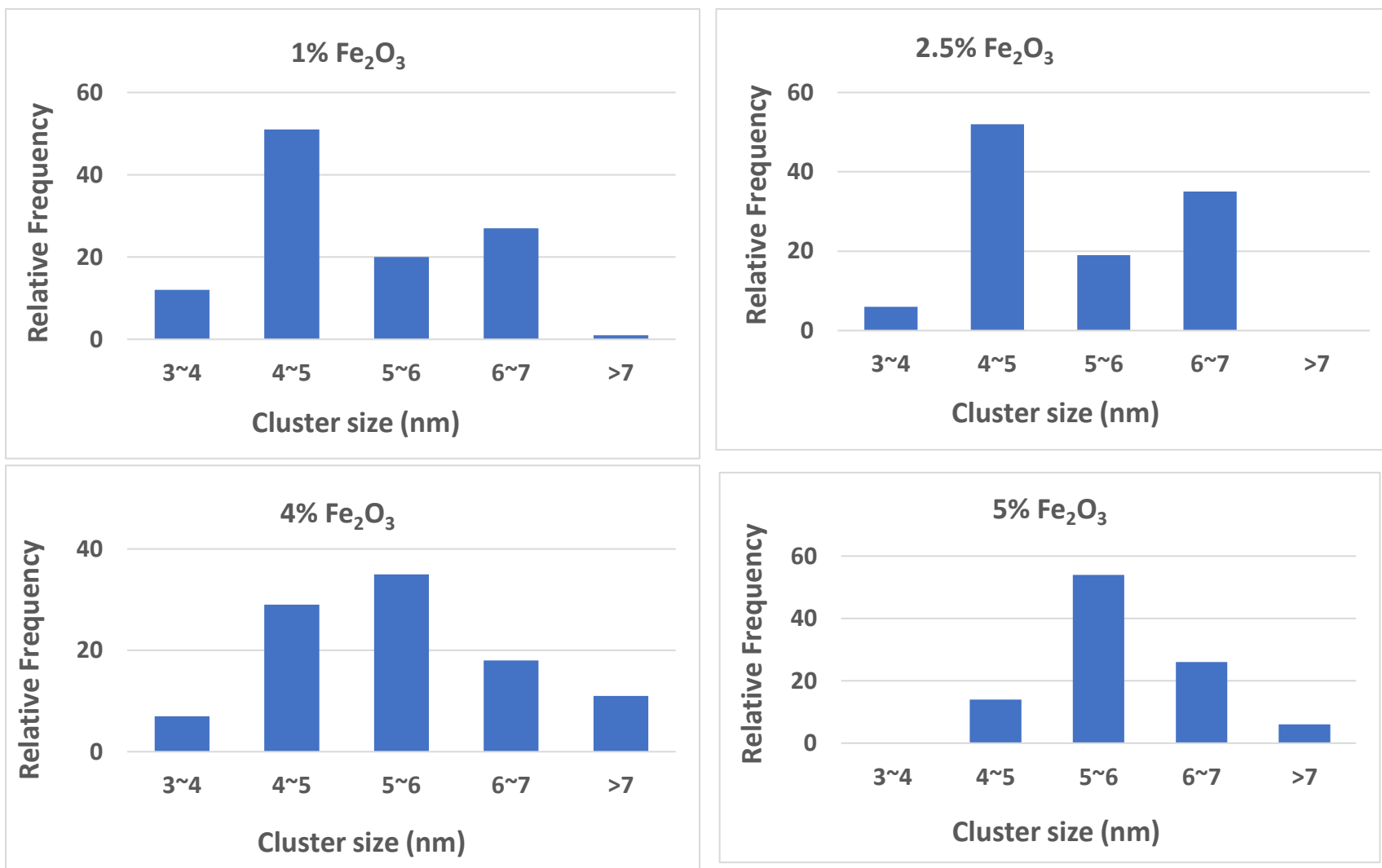
Figure 4.51. Size Distribution of Fe_2O_3 Nanoclusters

4.8.3 XRD Analysis of Fe₂O₃/SiO₂

XRD spectra show the diffraction patterns of iron oxide particles (Figure 4.52). The peaks at 33.18°, 35.67°, 40.74°, 49.51°, 53.90°, 62.17°, 63.97° and 72.03° are corresponding to the diffraction peaks of α-Fe₂O₃, indicating the fly ash surrogates are composed of α- Fe₂O₃ crystals and amorphous silica. XRD spectra confirmed that 1% of Fe₂O₃ fly ash surrogate is amorphous, with the increasing amount of iron, a larger number of crystals formed on and within amorphous silica.
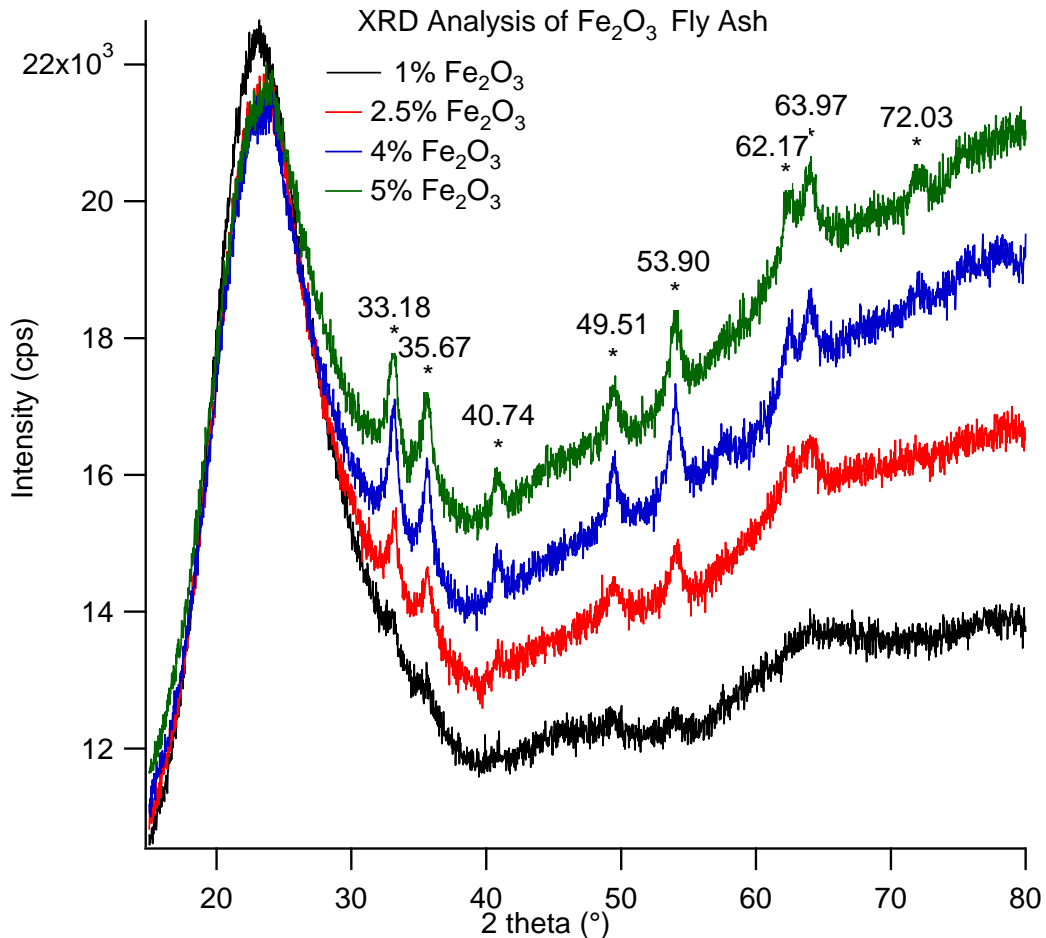
Figure 4.52. XRD Pattern of Fe₂O₃ Fly Ash Surrogates

4.9 References

1.   Jiang, J.-g.; Xin, X.; Jun, W.; Yang, S.-j.; Zhang, Y., Investigation of basic properties of fly ash from urban waste incinerators in China. *Journal of Environmental Sciences* **2007,** *19* (4), 458-463.

2.   Kiruri, L. W.; Khachatryan, L.; Dellinger, B.; Lomnicki, S., Effect of copper oxide concentration on the formation and persistency of environmentally persistent free radicals (EPFRs) in particulates. *Environmental science & technology* **2014,** *48* (4), 2212-2217.

3.   Lomnicki, S.; Truong, H.; Vejerano, E.; Dellinger, B., Copper oxide-based model of persistent free radical formation on combustion-derived particulate matter. *Environmental science & technology* **2008,** *42* (13), 4982-4988.

CHAPTER 5 DISCUSSION

5.1 Fe/Cu Synergy in PCDD/F Formation

Although metal-mediated PCDD/F formation has been studied extensively, [1-4] most of the studies were focused on the effect of single metal chloride or oxide. In the MSWI, fly ash is a complex mixture of components whose concentration can vary widely based on incinerator feedstock. How those components react to each other in terms of PCDD/F formation? Some synergistic or inhibitive effect might exist. How does the change of the metal content affect the PCDD/F output? Those questions need to be addressed. Iron and copper are the most commonly transition metals in combustion systems, it will be interesting to know their cooperative effect in terms of PCDD/F formation. Acutally, the synergy effect between iron and copper has been applied into many fields. A novel nanostructured Fe-Cu binary oxide was synthesized for efficiently removing arsenic from water. [5] Schuchardt's study showed copper oxide exhibits a synergistic effect on iron oxide supported silica for the oxidation of cyclohexane at room temperature. [6] Yang investigated the synergy between iron ore and copper ore as oxygen carriers in chemical-looping combustion and the mixture of iron ore and copper ore are expected to address simultaneously reactivity, recyclability, cost and environmental concerns of oxygen carriers. [7] Rossi prepared iron-copper composite catalysts to study the efficiecy in the Fenton Heterogeneous Process regarding organic charge removal and biodegradability enhancement. [8] For PCDD/F formation, Liao used different mixture of $CuCl_2$ and Fe_2O_3 for de novo synthesis of PCDD/F but no synegistic effects were observed. [9] In our study, different ratio of iron to copper mixed metal oxide model fly ashes were prepared to study their cooperative effects.

The conversion of 2-MCP over the three-studied mixed oxide Fe_2O_3/CuO surrogates is shown in Figure 5.1 and Figure 5.2. For reference, [10-11] previously obtained results from single oxide surrogates are also included in the figure. Under oxidative conditions, clear differences can be observed between the mixed oxide systems and single oxide catalysts in the catalytic oxidation of 2-MCP (Figure 5.1). All three mixed oxide surrogates convert > 99.5% of the 2-MCP precursor across the entire measured temperature range. On the contrary, single oxide systems gradually increase their activity in the oxidation process in the temperature range of 200-400 °C and level-off above 400 °C. In pyrolytic conditions, mixed oxide systems are also superior to single oxides in degradation of 2-MCP, though differences are less dramatic (Figure 5.2). The difference in the oxidative and pyrolytic degradation profiles indicates that 2-MCP is undergoing the Mars-Van Krevelen Mechanism.[12] Current experiments further confirm this theory, where in the absence of molecular oxygen, oxidation of 2-MCP still occurs. Higher activity of the mixed oxide systems at lower temperatures (below 400 °C) indicates a more energetically favorable abstraction of oxygen from the surface by the adsorbed molecules in mixed oxide samples compared to single oxides. This higher activity supports the hypothesis that synergy between iron and copper oxides is primarily due to weakened metal-oxygen bonds. Previous studies[13] have indicated that the adsorption of aromatic species on metal oxides leads to the formation of surface radicals and the mechanism for EPFR formation on individual transition metal oxides has been thoroughly characterized.[10, 14] Depending on the reactivity of the system and the reaction temperature, this leads to degradation/oxidation products or condensation of such radicals to form larger species (such as PCDD/Fs and others). The surface-mediated precursor mechanism for PCDD/F
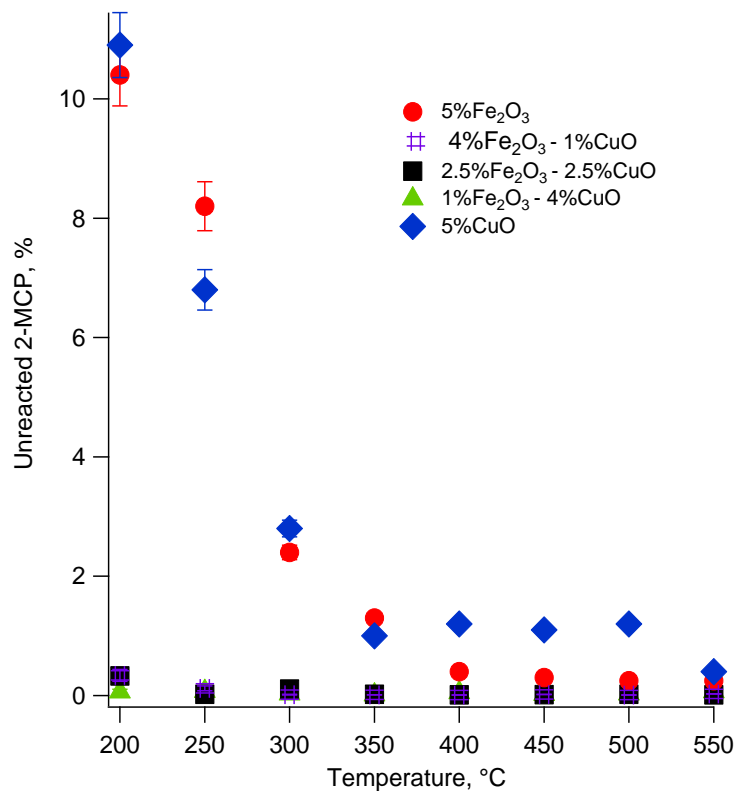
Figure 5.1. Catalytic Degradation of 2-MCP over Three Mixed Oxide Catalysts under Oxidation Conditions
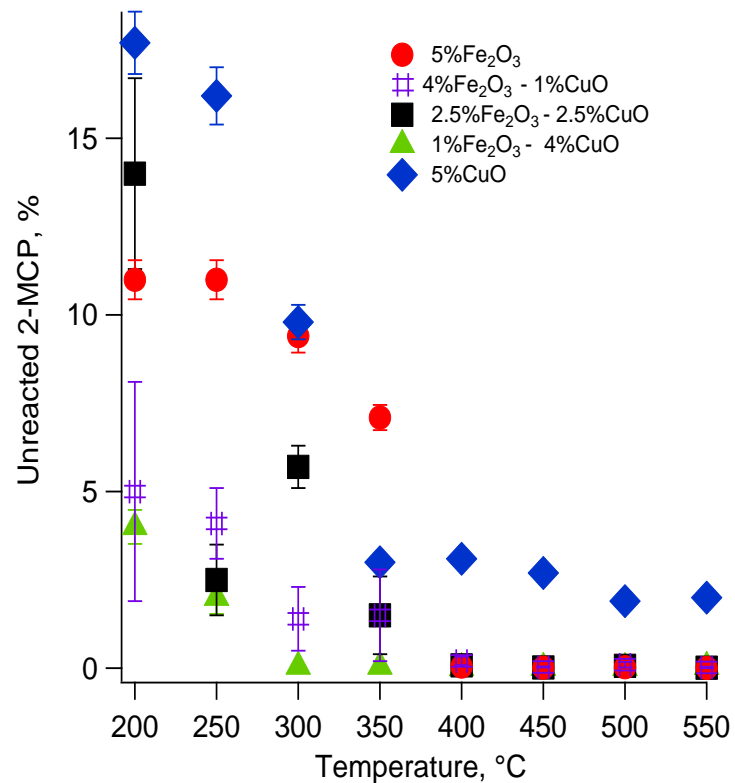
Figure 5.2. Catalytic Degradation of 2-MCP over Three Mixed Oxide Catalysts under Pyrolytic Conditions

100

formation can also be applied to mixed oxides. Indeed, the exposure of mixed metal oxide systems to the vapors of 2-MCP at 230 °C has shown the formation of EPFRs, similarly as described for the single metal systems.[4] These radicals are identified as a mixture of phenoxy- and semiquinone-type radicals.

There is an opposite relationship between the conversion of 2-MCP and the formation of PCDD/Fs on the mixed oxide catalysts. Under oxidative conditions, the yields of PCDD/Fs are very small. Surface-formed radicals are subject either to condensation process or further oxidation to smaller molecules and CO_2. There is a competition between the oxidation and condensation processes and under oxygen-rich conditions, the rate of destruction of 2-MCP surpasses the rate of condensation of PCDD/F intermediates, as indicated by almost complete destruction of 2-MCP. In the absence of molecular oxygen, the rate of catalytic oxidation of 2-MCP is suppressed and the rate of condensation of surface species increases the yields of PCDD/Fs (Figure 5.3). In fact, PCDD/F yields on the mixed oxide catalysts under pyrolytic conditions are up to five times higher than any previously measured yield from a single oxide catalyst. This applies particularly to the mixed oxide samples containing 2.5% of CuO and less (Fe:Cu ratios 0.9 and 3.5). The samples containing 1% Fe_2O_3 still formed higher yields of PCDD/Fs than either single oxide samples, however much less than the other two studied mixed oxide catalysts.

Mixed oxide systems have shown a clear temperature shift in the PCDD/F formation window under pyrolytic conditions. While for the single oxides, formation of PCDD/Fs started above 300 °C (for Fe) and 350 °C (for Cu), mixed oxide systems have
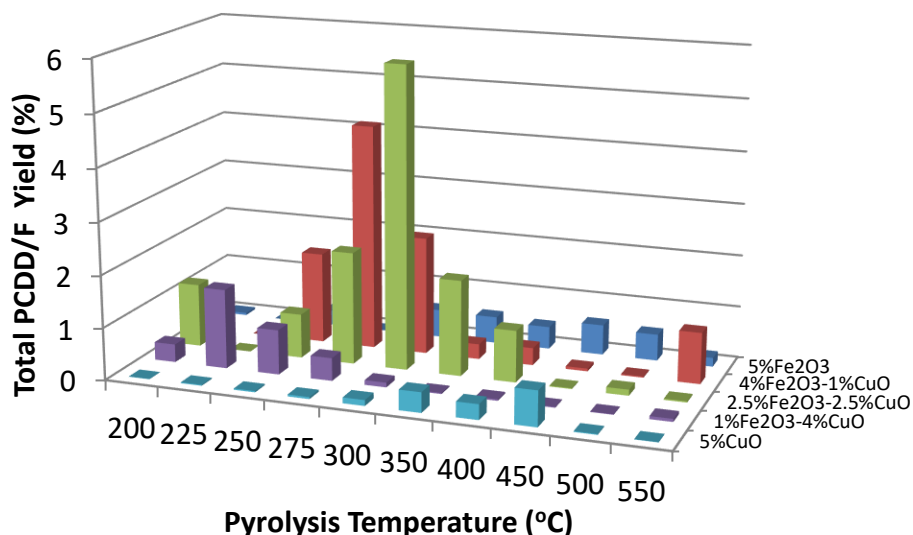
Figure 5.3. Total PCDD/F Yields from the Pyrolytic Degradation of 2-MCP over Fe/Cu Mixed Oxide Catalysts

shown formation of PCDD/Fs already at 200 °C with a clear maximum at ~ 275-300 °C.

A correlation between the degradation of 2-MCP and the beginning of PCDD/F formation

shows the point at which the surface is sufficiently activated to form surface-bound

intermediates. Comparing the onset of the PCDD/Fs formation temperature with the 2-

MCP degradation profiles, it appears that ~ 93-94% degradation of MCP marks the

activity threshold for the PCDD/F formation onset (with the exception of Fe:Cu = 1:1 at

200 °C, where 2-MCP degradation is at 86%).

We have shown previously a significant difference in the PCDD and PCDF yields

for copper and iron oxides from 2-MCP: [10-11] copper oxides preferentially formed PCDDs,

while iron oxide formed primarily PCDFs. By using 2-MCP in current studies, we were

hoping to identify which metal center dominates the PCDD/F formation process in mixed

oxide systems. PCDD: PCDF ratios for all samples are shown in Figure 5.4. The congener

profiles of all three mixed oxide systems contain higher quantities of PCDDs across the
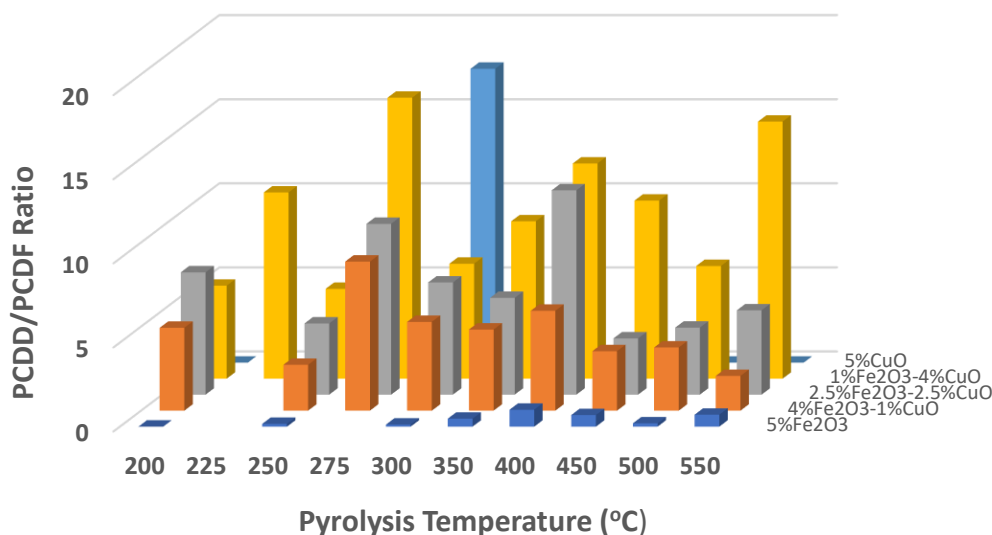
Figure 5.4. PCDD/PCDF Ratios from the Pyrolytic Degradation of 2-MCP over Fe/Cu
Mixed Oxide Catalysts

entire studied temperature range. The mechanistic reason for the increased PCDD/F yield

for samples containing less copper or "diluted" by iron oxides is at present not known. It

might be associated with the electronic effects of iron oxide presence and potential

stabilization of the surface radicals. PCDDs are formed through Eley-Rideal (E-R)

reactions of surface bound EPFRs with gas phase precursors, and PCDFs are formed

through the condensation of surface radicals. Surface immobilization of EPFRs prevents

their lateral-movement, affecting either condensation with other surface species or

subsequent surface oxidation. In fact, it is most likely the fast-surface oxidation of PCDF

precursors that is responsible for the smaller yields of PCDFs. For example, 4,6-

dichlorodibenzofuran (DCDF) formation on the surface of mixed metal oxides reaches maximum at 300 °C (0.8% yield) for samples containing 1:1 ratio of iron and copper and quickly drops to zero with increasing temperatures (Figure 5.5). As a result, such species become more available for reaction with the gas phase precursor to form PCDDs.
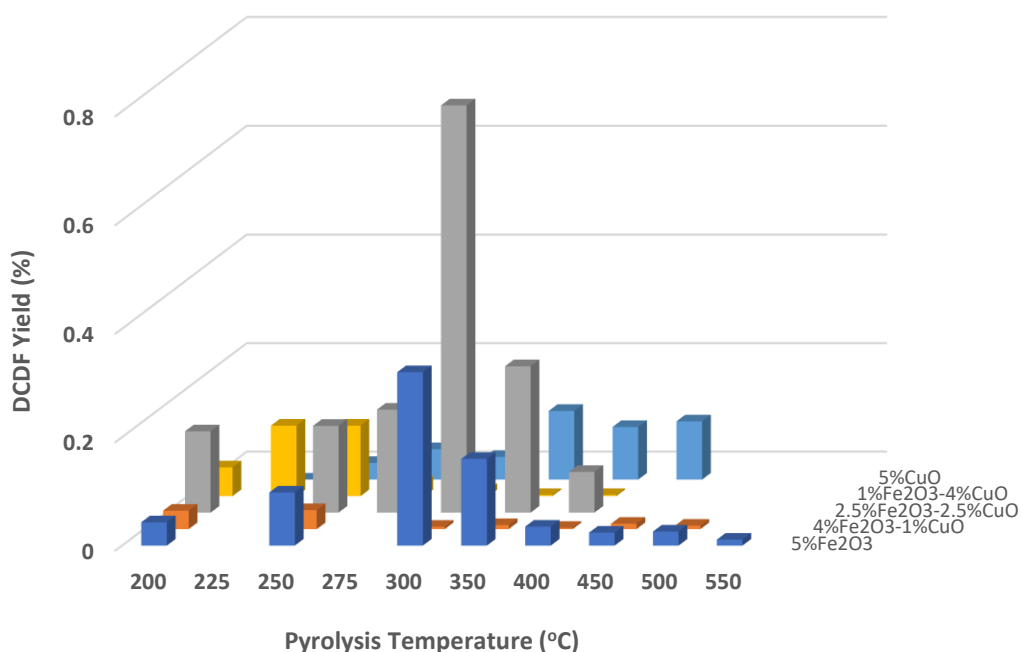
Figure 5.5. 4,6-Dichlorodibenzofuran (DCDF) Yields from the Pyrolytic Degradation of 2-MCP over Fe/Cu Mixed Oxide Catalysts

5.2 Role of Fe_2O_3 and CuO in PCDD/F Formation

The observed synergistic effects indicate a likelihood of direct contact between the Fe_2O_3 and CuO on the surface of the fly ash surrogate. Such co-location could explain the increased PCDD/F yield for samples with decreasing copper concentration – one can anticipate a dilution of surface copper sites (*vide supra*) within the iron oxide phase and increased iron-copper electronic interaction. In fact, higher activity of mixed metal systems (at the same metal load) prompts the hypothesis that synergy between iron and

copper oxides affects the metal-oxygen bonds and enhances reactivity in Mars-Van Krevelen type oxidation. Figure 5.6 presents the binding energy shift with the change of iron/copper content in fly ashes between fresh and used catalysts. The binding energy of copper decreased with the increasing iron content. Shift of electron clouds indicates copper is more reduced. Addition of Fe_2O_3 into the CuO samples results in graduation
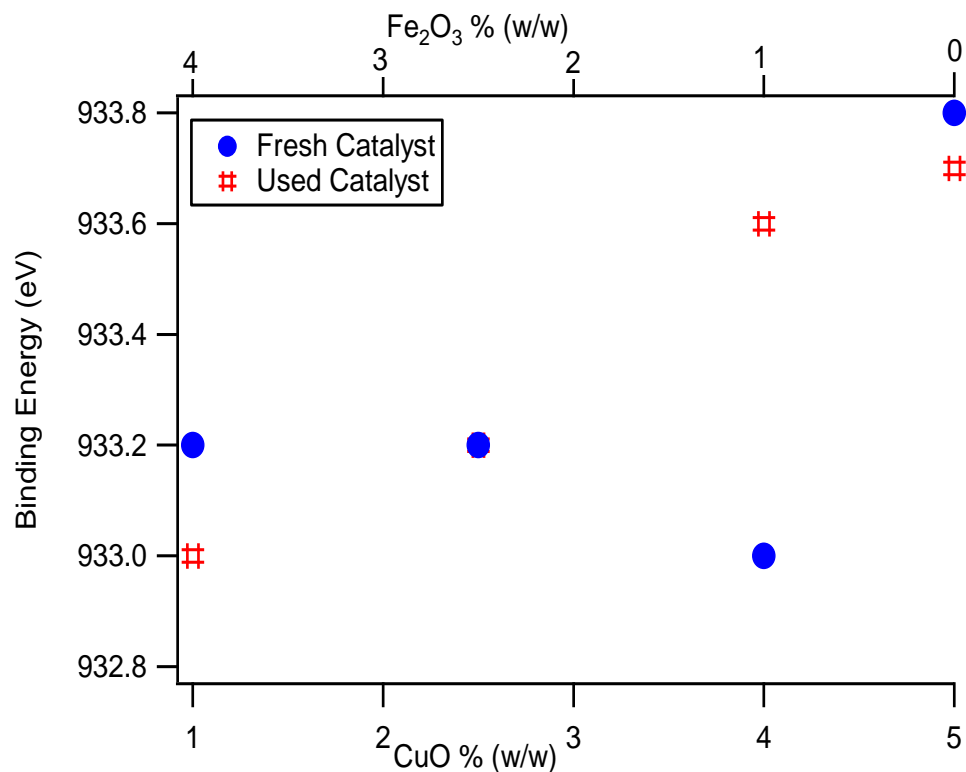
Figure 5.6. Binding Energy Shift with Iron/Copper Content in Fe_2O_3/CuO/SiO$_2$ Fly Ash Surrogates

increase of the copper reduction (ref. Figure 4.48). The increased reducibility of copper in mixed oxide systems implies an interaction between iron and copper ions and their direct contact. In such case, Iron(III)-Cu(II)O long distance interaction pushes the electron cloud towards copper resulting in an increased affinity of Cu^{2+} to accept an electron. Such effects were observed earlier for Cr(III)-Cu(II) systems. [15] Because EPFRs are formed by an electron transfer between an adsorbed species and a metal center, one can anticipate

that increased affinity of Cu^{2+} ions to electrons will also accelerate the formation of EPFRs and/or increase their stabilization on the surface. Since PCDD/F formation is dependent on surface coverage by EPFRs, higher concentration of longer lasting EPFRs results in higher PCDD/F yields. No significant changes were observed within the iron binding energy range in respect of changing iron content. Since PCDD/F formation is dependent on surface coverage by EPFRs, higher concentration of longer lasting EPFRs results in higher PCDD/F yields.

The effect of Fe-Cu electronic interaction in mixed metal oxide catalysts are manifested in dibenzo-*p*-dioxin (DD) (Figure 5.7) and 1-monochlorodibenzo-*p*-dioxin (MCDD) (Figure 5.8). Both DD and MCDD are formed by similar E-R mechanisms, the difference being the reaction site of gas-phase molecule attack, either at the hydroxyl group or the chlorine of the adsorbed EPFR.[16] As seen in Figure 5.7 and Figure 5.8, the single oxide and mixed oxide surrogates primarily form DD and MCDD, respectively. We infer that as the Fe-Cu interaction affects the reducibility of copper sites, the electron density of the associated Cu-adsorbate can be affected, increasing the rate of Cl abstraction/substitution by copper sites. Alternatively, since reaction at the OH site results in the stronger adsorbed species, [17] this can lead to oxidation of surface-bound DD (mixed oxide systems indicate much higher oxidative potential. cf. Figure 5.1).

The results indicate the synergy between iron and copper promotes PCDD/F formation. Under pyrolytic conditions, synergy of Iron and copper oxides produced almost 5-fold yields of PCDD/F compared to single CuO or Fe_2O_3. Under oxidative conditions, iron and copper synergy enhances the oxidation of PCDD/F precursor.
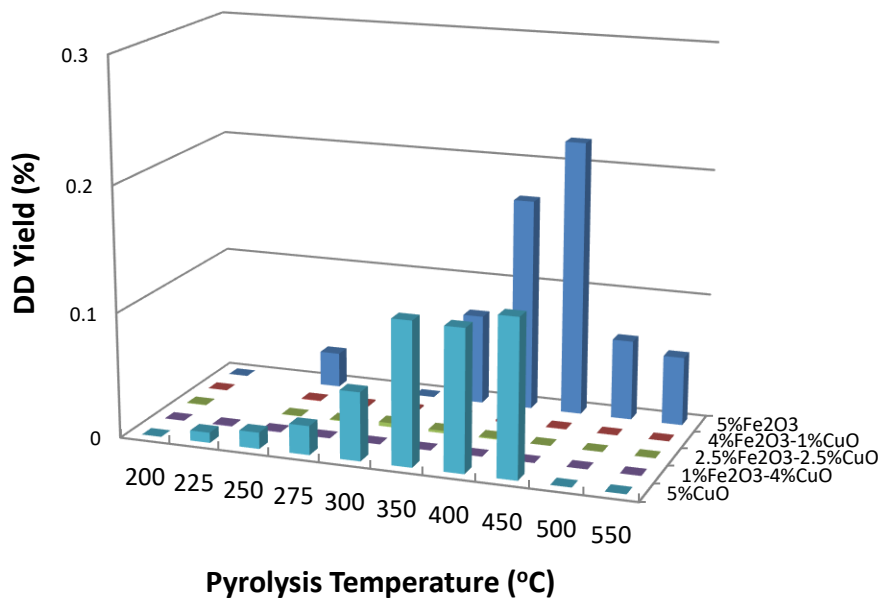
Figure 5.7. Dibenzo-*p*-dioxin Yields from the Pyrolytic Degradation of 2-MCP over Fe/Cu Mixed Oxide Catalysts
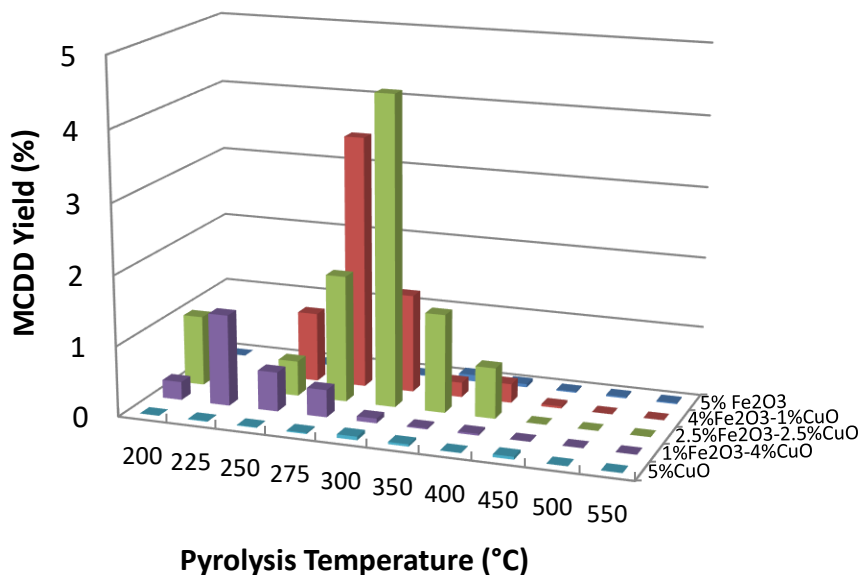
Figure 5.8. Monochlorodibenzo-*p*-dioxin Yields from the Pyrolytic Degradation of 2-MCP over Fe/Cu mixed Oxide Catalysts

5.3 Content and Morphology of Fe_2O_3 in PCDD/F Formation

5.3.1 Content and Morphology of Fe_2O_3 on EFPRs and PCDD/F Formation

As one of the highest concentration transition metals in fly ash, the effect of iron (III) on the PCDD/F formation has been extensively studied both in de novo pathway [18-21] and in precursor pathway. [10, 22] Depending on the MSWI facilities and sampling time, the content of iron oxide in fly ashes is from 0.85-5.02 %. [23] From Fe_2O_3 and CuO mixed metal oxide fly ash study, we know that iron contributed to PCDD/F yields. In order to further understand the relationship between physical properties of iron oxide and its catalytic activities in PCDD/F formation, we prepared 1%, 2.5% and 4% (wt) of iron oxide fly ash surrogates and compared the results with that of typical 5% iron oxide model fly ash.

Figure 5.9 and Figure 5.10 present the catalytic degradation of 2-MCP over Fe_2O_3 fly ash surrogates under pyrolysis and oxidation conditions, respectively. Degradation of 2-MCP is lower with decreasing amount of iron, particularly in pyrolysis conditions. Under oxidation conditions, more than 90% of 2-MCP has been destructed at 250 °C on four fly ash surrogates, almost none of 2-MCP is left at 350 °C. Pyrolytic conditions result in a significant surface oxygen deficit, due to Mars-Van Krevelen mechanism. At 200 °C, 5% Fe_2O_3 decomposed 90% of 2-MCP while 1% to 4% Fe_2O_3 degraded 70% to 80% of 2-MCP. Above 300 °C, 2-MCP degraded similarly on all fly ash surrogates.

Although 5% Fe_2O_3 destroyed 2-MCP at the initial temperature we studied, under pyrolysis conditions, total PCDD/F yield increased with the content of iron oxide in the model fly ash (Figure 5.11). The typical maximum formation window for dioxin is between 280-350°C. This is also true in our case for pyrolytic conditions. However, total PCDD/F
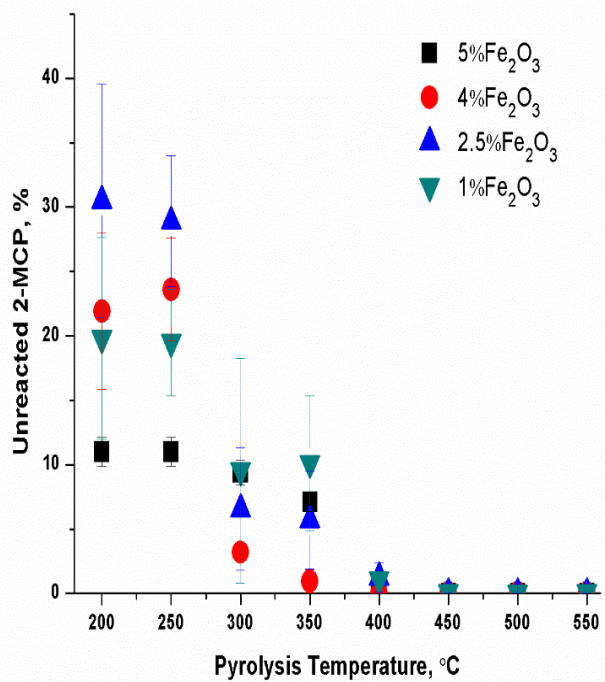
Figure 5.9. Catalytic Degradation of 2-MCP over Fe_2O_3 Catalysts under Pyrolysis Conditions
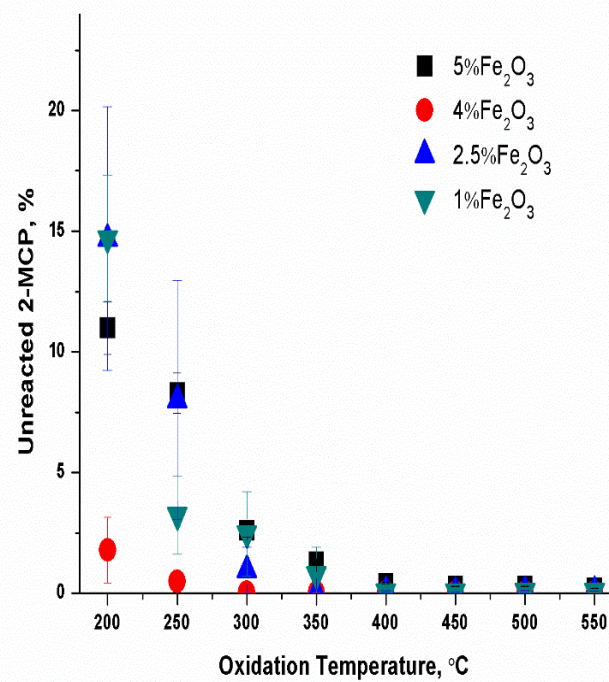
Figure 5.10. Catalytic Degradation of 2-MCP over Fe_2O_3 Catalysts under Oxidation Conditions

yield did not change too much between 2.5% and 4% Fe_2O_3, when Fe_2O_3 increased from 4% to 5%, total PCDD/F yield doubled from 0.45% to 0.9%. One interesting phenomenon is that under oxidation, 5% Fe_2O_3 produced approximately the same amount of PCDD/Fs as that under pyrolysis during the entire temperature range (Figure 5.12). But lower than 5% Fe_2O_3 of fly ashes produced neglectable amount of PCDD/Fs compared to which under pyrolysis. We can anticipate that 5% is a critical point for the yield of PCDD/Fs in terms of the Fe_2O_3 content in the fly ashes.

We have previously demonstrated that 2-MCP interacts with the surfaces of metal oxides through a chemisorption mechanism. [16] Once chemisorbed to the surface, the adsorbed species can undergo multiple transformations to form EPFRs, which are the intermediates of dioxins and other products. The results of EPFRs concentration for different amount of iron oxide in the fly ash surrogates are presented in Figure 5.13. The EPFRs concentration increases quadratically as a function of the amount of iron oxide following the dependence $y = 2*10^{16} x^2 - 6*10^{16} x + 1*10^{17}$ with R^2 of 0.9969. According to the surface theory of dioxins formation, this indicates the potential for increasing yield of dioxins with increasing Fe_2O_3 content: condensation of radicals to PCDD/Fs is dependent on the concentration of surface bound species. Indeed, PCDD/F yield follows the same trend as EPFRs (Figure 5.13) in respect to Fe_2O_3 content. The correlation between the concentration of EPFRs and the average integrated PCDD/F yield is presented in Figure 5.14. It follows a linear correlation $y = -0.02+1.4*10^{-18} x$ with adjusted $R^2 = 0.915$. This correlation strongly confirms the validity of the surface radicals being the precursors in the dioxins formation mechanism.
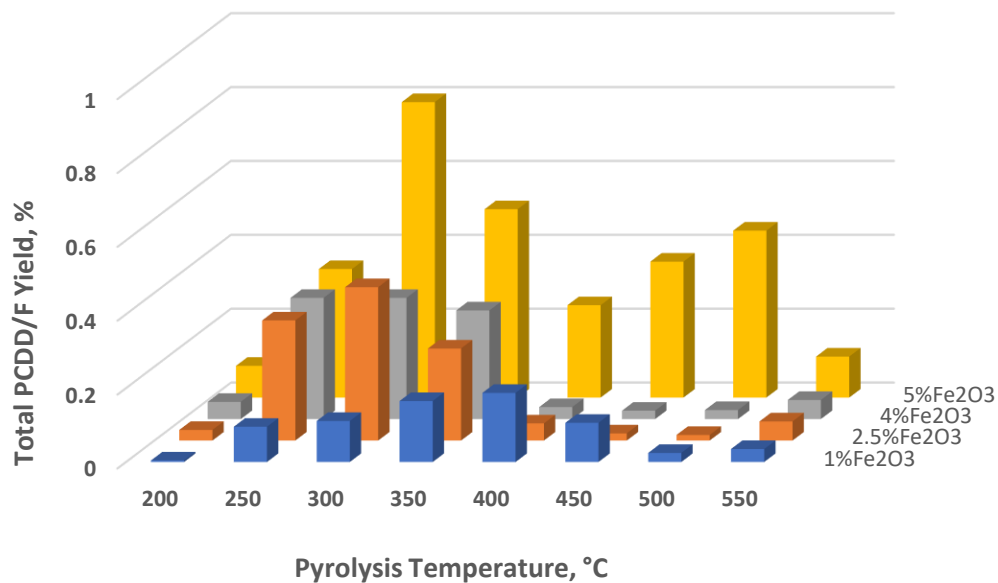
Figure 5.11. Total PCDD/F Yields from the Pyrolytic Degradation of 2-MCP over Iron Oxide Fly Ash Surrogates
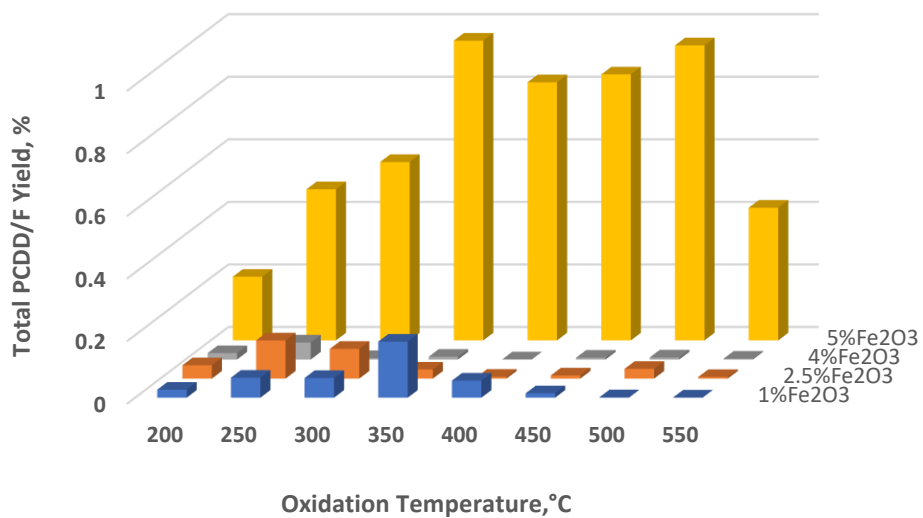
Figure 5.12. Total PCDD/F Yields from the Oxidation Degradation of 2-MCP over Iron Oxide Fly Ash Surrogates
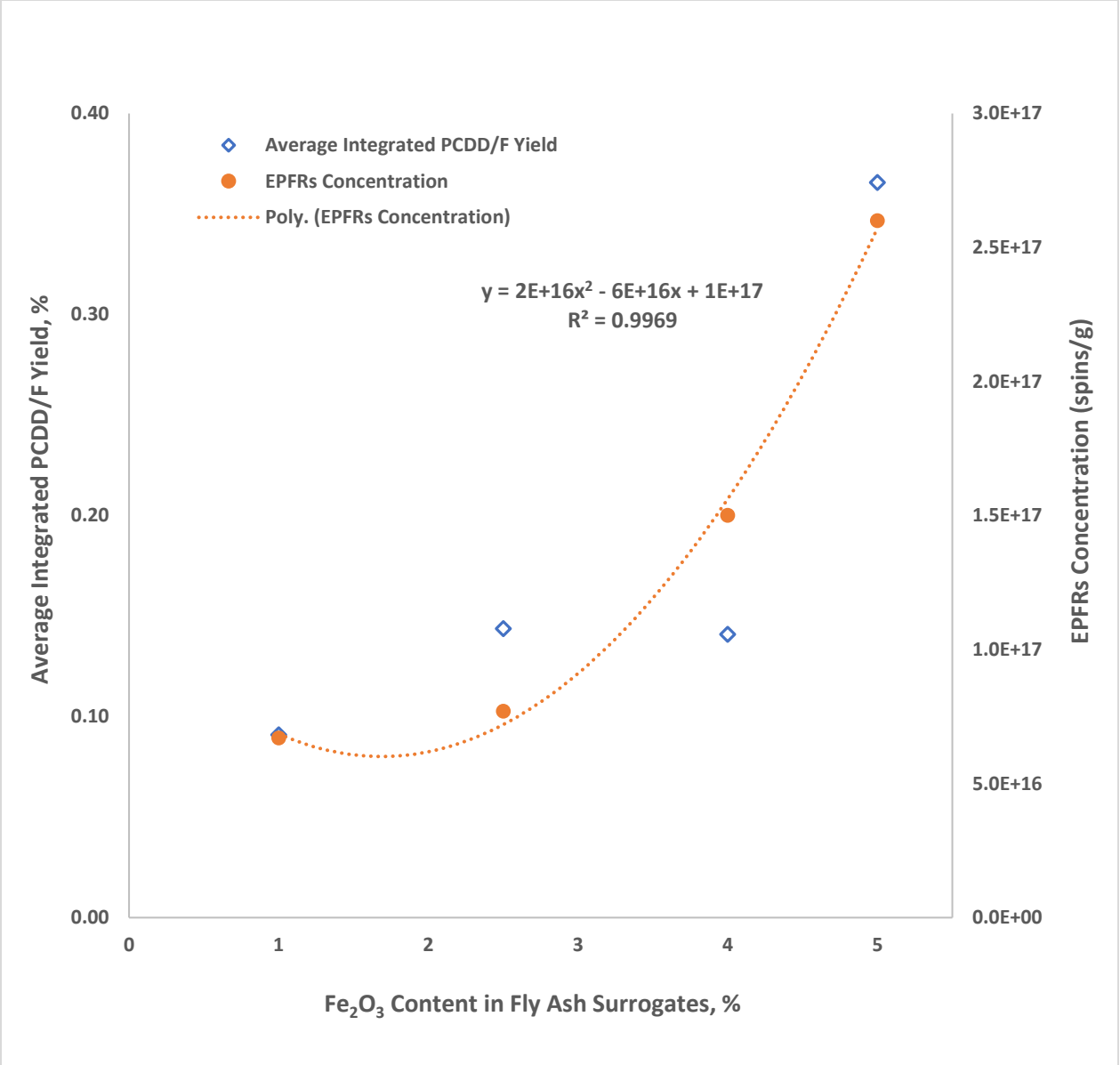
Figure 5.13. EPFRs Concentration and Average Integrated PCDD/F Yield for Different Amount of Iron Oxide in Fly Ash Surrogates
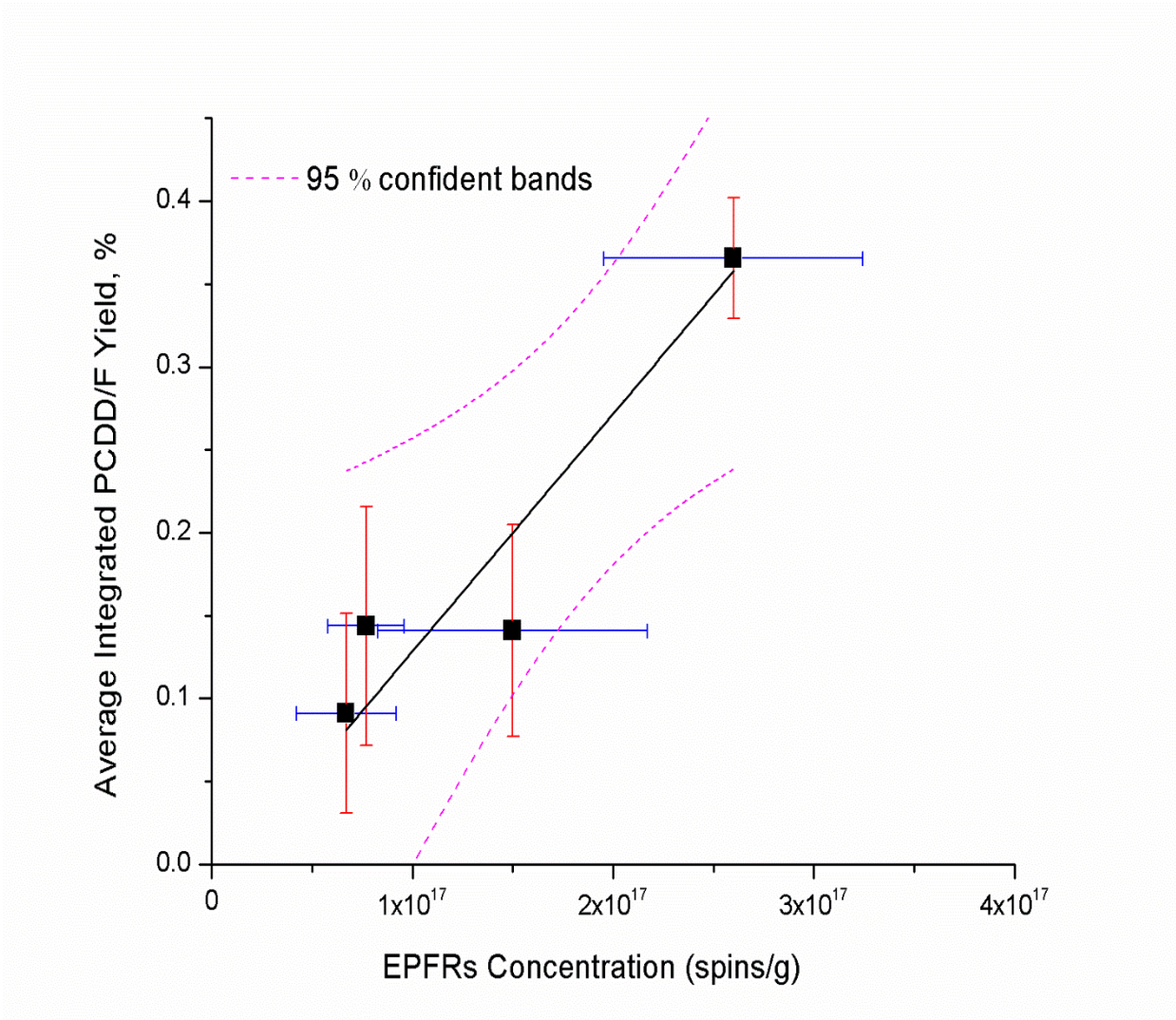
Figure 5.14. Correlation between EPFRs Concentration and Average Integrated Yield of PCDD/F

As is known, the particle size, morphology, oxidation state, and chemical/physical environment are strongly related to their properties and catalytic activities. [24] We can anticipate that changing the concentration of metal in fly ashes will affect the metal/metal oxide cluster size and its activities. In order to understand the composition of iron oxide fly ash and its relationship with size, morphological, structural properties, the fly ash surrogates were investigated by using transmission electron microscopy and X-ray diffraction. High resolution TEM images and diffraction patterns of different Fe_2O_3 content fly ash surrogates are depicted in Figure 4.49. Determined from TEM images, the size of the single Fe_2O_3 nanoclusters ranges from ~3-10 nm. With the amount of iron increasing in the model fly ash, the average size of Fe_2O_3 nanoparticles is increasing, as shown in Figure 5.15. Based on TEM images and diffraction pattern, larger nanoparticle clusters
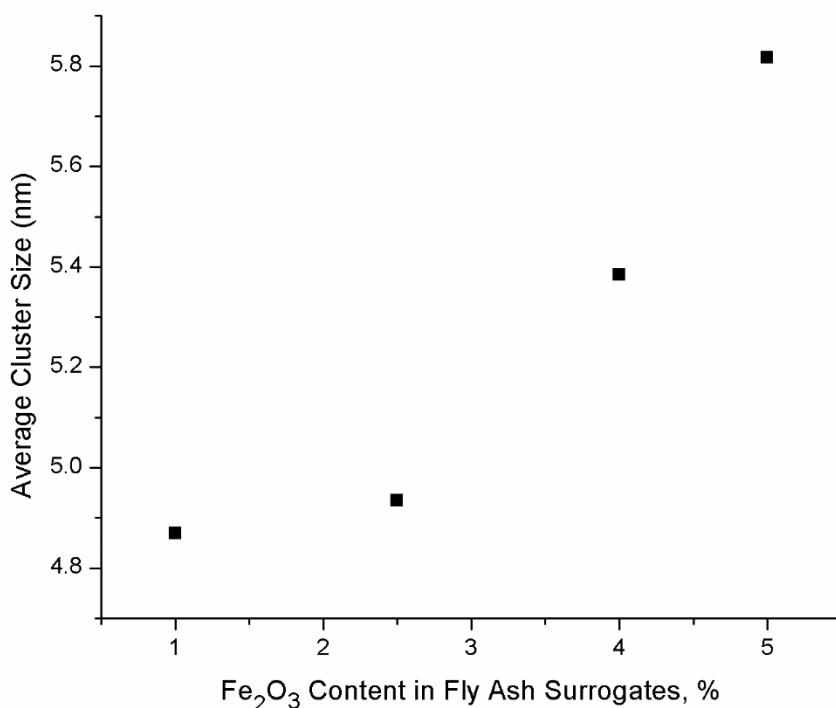
Figure 5.15. Average Fe_2O_3 nanoparticle Size for different Content of Fe_2O_3 Fly Ash Surrogates

and more crystals are easily formed on the 5% Fe_2O_3. XRD spectra also confirmed that 1% Fe_2O_3 model fly ash is amorphous and does not contain α-Fe_2O_3 crystals, with the increasing content of iron, a lot more α-Fe_2O_3 crystals formed within the amorphous phase of silica.

5.3.2 Competition between 4-MCDF and DF Formation Reactions

From previous studies of the Fe_2O_3 mediated formation of PCDD/Fs from 2-MCP, we indicated PCDD/F formation mechanism. Specifically, chlorinated phenols chemisorb to metal oxide or hydroxide surface sites to form a phenoxy-type, environmentally persistent free radicals (EPFRs). These surface-associated EPFRs can react with each other to form PCDD/Fs and other products. Two pathways of chemisorption have been identified for 2-MCP (cf. Scheme 5.1): (1) elimination of H_2O to form 2-chlorophenoxy radical (II), which can proceed to form 4,6-DCDF; (2) elimination of both H_2O and HCl to form the bidentate species (V), which could produce phenoxy radicals that forms DF.

Surface-medicated formation of 4,6-DCDF, DD, MCDD [16] and DF[10] have been described and Langmuir-Hinshelwood mechanism is proposed for the formation reactions of 4,6-DCDF and DF, i.e., both reacting species are adsorbed on the surface. 4,6-DCDF is formed directly from condensation of 2-chlorophenoxy radical [16] at lower temperatures. DF is formed through the bidentate intermediate V depicted in Scheme 5.1 leading to the formation of phenoxy radical. Phenoxy radical, in turn, converts to keto mesomer; and two of the surface-bound mesomers react to form DF at higher temperature range.
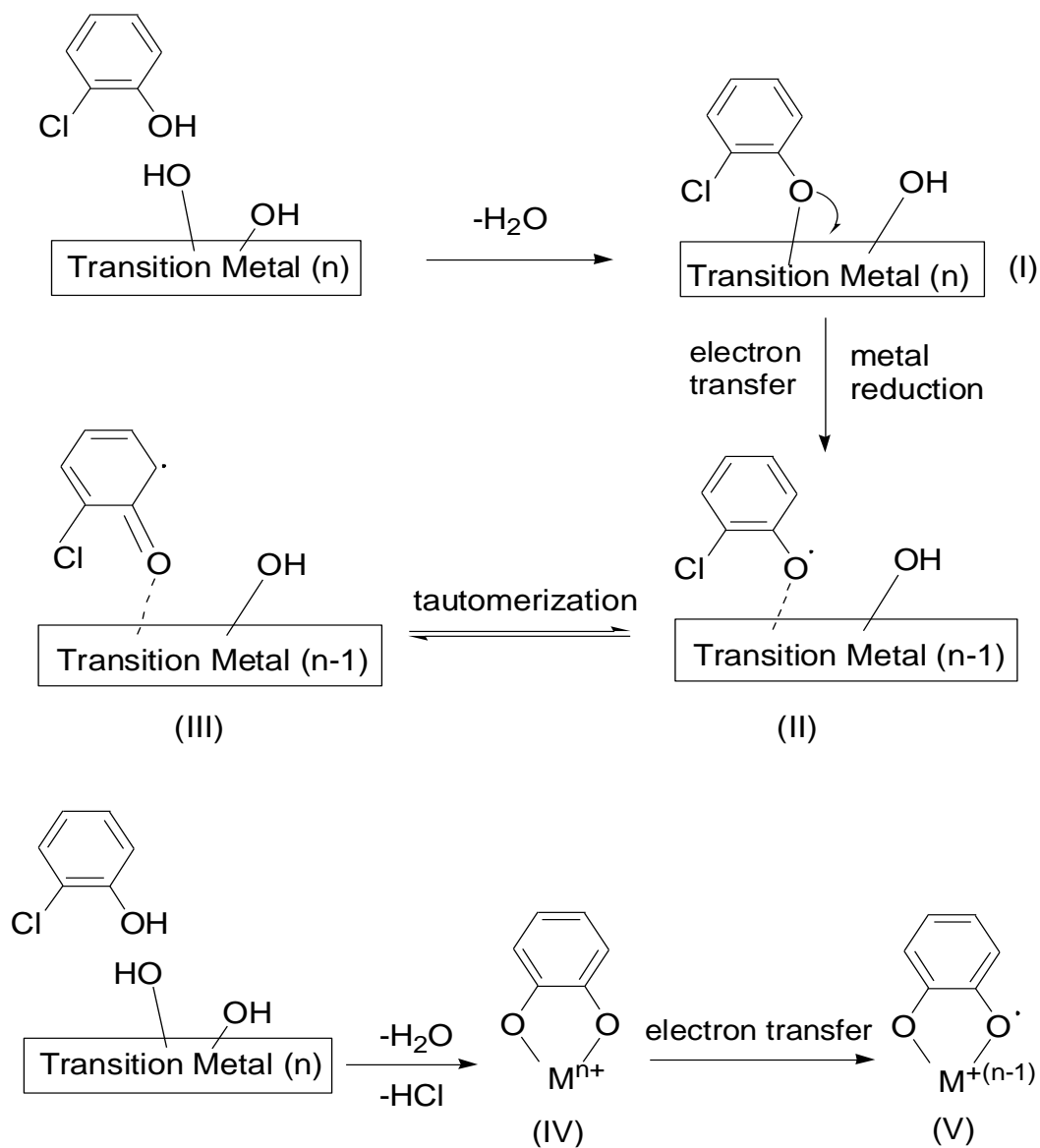
Scheme 5.1. EPFRs Formation Mechanisms (adapted from [10])

Our data also indicate the formation of 4-MCDF over lower content iron samples, within the maximum yield at 300-450 °C; but 4-MCDF was not observed over 5% Fe_2O_3 fly ash (Figure 5.16). On the contrary, DF was only detected over 5% Fe_2O_3/silica surface within the maximum yield at 450-500 °C. The phenomenon implies different mechanism of formation of PCDFs over low iron content of fly ashes.
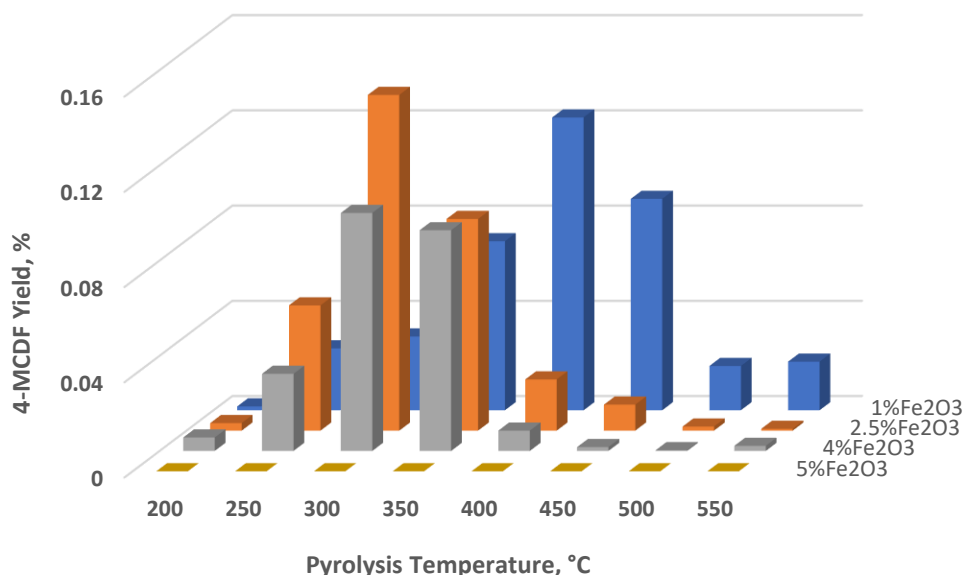
Figure 5.16. 4-MCDF Yields from the Pyrolytic Degradation of 2-MCP over Fe_2O_3

When the content of iron oxide is less than 5%, the surface formation of bidentate species seems to be hindered. This may result from lower concentration of sites capable of simultaneous binding of two carbons. Since the iron oxide cluster size decreases with lowing the iron content, a geometric or electronic effect can contribute to those limitations. As a result, it is more likely that smaller concentration of iron resulting phenoxy species will lead to the "mixed" condensation of phenoxy and 2-chlorophenoxy radicals giving rise to 4-MCDF, as depicted in Scheme 5.2 (reaction between species VII and II). Thus, the iron oxide content (through cluster size differentiations) determines the furan product distribution. At increasing iron content, 4,6-DCDF product is increasingly favored with maximum at 5% of Fe_2O_3 (Figure 5.17). The summary of the PCDFs congener yield over different Fe_2O_3 fly ash surrogates is in table 5.1.
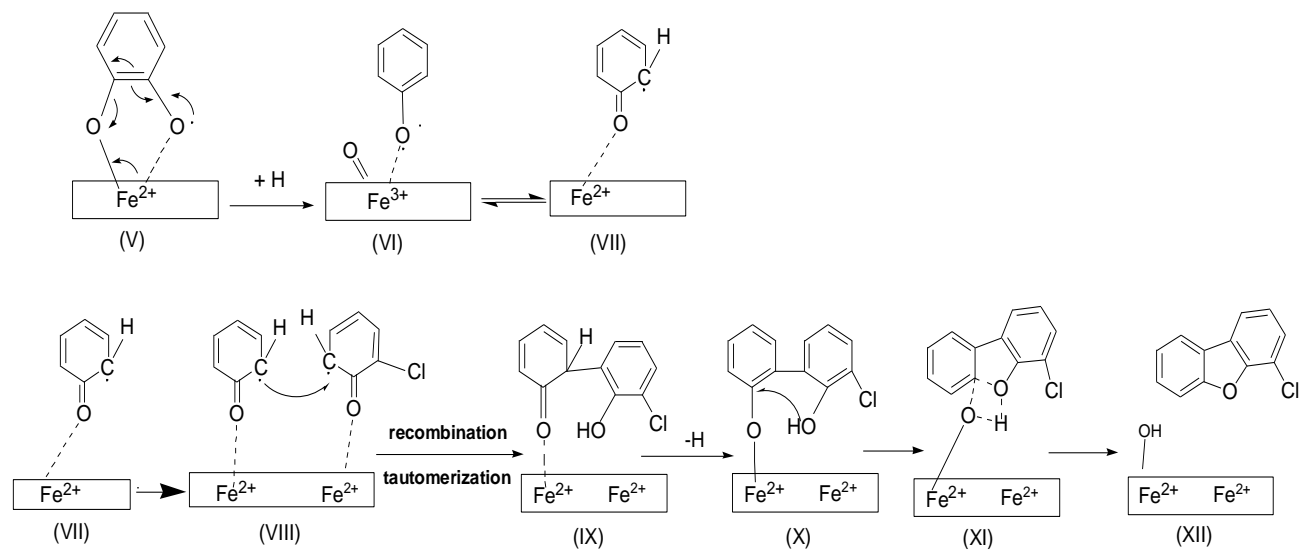
Scheme 5.2. Surface-Mediated Formation of 4-MCDF
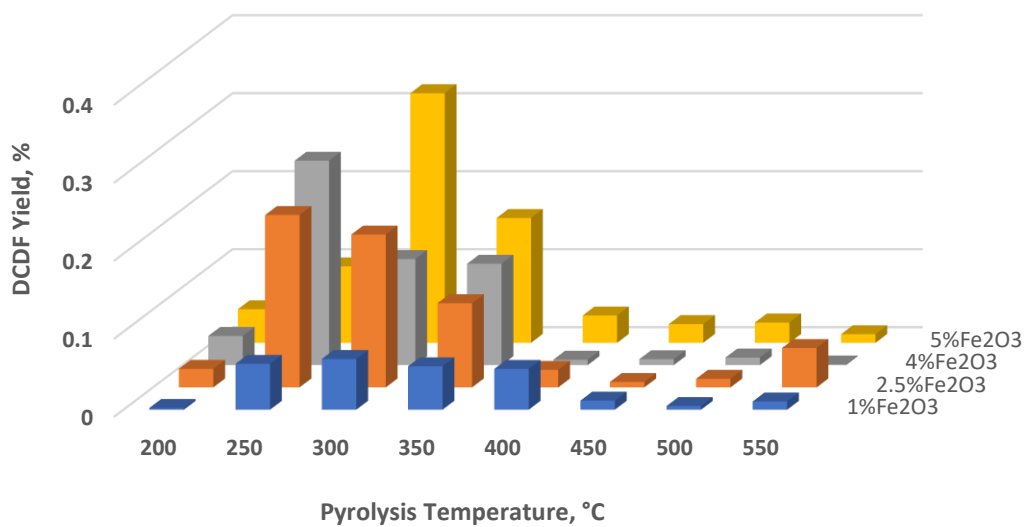
Figure 5.17. 4,6-DCDF Yields from the Pyrolytic Degradation of 2-MCP over Fe_2O_3

Table 5.1. Summary of PCDF Congener Yield Over Different Fly Ash Surrogates			
Product	Maximum Yield and Temperature	% (w/w) of Fe_2O_3 in Fly Ash Surrogates	Surface Radical
4,6-DCDF	0.07% at 300 °C	1%	
	0.22% at 250 °C	2.5%	
	0.26% at 250 °C	4%	
	0.32% at 300 °C	5%	
4-MCDF	0.12% at 400 °C	1%	
	0.14% at 300 °C	2.5%	
	0.10% at 300 °C	4%	
	0	5%	
DF	0.05% at 550 °C	1%	
	0.03% at 550 °C	2.5%	
	0.05% at 550 °C	4%	
	0.40% at 500 °C	5%	
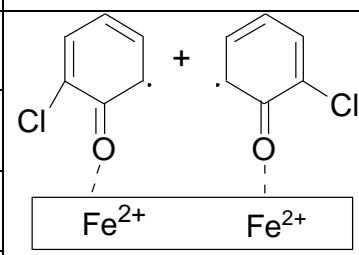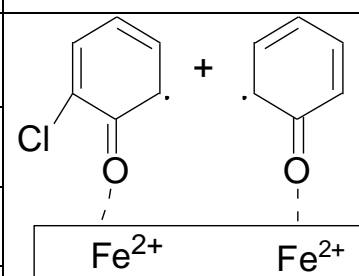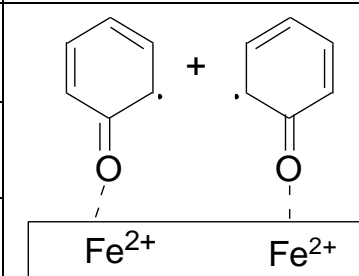
5.3.3 PCDDs vs PCDFs

A closer look at the total PCDD and PCDF yields as a function of iron oxide content in fly ash surrogates indicates interesting differences in reactivities. Figure 5.18 presents the average integrated yield of PCDDs and PCDFs over entire temperature range (the average integrated yield is defined as a sum of all products in a category divided by the number of measurement points). PCDDs include DD, 1-MCDD, DCDD, TriCDD and PCDFs include DF, 4-MCDF, 4,6-DCDF. A clear trend is that with the increasing content of iron, both the yields of PCDDs and PCDFs are increasing accordingly, which is consistent with the EPFRs formation. Over all the iron oxide fly ash surrogates, PCDFs' formation is dominant over PCDDs because the chemisorption mechanisms over copper and iron oxides surfaces are different (rf. Scheme 5.1). Bidentate species could only form on iron oxide surface as the intermediate of DF.
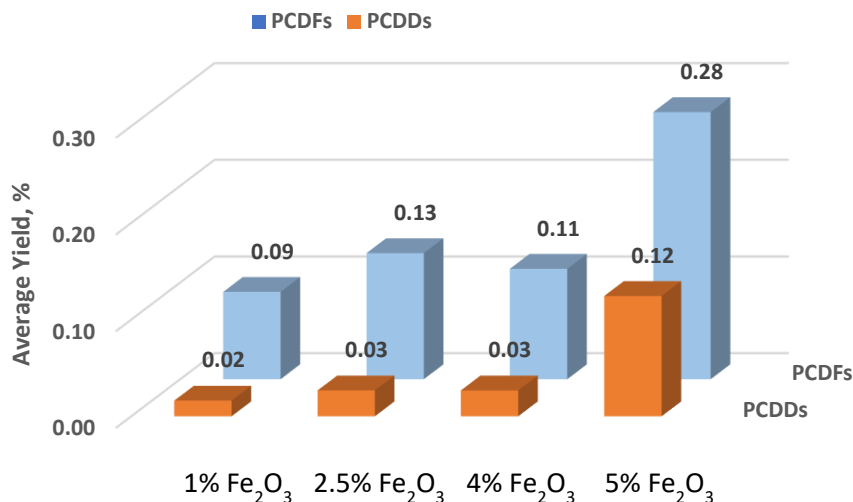
Figure 5.18. Average Integrated Yield of PCDDs and PCDFs Depending on Fe_2O_3 Content under Pyrolysis

The ratio of PCDD/PCDF is increasing with the increasing content of Fe_2O_3 in the model fly ash, shown in Figure 5.19. And this ratio is even increasing more dramatically on the mixed metal oxides with the increasing content of CuO in the fly ash surrogates. The yield of MCDD, DCDD, TriCDD, DD follow an increasing trend with adding more iron oxide in the model fly ash (DD was only found on 5% Fe_2O_3/silica, which indicates the surface catalyzed chlorination reactions preferably happen on low content of iron). See Figure 5.20 for the 1-MCDD yields from the pyrolytic degradation of 2-MCP over Fe_2O_3. For the PCDFs, although 4,6-DCDF yield increased with content of iron; for 4-MCDF, less difference is found when iron oxide is less than 5% and none of 4-MCDF was formed on 5% Fe_2O_3.
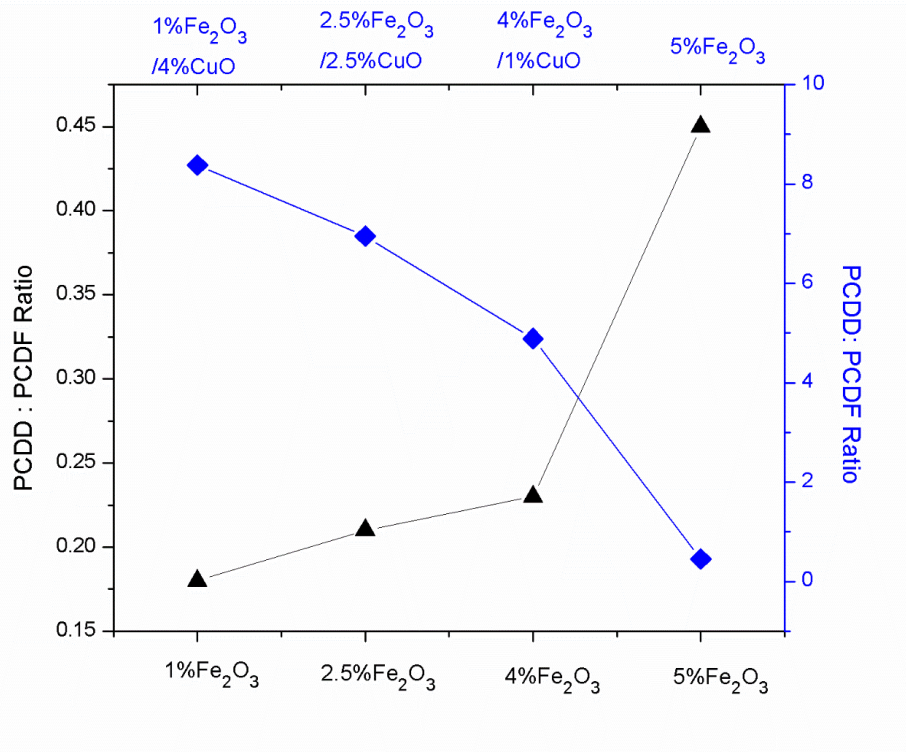
Figure 5.19. PCDF/PCDD Ratio for Different Fe_2O_3 Content in Fly Ashes (under Pyrolysis)
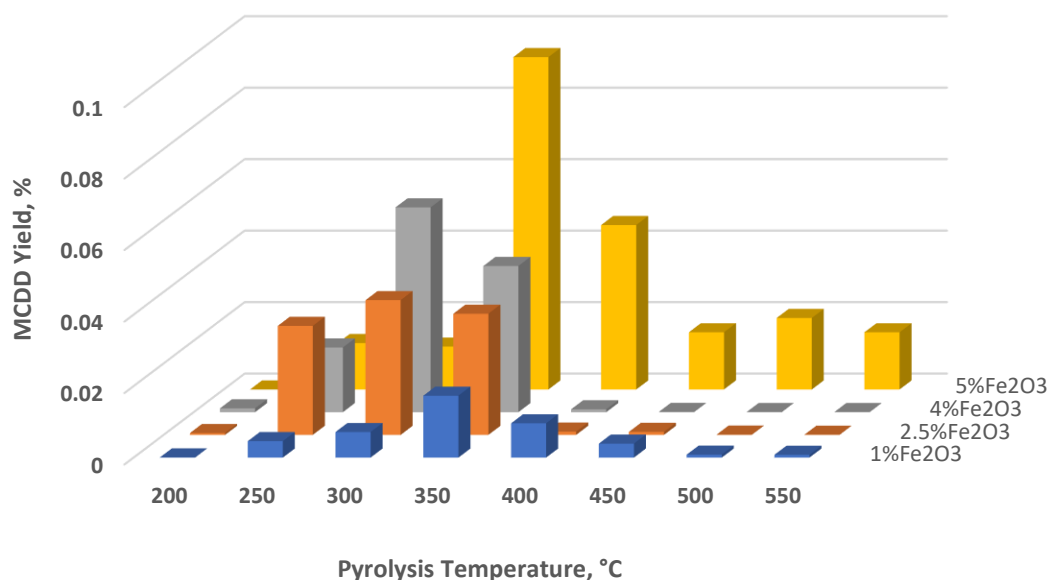
Figure 5.20. 1-MCDD Yields from the Pyrolytic Degradation of 2-MCP over Fe_2O_3

Conclusions can be drawn that in the fly ashes of the incinerator, not only the content, but also the cluster size of iron oxide nanoparticle will affect the formation of the surface associated EPFRs. These EPFRs further react either through Eley-Rideal mechanism or Langmuir-Hinshelwood mechanism to form different PCDD/F congeners. Generally, higher content of iron will form larger nanoparticle clusters and more crystals, which contributes producing higher yields of PCDD/F.

5.4 References

1.   Ryu, J.-Y.; Mulholland, J. A., Metal-mediated chlorinated dibenzo-p-dioxin (CDD) and dibenzofuran (CDF) formation from phenols. *Chemosphere* **2005,** *58* (7), 977-988.

2.   Öberg, T.; Bergbäck, B.; Filipsson, M., Catalytic effects by metal oxides on the formation and degradation of chlorinated aromatic compounds in fly ash. *Chemosphere* **2008,** *71* (6), 1135-1143.

3.   Chin, Y.-T.; Lin, C.; Chang-Chien, G.-P.; Wang, Y.-M., PCDD/F formation catalyzed by the metal chlorides and chlorinated aromatic compounds in fly ash. *Aerosol Air Qual. Res* **2012,** *12* (2), 228-236.

4.   Kiruri, L. W.; Khachatryan, L.; Dellinger, B.; Lomnicki, S., Effect of copper oxide concentration on the formation and persistency of environmentally persistent free radicals (EPFRs) in particulates. *Environmental science & technology* **2014,** *48* (4), 2212-2217.

5.   Zhang, G.; Ren, Z.; Zhang, X.; Chen, J., Nanostructured iron (III)-copper (II) binary oxide: a novel adsorbent for enhanced arsenic removal from aqueous solutions. *Water research* **2013,** *47* (12), 4022-4031.

6.   Schuchardt, U.; Pereira, R.; Krähembühl, C. E.; Rufo, M.; Buffon, R., Synergistic effect of iron and copper oxides supported on silica in the room temperature oxidation of cyclohexane. *Applied Catalysis A: General* **1995,** *131* (1), 135-141.

7.   Yang, W.; Zhao, H.; Wang, K.; Zheng, C., Synergistic effects of mixtures of iron ores and copper ores as oxygen carriers in chemical-looping combustion. *Proceedings of the Combustion Institute* **2015,** *35* (3), 2811-2818.

8.   Rossi, A. F.; Martins, R. C.; Quinta-Ferreira, R. M., Composition effect of iron–copper composite catalysts in the Fenton heterogeneous process efficiency and cooxidation synergy assessment. *Industrial & Engineering Chemistry Research* **2014,** *53* (40), 15369-15373.

9.   Liao, J.; Buekens, A.; Olie, K.; Yang, J.; Chen, T.; Li, X., Iron and copper catalysis of PCDD/F formation. *Environmental Science and Pollution Research* **2016,** *23* (3), 2415-2425.

10.   Nganai, S.; Lomnicki, S.; Dellinger, B., Ferric oxide mediated formation of PCDD/Fs from 2-monochlorophenol. *Environmental science & technology* **2008,** *43* (2), 368-373.

11.   Lomnicki, S.; Dellinger, B., Formation of PCDD/F from the pyrolysis of 2-chlorophenol on the surface of dispersed copper oxide particles. *Proceedings of the Combustion Institute* **2002,** *29* (2), 2463-2468.

12.   Doornkamp, C.; Ponec, V., The universal character of the Mars and Van Krevelen mechanism. *Journal of Molecular Catalysis A: Chemical* **2000,** *162* (1), 19-32.

13.   Vejerano, E.; Lomnicki, S.; Dellinger, B., Formation and stabilization of combustion-generated environmentally persistent free radicals on an Fe (III) 2O3/silica surface. *Environmental science & technology* **2010,** *45* (2), 589-594.

14.   Dellinger, B.; Lomnicki, S.; Khachatryan, L.; Maskos, Z.; Hall, R. W.; Adounkpe, J.; McFerrin, C.; Truong, H., Formation and stabilization of persistent free radicals. *Proceedings of the Combustion Institute* **2007,** *31* (1), 521-528.

15.   Wojciechowska, M.; Haber, J.; Łomnicki, S.; Stoch, J., Structure and catalytic activity of double oxide system: Cu–Cr–O supported on MgF2. *Journal of Molecular Catalysis A: Chemical* **1999,** *141* (1), 155-170.

16.   Lomnicki, S.; Dellinger, B., A detailed mechanism of the surface-mediated formation of PCDD/F from the oxidation of 2-chlorophenol on a CuO/silica surface. *The Journal of Physical Chemistry A* **2003,** *107* (22), 4387-4395.

17.   Khachatryan, L.; Vejerano, E.; Lomnicki, S.; Dellinger, B., Environmentally persistent free radicals (EPFRs). 1. Generation of reactive oxygen species in aqueous solutions. *Environmental science & technology* **2011,** *45* (19), 8559-8566.

18.   Zhang, M.; Buekens, A.; Ma, S.; Li, X., Iron chloride catalysed PCDD/F-formation: Experiments and PCDD/F-signatures. *Chemosphere* **2018,** *191*, 72-80.

19.   Heeb, N. V.; Zennegg, M.; Haag, R.; Wichser, A.; Schmid, P.; Seiler, C.; Ulrich, A.; Honegger, P.; Zeyer, K.; Emmenegger, L., PCDD/F formation in an iron/potassium-catalyzed diesel particle filter. *Environmental science & technology* **2013,** *47* (12), 6510-6517.

20.   Ryan, S. P.; Altwicker, E. R., Understanding the role of iron chlorides in the de novo synthesis of polychlorinated dibenzo-p-dioxins/dibenzofurans. *Environmental science & technology* **2004,** *38* (6), 1708-1717.

21.   Ryan, S. P.; Altwicker, E. R., The formation of polychlorinated dibenzo-p-dioxins/dibenzofurans from carbon model mixtures containing ferrous chloride. *Chemosphere* **2000,** *40* (9-11), 1009-1014.

22.   Nganai, S.; Lomnicki, S.; Dellinger, B., Formation of PCDD/Fs from oxidation of 2-monochlorophenol over an Fe2O3/silica surface. *Chemosphere* **2012,** *88* (3), 371-376.

23.   Jiang, J.-g.; Xin, X.; Jun, W.; Yang, S.-j.; Zhang, Y., Investigation of basic properties of fly ash from urban waste incinerators in China. *Journal of Environmental Sciences* **2007,** *19* (4), 458-463.

24.   Cuenya, B. R., Synthesis and catalytic properties of metal nanoparticles: Size, shape, support, composition, and oxidation state effects. *Thin Solid Films* **2010,** *518* (12), 3127-3150.

CHAPTER 6 CONCLUSIONS

Transition metal-mediated PCDD/F formation reactions occurring in the cool zone of the combustors account for most of the PCDD/F emission in combustion systems. Both copper and iron are present in fly ashes and considered the most active metals in catalyzing PCDD/F formation. Previous research has focused on the effect of single metal oxide or chloride on the formation of PCDD/F and there are rarely studies on the multi-metal effect and a quantitative link between the content of metal in the fly ash and PCDD/F yields.

We studied the cooperative effect between iron and copper on the PCDD/F formation. The results indicate the synergy between iron and copper promotes PCDD/F formation. Under pyrolytic conditions, synergy of iron and copper oxides produced almost 5-fold yields of PCDD/F compared to single CuO or Fe_2O_3. Under oxidative conditions, iron and copper synergy enhances the oxidation of PCDD/F precursor. After comparing PCDD/F congener profiles and yields with that of single CuO or Fe_2O_3, we found that in the iron and copper mixed oxide system, CuO contributes to the formation of PCDD/F congener profile while Fe_2O_3 is affecting the PCDD/F yields.

The effect of iron content and Fe_2O_3 cluster size on the PCDD/F formation was investigated. Under pyrolytic conditions, EPFRs concentration increased with the increasing of the iron content in the fly ash surrogates. Total PCDD/F yield followed the same trend. The catalytic activity of Fe_2O_3 fly ash surrogates relates to not only the content, but also the cluster size of Fe_2O_3. 1% Fe_2O_3 sample is amorphous containing smaller nanoclusters and 5% Fe_2O_3 contains a larger number of crystals with larger nanoclusters. Fe_2O_3 content and morphology determines PCDF congeners' distribution.

124

In the waste incineration, single metal oxide does affects the PCDD/F formation and yields, however, interaction and collective effects between transition metals, particularly between copper and iron contribute to the PCDD/F formation overall.

Sulfur has been applied to MSWI as an effective inhibitor of dioxin formation, however, the mechanism on how sulfur affects the redox potential of iron or copper and poison their catalytic activity, thus the formation of EPFRs for PCDD/F has not been fully understood. Our future work is to introduce sulfur by impregnating the sulfur compound into fly ash surrogates or introducing gaseous SO_2 to study the sulfur's inhibitive effect on the formation of PCDD/Fs.

VITA

Xia Guan was born in Henan, China. She received the degree of Bachelor of Engineering in Environmental Monitoring from Henan Normal University. She began to work as a chemistry teacher for several years and went on further her chemistry education at Fudan University and received a Doctor of Philosophy degree in Analytical Chemistry in 2011. She joined Louisiana State University graduate program in the summer of 2014. She studied under Dr. Slawo Lomnicki at Environmental Sciences Department and LSU Superfund Research Program. She is a candidate to receive a Doctor of Philosophy degree in Environmental Sciences in May 2018.